Supporting Information

“Cold” Photo-Induced Crystal-to-Liquid Transition of Acylhydrazones: Leveraging Slight Molecular Modification to Expand Usable Temperature Range

Ryo Koibuchi[1], Isao Yoshikawa[1], Hirohiko Houjou*[1,2]
[1] Institute of Industrial Science, The University of Tokyo, 4-6-1 Komaba, Meguro-ku, Tokyo 153-8505, Japan.
[2] Environmental Science Center, The University of Tokyo, 3-7-1 Hongo, Bunkyo-ku, Tokyo 113-0033, Japan.
*corresponding author: houjou@iis.u-tokyo.ac.jp

Contents

1 Experimental details

Materials

Starting materials and reagents were commercially available and used as obtained from Tokyo Chemical Industry Co., Ltd. or Kanto Chemical Co., Inc. without further purification.

NMR spectroscopy

^{1}H and ^{13}C NMR spectra were recorded on a JEOL JNM-ECS400 spectrometer. For the ^{1}H NMR spectra of the UV-irradiated sample, 365 nm light irradiation was performed using an ASAHI SPECTRA LAX-103.

UV-Vis absorption spectroscopy

The UV-Vis absorption spectra were measured with a JASCO V-630 spectrometer. The 365 nm light irradiation of the measurement sample was performed with a Funakoshi UVGL-58 handheld UV lamp.

Photographic images of the PCLT

The photographic images of the PCLT were recorded using a conventional optical microscope equipped with a temperature-controlled stage (Linkam THMS600).[1] The UV irradiation was carried out from a high-pressure Hg lamp (100 W) via a 330–380 nm bandpass filter. The measurement light was emitted from a halogen lamp (100 W).

DSC measurement

The DSC measurements were carried out with a Pyris 1 DSC. The samples were sealed in 20 μL aluminum pans (Perkin-Elmer, KIT NO. 0219-0062) for measurement.

Mass spectrometry

Mass spectra were recorded on a JEOL JMS-S3000 MALDI-TOF-MS equipment, for which trans-2-[3-(4-tertButylphenyl)-2-methyl-2-propenylidene]malononitrile was used as matrix.

IR spectroscopy

The IR spectra were measured with a JASCO FT/IR-4X spectrometer. The 365 nm light irradiation of the crystal sample for the IR spectra measurement was carried out with an ASAHI SPECTRA LAX-103. Heating of the sample was controlled using a Spectra-Tech HT32 high-temperature cell. The IR spectra at −15 °C were measured using a temperature-controlled stage (Linkam THMS600) and JASCO FTIR 6600.

X-ray Diffraction (XRD)

The *E*-isomer crystals were obtained by recrystallization from a methanol solution. As an exception, the *S*-type crystals of **d7** and **e7** were obtained by recrystallization from the molten state. The *Z*-isomer crystals were recrystallized from a methanol solution under 365 nm light irradiation. Crystallographic data were collected on a Rigaku XtaLAB P200, λ (Cu-K$_\alpha$) = 1.54187 Å. The structures were solved by direct method (SHELXS-2013)[2] or dual method (SHELXT-2014)[3], and refined on F^2 by full-matrix leastsquare techniques (SHELXL-2018)[4] using the Yadokari-XG software package[5]. Crystallographic data were deposited with Cambridge Crystallographic Data Centre: Deposition number CCDC-2431293-2431303.

2 Synthesis

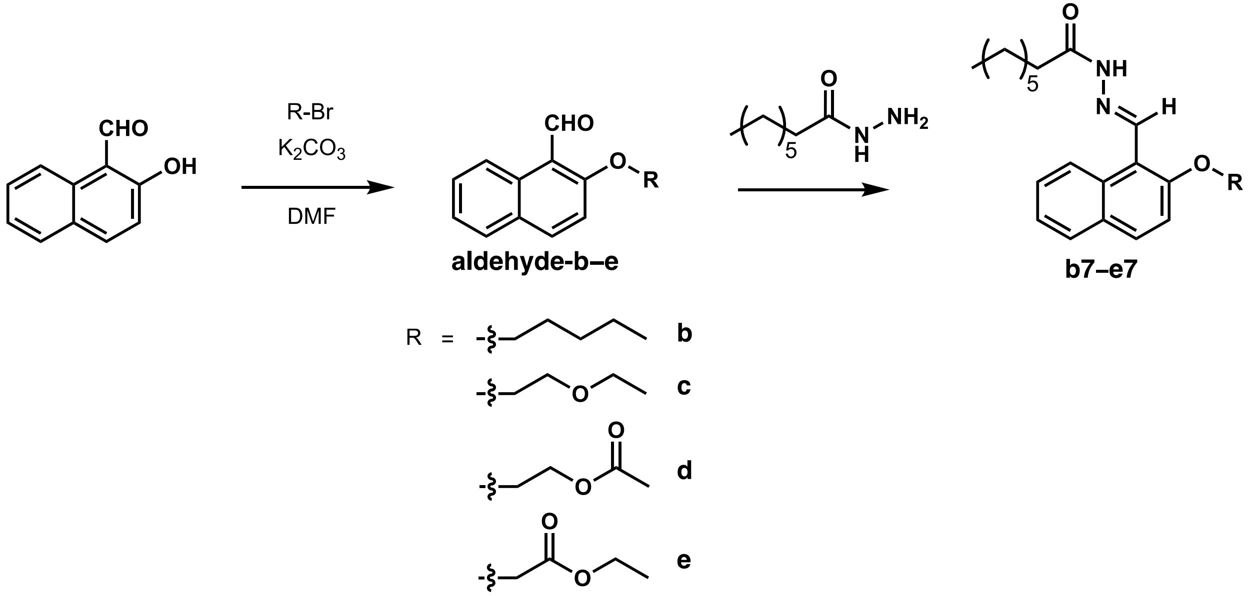

Scheme S1. Scheme for synthesizing of acylhydrazones.

Synthesis of aldehyde-b–e (Scheme S1): 2-Hydroxy-1-naphthaldehyde (1 equiv), R-Br (Scheme S1) (1.1 equiv), potassium carbonate (1.1 equiv), and potassium iodide (0.05 equiv) were dissolved in *N*,*N*-dimethylformamide (DMF) and stirred for 24 hours. The resulting brown solution was concentrated using a rotary evaporator and then diluted with water. The mixture was extracted with dichloromethane (DCM), and the combined organic layers were dried over Na_2SO_4. The solvent was removed using a rotary evaporator, and the resulting precipitant was collected by filtration. All aldehydes were used as intermediates for the synthesis of **b7**–**e7** without further purification.

Synthesis of Octanohydrazide

Octanohydrazide was prepared according to method previously reported.[6]

Synthesis of a7–e7

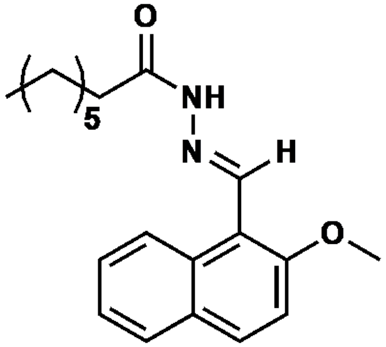

a7: **a7** was prepared according to method previously reported.[6] To an ethanol solution (12.5 mL) of octanohydrazide (728.0 mg, 4.6 mmol), 2-methoxy-1-naphthaldehyde (856.6 mg, 4.6 mmol) was added. After refluxing for 1 h, the solution was cooled at room temperature to afford a non-colored crystalline solid. Yield 1.138 g (76%). ^{1}H NMR (400 MHz, DMSO-d_6) : δ = 11.40 (s, 0.5H), 11.24 (s, 0.5H), 9.30 (d, *J* = 8.7 Hz, 0.5H), 9.05 (d, *J* = 8.7 Hz, 0.5H), 8.85 (s, 0.5H), 8.69 (s, 0.5H), 8.03 (dd, *J* = 9.0, 4.2 Hz, 1H), 7.91 (dd, *J* = 7.5, 4.0 Hz, 1H), 7.58 − 7.50 (m, 2H), 7.42 (t, *J* = 8.0, 1H), 3.99 and 3.97 (both s, total 3H), 2.64 (t, *J* = 7.5 Hz, 1H), 2.23 (t, *J* = 7.4 Hz, 1H), 1.67 – 1.57 (m, 2H), 1.40 – 1.21 (m, 8H), 0.89 – 0.81 (m, 3H); ^{13}C NMR (100 MHz, DMSO-d_6) : δ = 174.25, 168.51, 157.60, 157.46, 143.22, 140.30, 132.51, 132.17, 130.67, 130.62, 128.82, 128.76, 128.64, 128.47, 127.97, 127.76, 125.87, 125.06, 124.05, 123.95, 114.34, 114.23, 113.48, 113.42, 56.67, 34.17, 32.43, 31.24, 31.21, 28.96, 28.72, 28.51, 25.12, 24.53, 22.13, 22.10, 13.99, 13.96; MALDI-TOF-MS m/z calcd for $[MH]^+$ 327.2, found 327.2; Analysis for $C_{20}H_{26}N_2O_2$, calcd C 73.59, H 8.03, N 8.58, found C 73.56, H 8.17, N 8.56.

Note: owing to the equilibrated conformers with respect to amide bond rotation, some ^{1}H and ^{13}C NMR signals of acylhydrazones are observed as two sets of peaks.

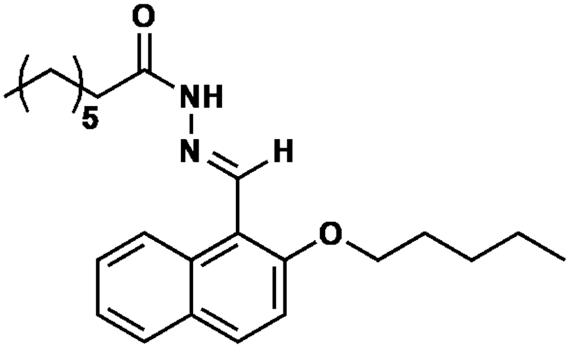

b7: To a methanol solution (5 mL) of octanohydrazide (364.0 mg, 2.3 mmol), aldehyde-**b** (557.3 mg, 2.3 mmol) was added. After refluxing for 1 h, the solution was cooled at room temperature to afford a non-colored crystalline solid. Washed with ethanol Yield 732.6 mg (83%). ^{1}H NMR (400 MHz, DMSO-d_6) : δ = 11.38 (s, 0.5H), 11.32 (s, 0.5H), 9.31 (d, *J* = 8.3 Hz, 0.5H), 9.05 (d, *J* = 8.7 Hz, 0.5H), 8.85 (s, 0.5H), 8.72 (s, 0.5H), 7.99 (dd, *J* = 9.2, 4.0 Hz, 1H), 7.89 (dd, *J* = 7.6, 4.7 Hz, 1H), 7.56 − 7.46 (m, 2H), 7.41 (t, *J* = 7.5, 1H), 4.22 – 4.16 (m, 2H), 2.65 (t, *J* = 7.6 Hz, 1H), 2.24 (t, *J* = 7.5 Hz, 1H), 1.82 – 1.76 (m, 2H), 1.66 – 1.59 (m, 2H), 1.48 – 1.24 (m, 12H), 0.94 – 0.81 (m, 6H); ^{13}C NMR (100 MHz, DMSO-d_6) : δ = 174.27, 168.52, 157.10, 157.01, 143.27, 140.59, 132.41, 132.08, 130.75, 130.69, 128.80, 128.75, 128.60, 128.42, 127.89, 127.69, 125.93, 125.06, 124.02, 123.93, 114.69, 114.61, 114.50, 69.19, 34.16, 32.39, 31.23, 28.96, 28.73, 28.64, 28.51, 27.66, 27.63, 25.12, 24.51, 22.11, 22.09, 21.97, 21.92, 13.97, 13.95; HRMS m/z calcd for $[MH]^+$ 383.2694, found 383.2688.

Note: owing to the equilibrated conformers with respect to amide bond rotation, some ^{1}H and ^{13}C NMR signals of acylhydrazones are observed as two sets of peaks.

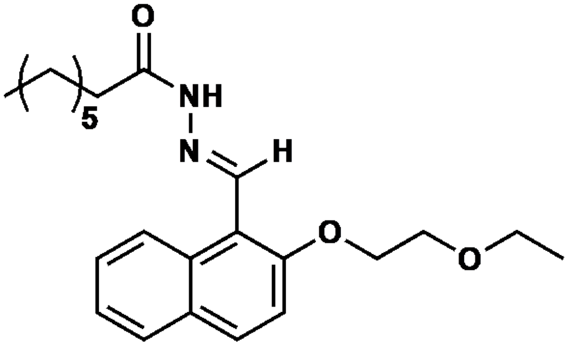

c7: To a methanol solution (5 mL) of octanohydrazide (364.0 mg, 2.3 mmol), aldehyde-**c** (561.9 mg, 2.3 mmol) was added. After refluxing for 1 h, the solution was cooled at room temperature to afford a non-colored crystalline solid. Washed with ethanol Yield 498.2 mg (56%). ^{1}H NMR (400 MHz, DMSO-d_6) : δ = 11.42 (s, 0.5H), 11.30 (s, 0.5H), 9.33 (d, *J* = 8.7 Hz, 0.5H), 9.06 (d, *J* = 8.6 Hz, 0.5H), 8.84 (s, 0.5H), 8.71 (s, 0.5H), 8.03 (dd, *J* = 9.0, 3.7 Hz, 1H), 7.91 (dd, *J* = 7.9, 4.6 Hz, 1H), 7.57 − 7.41 (m, 2H), 7.42 (t, *J* = 7.4, 1H), 4.31 – 4.36 (m, 2H), 3.76 (t, *J* = 4.6 Hz, 2H), 3.56 – 3.50 (m, 2H), 2.65 (t, *J* = 7.5 Hz, 1H), 2.24 (t, *J* = 7.4 Hz, 1H), 1.66 – 1.60 (m, 2H), 1.36 – 1.24 (m, 8H), 1.13 (t, *J* = 7.1 Hz, 3H), 0.87 – 0.81 (m, 3H);

^{13}C NMR (100 MHz, DMSO-d_6) : δ = 174.29, 168.56, 157.02, 156.96, 143.35, 140.63, 132.37, 132.04, 130.73, 130.67, 129.01, 128.97, 128.61, 128.43, 127.91, 127.70, 126.02, 125.14, 124.19, 124.09, 115.15, 115.09, 115.02, 69.26, 69.10, 65.86, 65.78, 34.16, 32.41, 31.24, 31.22, 28.96, 28.74, 28.53, 28.51, 25.14, 24.53, 22.12, 22.10, 15.16, 15.14, 13.98, 13.96; HRMS m/z calcd for [MH]$^+$ 407.2306, found 407.2299. *Note*: owing to the equilibrated conformers with respect to amide bond rotation, some ^{1}H and ^{13}C NMR signals of acylhydrazones are observed as two sets of peaks.

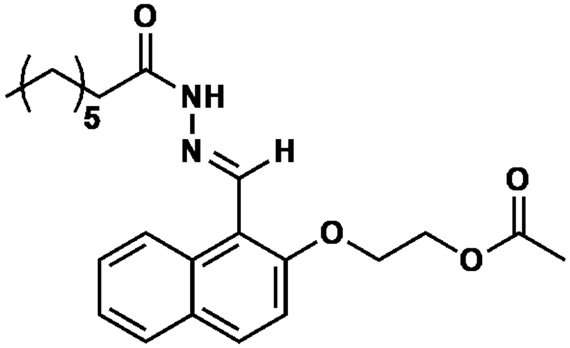

d7: To an ethanol solution (5 mL) of octanohydrazide (364.0 mg, 2.3 mmol), aldehyde-**d** (594.0 mg, 2.3 mmol) was added. After refluxing for 1 h, the solution was cooled at room temperature to afford a non-colored crystalline solid. Washed with ethanol Yield 685.9 mg (75%). ^{1}H NMR (400 MHz, DMSO-d_6) : δ = 11.41 (s, 0.5H), 11.29 (s, 0.5H), 9.33 (d, J = 8.7 Hz, 0.5H), 9.06 (d, J = 8.6 Hz, 0.5H), 8.84 (s, 0.5H), 8.70 (s, 0.5H), 8.01 (dd, J = 9.2, 3.2 Hz, 1H), 7.91 (dd, J = 7.7, 4.9 Hz, 1H), 7.58 − 7.49 (m, 2H), 7.44 (t, J = 6.9, 1H), 4.45 – 4.36 (m, 4H), 2.65 (t, J = 7.5 Hz, 1H), 2.24 (t, J = 7.4 Hz, 1H), 2.05 (s, 3H), 1.66 – 1.59 (m, 2H), 1.36 – 1.24 (m, 8H), 0.87 – 0.81 (m, 3H); ^{13}C NMR (100 MHz, DMSO-d_6) : δ = 174.29, 170.48, 168.56, 156.67, 156.58, 143.19, 140.50, 132.44, 132.12, 130.92, 130.69, 130.62, 129.14, 129.10, 128.64, 128.47, 127.98, 127.78, 126.05, 125.18, 124.32, 124.24, 115.38, 115.26, 115.08, 114.93, 67.66, 62.78, 62.75, 34.17, 32.39, 31.24, 28.96, 28.74, 28.53, 28.51, 25.12, 24.51, 22.12, 20.71, 13.99, 13.96; HRMS m/z calcd for [MNa]$^+$ 421.2098, found 421.2086.

Note: owing to the equilibrated conformers with respect to amide bond rotation, some ^{1}H and ^{13}C NMR signals of acylhydrazones are observed as two sets of peaks.

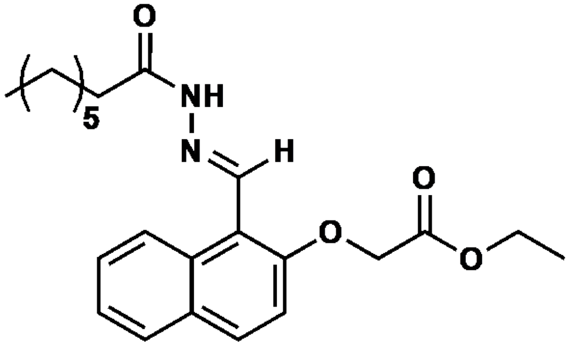

e7: To an ethanol solution (5 mL) of octanohydrazide (364.0 mg, 2.3 mmol), aldehyde-**e** (594.0 mg, 2.3 mmol) was added. After refluxing for 1 h, the solution was cooled at room temperature to afford a non-colored crystalline solid. Washed with ethanol Yield 586.9 mg (64%). ^{1}H NMR (400 MHz, DMSO-d_6) : δ = 11.46 (s, 0.5H), 11.30 (s, 0.5H), 9.31 (d, J = 8.6 Hz, 0.5H), 9.04 (d, J = 8.6 Hz, 0.5H), 8.90 (s, 0.5H), 8.73 (s, 0.5H), 7.98 (dd, J = 9.2, 4.5 Hz, 1H), 7.90 (dd, J = 7.6, 3.9 Hz, 1H), 7.59 − 7.53 (m, 1H), 7.46 − 7.39 (m, 2H), 5.06 (d, J = 10.6 Hz, 2H), 4.18 (q, J = 7.2 Hz, 2H), 2.65 (t, J = 7.5 Hz, 1H), 2.24 (t, J = 7.4 Hz, 1H), 1.66 – 1.59 (m, 2H), 1.38 – 1.19 (m, 11H), 0.88 – 0.81 (m, 3H); ^{13}C NMR (100 MHz, DMSO-d_6) : δ

= 174.32, 168.79, 168.77, 168.62, 156.02, 155.85, 143.20, 140.25, 132.22, 131.85, 130.69, 130.66, 129.21, 129.17, 128.59, 128.43, 127.80, 126.02, 125.19, 124.41, 124.31, 115.33, 115.23, 114.18, 114.13, 65.80, 60.86, 34.14, 32.42, 31.24, 31.21, 28.95, 28.73, 28.51, 25.12, 24.53, 22.12, 22.10, 14.05, 13.99, 13.96; HRMS m/z calcd for $[MNa]^+$ 421.2098, found 421.2077.

Note: owing to the equilibrated conformers with respect to amide bond rotation, some ^1H and ^{13}C NMR signals of acylhydrazones are observed as two sets of peaks.

3 Tracking the *E*/*Z* isomerization by ^{1}H NMR spectra

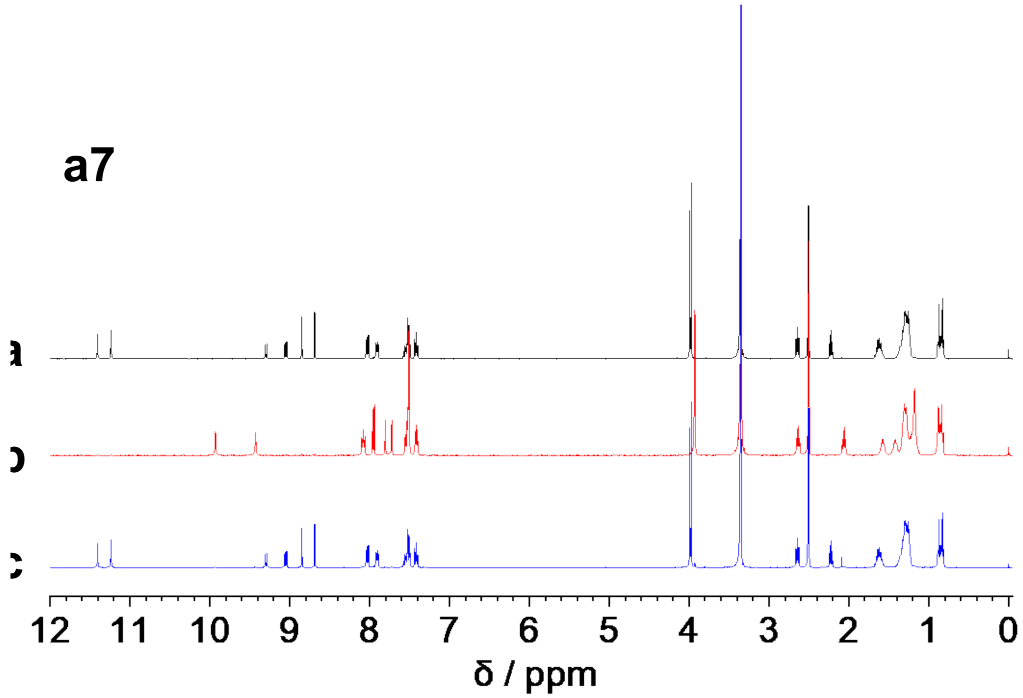

Figure S1 ^{1}H NMR spectra of **a7** in DMSO-d_6: (a) as-prepared, (b) irradiated with 365 nm light for 90 min, and (c) heated at 130 °C for 2h after UV irradiation.

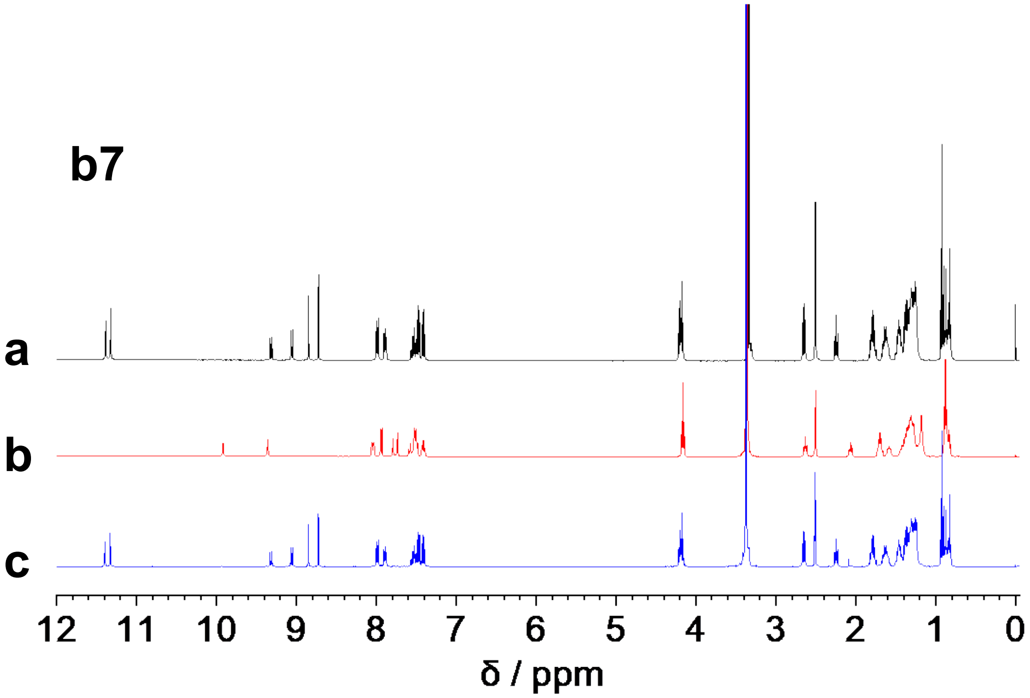

Figure S2 ^{1}H NMR spectra of **b7** in DMSO-d_6: (a) as-prepared, (b) irradiated with 365 nm light for 90 min, and (c) heated at 130 °C for 2h after UV irradiation.

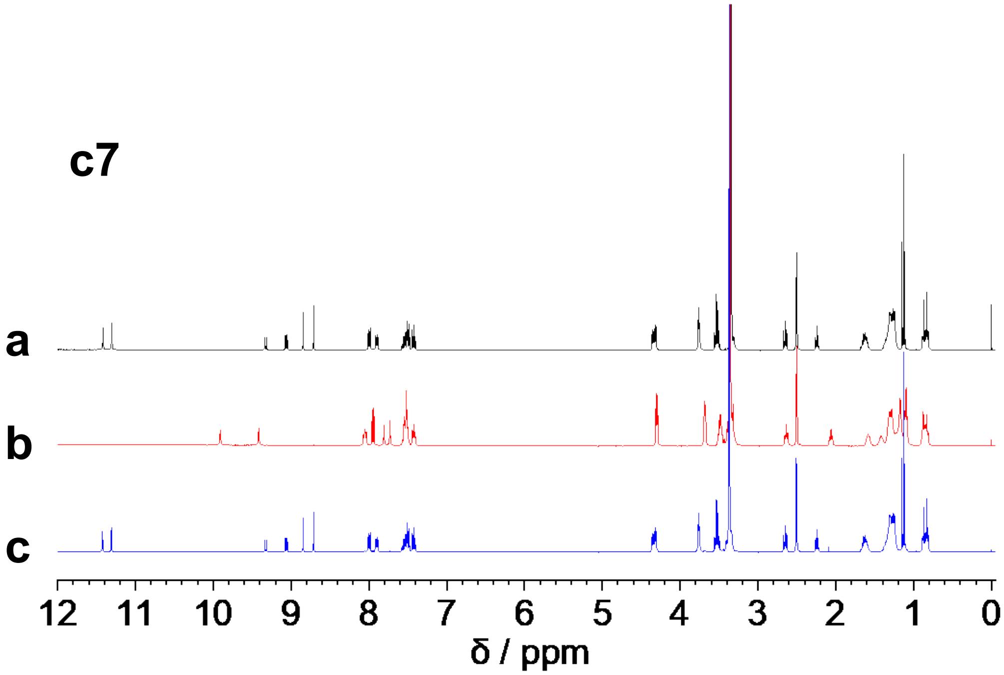

Figure S3 ^{1}H NMR spectra of **c7** in DMSO-d_6: (a) as-prepared, (b) irradiated with 365 nm light for 90 min, and (c) heated at 130 °C for 2h after UV irradiation.

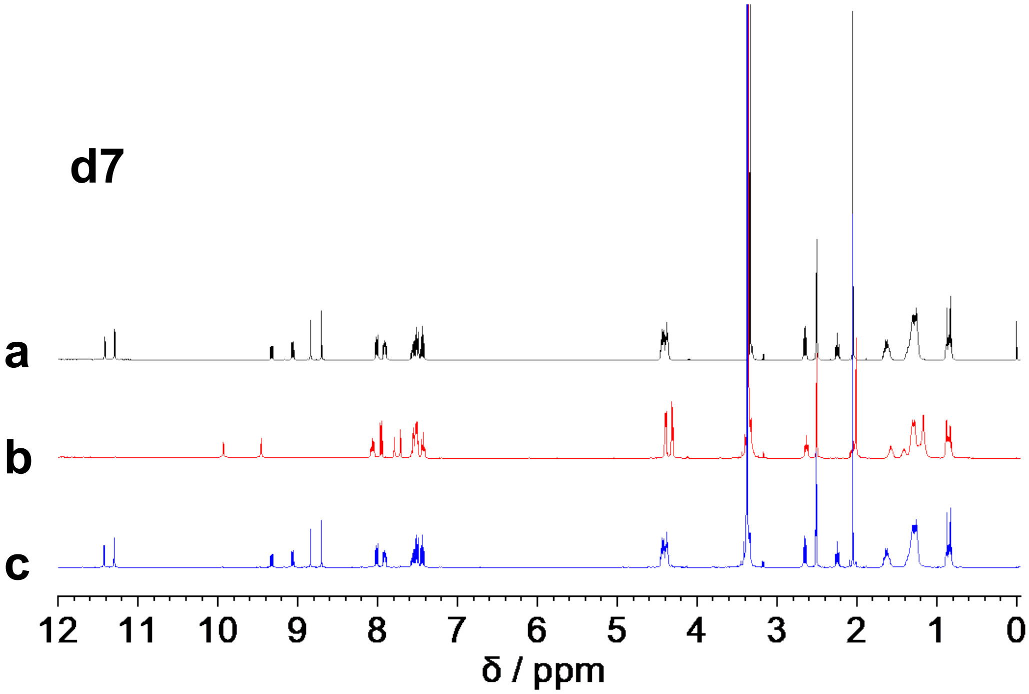

Figure S4 ^{1}H NMR spectra of **d7** in DMSO-d_6: (a) as-prepared, (b) irradiated with 365 nm light for 90 min, and (c) heated at 130 °C for 2h after UV irradiation.

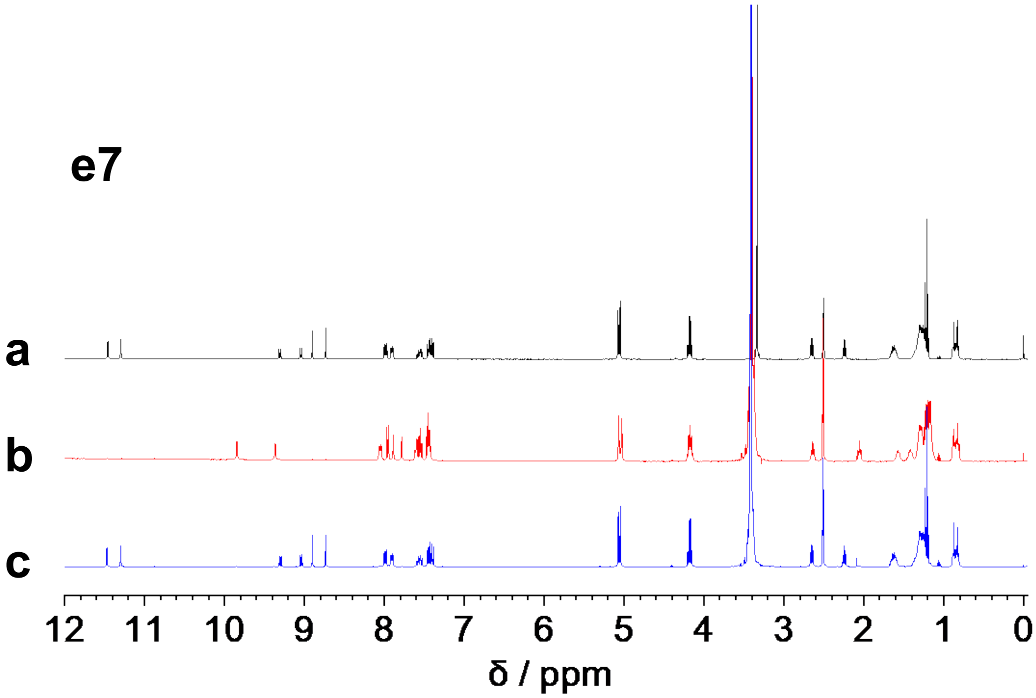

Figure S5 ^{1}H NMR spectra of **e7** in DMSO-d_6: (a) as-prepared, (b) irradiated with 365 nm light for 90 min, and (c) heated at 130 °C for 2h after UV irradiation.

4 UV-Vis spectroscopy

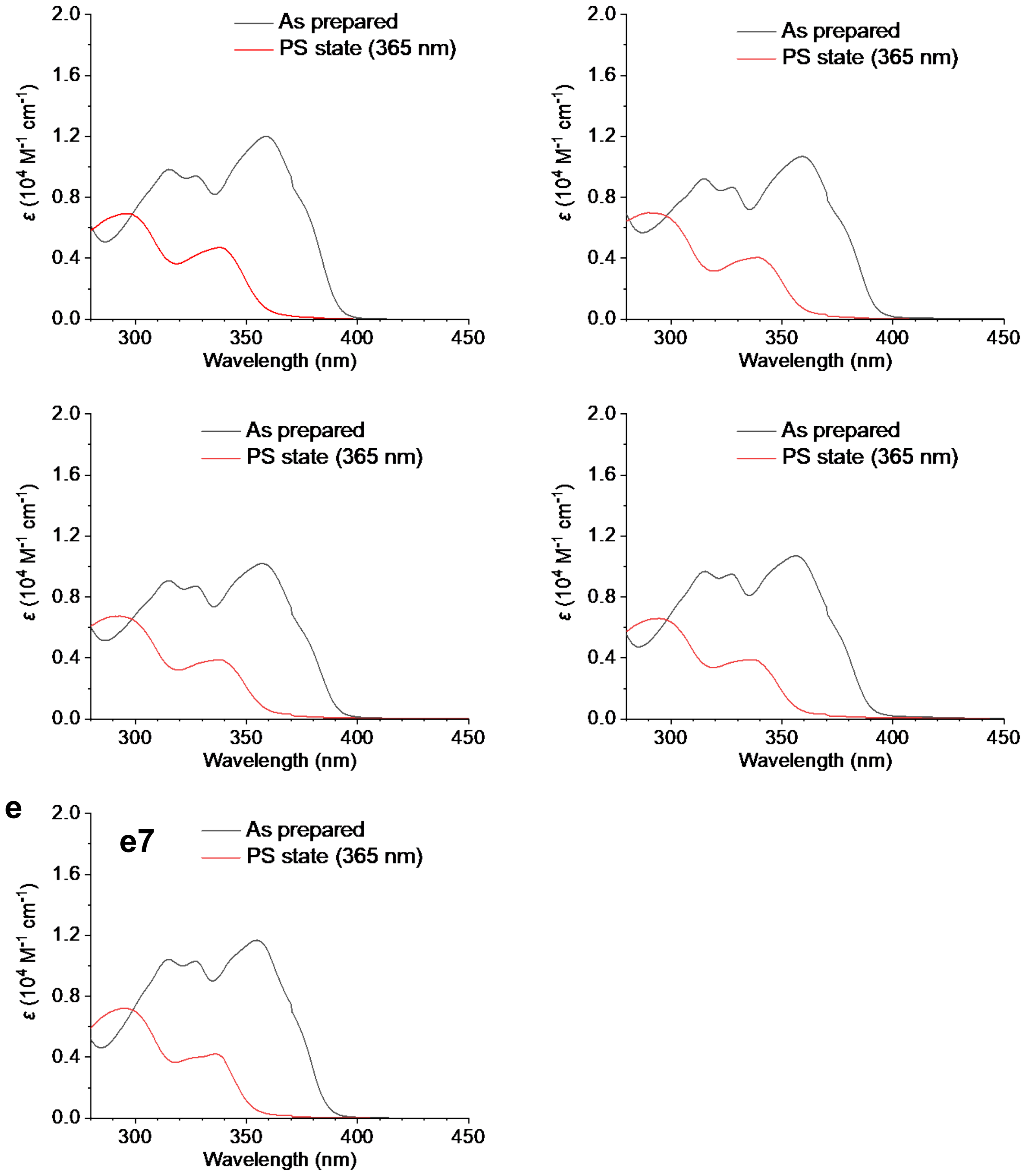

Figure S6 UV-Vis spectra of acylhydrazones in DMSO solution (5.0×10^{-5} M): as prepared (black), PS state under 365 nm irradiation for 10 min (red).

5 Thermal *Z*-to-*E* isomerization kinetics

According to the literatures[7,8], the experimental kinetics data were analyzed through Arrhenius plot and Eyring plot. Thermal *Z*-to-*E* isomerization was measured in DMSO solution (5.0×10^{-5} M) at various temperatures (60, 70, and 80 °C).

The Arrhenius equation is as following:

$$\ln k = -\frac{E_\mathrm{a}}{RT} + \ln A$$

where k is the rate constant; E_a is the activation energy; R is the gas constant; T is the absolute temperature; and A is the pre-exponential factor.

The Eyring equation is as following:

$$\ln\frac{kh}{k_\mathrm{B}T} = -\frac{\Delta H^{\ddagger}}{RT} + \frac{\Delta S^{\ddagger}}{R}$$

where k is the rate constant; h is Planck's constant; k_B is the Boltzmann constant; T is the absolute temperature; R is the gas constant; $\Delta H^{\ddagger}$ is the enthalpy of activation; and $\Delta S^{\ddagger}$ is the entropy of activation.

Free energy of activation ($\Delta G^{\ddagger}$) is as following:

$$\Delta G^{\ddagger} = \Delta H^{\ddagger} - T\Delta S^{\ddagger}$$

Table S1 Thermal *Z*-to-*E* isomerization properties of acylhydrazones.

	E isomer	*Z* isomer	Photoconversion	Quantum yield	Thermal *Z*→*E* isomerization			
	π-π* $\lambda_{\max}$ (nm)	π-π* $\lambda_{\max}$ (nm)	*E*→*Z* (%)	*E*→*Z* (%)	$t_{1/2}$ (d)	$\Delta G^{\ddagger}$ (kJ/mol)	$\Delta H^{\ddagger}$ (kJ/mol)	$\Delta S^{\ddagger}$ (J/mol K)
a7	359	338	98	0.24	24	110.0	57.3	−176.9
b7	360	340	99	0.33	138	114.3	80.1	−114.6
c7	357	338	99	0.27	91	113.3	74.4	−130.4
d7	356	336	99	0.27	113	113.8	77.4	−122.0
e7	355	336	97	0.31	144	114.4	74.4	−134.0

[1] Values at 25 °C in DMSO, extrapolated from the experimental kinetics data at elevated temperatures in the Arrhenius equation.

[2] Values at 25 °C in DMSO, calculated through Eyring plot based on the extrapolated from the experimental kinetics data.

Table S2 Thermal relaxation kinetics results of **a7** in DMSO.

	Experimental			Calculated			
	60 °C	70 °C	80 °C		25 °C		
k ($\times 10^{-5}$ min^{-1})	26.6	43.0	91.3	*k* ($\times 10^{-5}$ min^{-1})	1.98	E_a (kJ/mol)	60.1
$t_{1/2}$ (min)	2602	1613	759	$t_{1/2}$ (d)	24	ln*A*	13.4

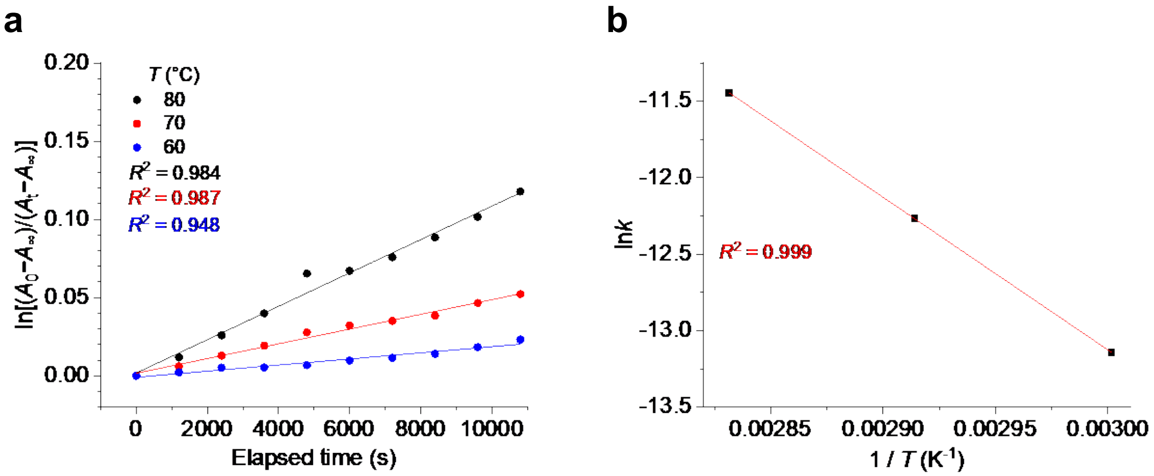

Figure S7 (a) Kinetic analysis of **b7** in DMSO solution (5.0×10^{-5} M). Absorption change at 354.5 nm was monitored and fitted with first-order kinetics to obtain the rate constant of *Z*-to-*E* thermal relaxation. (b) Arrhenius plot for thermal relaxation of **b7** in DMSO.

Table S3 Thermal relaxation kinetics results of **b7** in DMSO.

	Experimental			Calculated			
	60 °C	70 °C	80 °C		25 °C		
k ($\times 10^{-6}$ s^{-1})	2.0	4.7	10.7	*k* ($\times 10^{-8}$ s^{-1})	5.8	E_a (kJ/mol)	83.0
$t_{1/2}$ (s)	354488	147180	64970	$t_{1/2}$ (d)	138	ln*A*	16.8

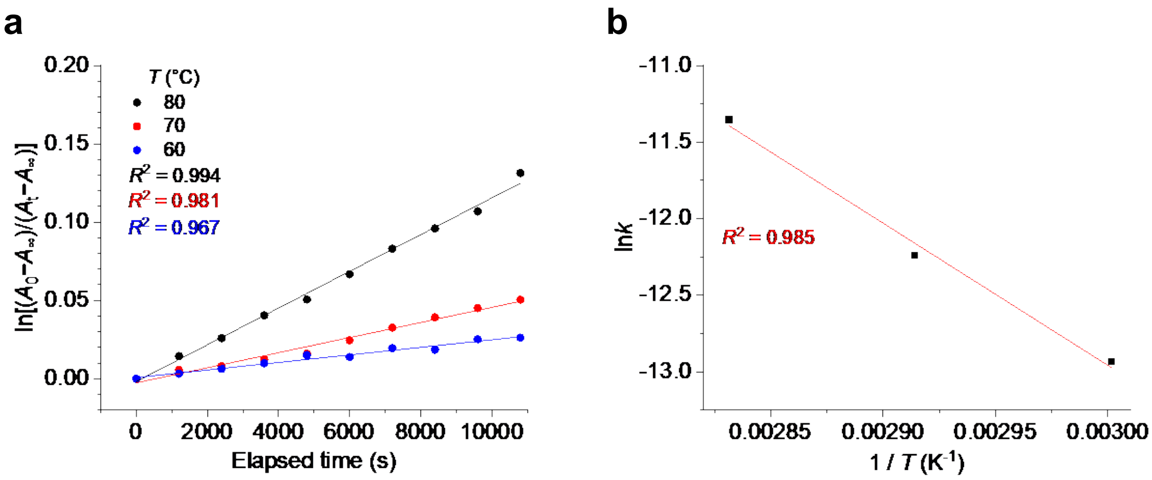

Figure S8 (a) Kinetic analysis of **c7** in DMSO solution (5.0×10^{-5} M). Absorption change at 354.5 nm was monitored and fitted with first-order kinetics to obtain the rate constant of *Z*-to-*E* thermal relaxation. (b) Arrhenius plot for thermal relaxation of **c7** in DMSO.

Table S4 Thermal relaxation kinetics results of **c7** in DMSO.

	Experimental			Calculated			
	60 °C	70 °C	80 °C		25 °C		
k ($\times10^{-6}$ s^{-1})	2.4	4.8	11.7	k ($\times10^{-8}$ s^{-1})	8.8	E_a (kJ/mol)	77.3
$t_{1/2}$ (s)	287386	143678	59084	$t_{1/2}$ (d)	91	ln$A$	14.9

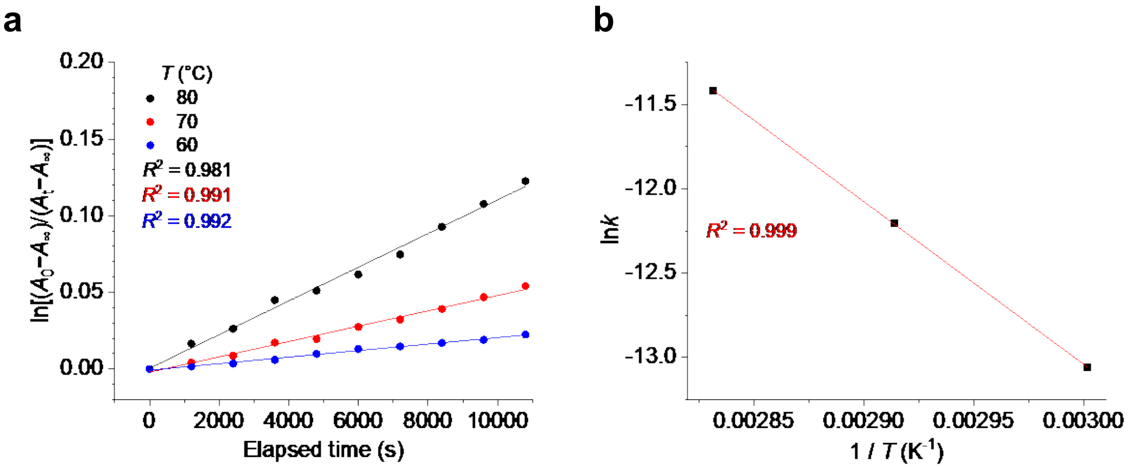

Figure S9 (a) Kinetic analysis of **d7** in DMSO solution (5.0×10^{-5} M). Absorption change at 354.5 nm was monitored and fitted with first-order kinetics to obtain the rate constant of *Z*-to-*E* thermal relaxation. (b) Arrhenius plot for thermal relaxation of **d7** in DMSO.

Table S5 Thermal relaxation kinetics results of **d7** in DMSO.

	Experimental			Calculated			
	60 °C	70 °C	80 °C		25 °C		
k ($\times10^{-6}$ s^{-1})	2.1	5.0	11.0	k ($\times10^{-8}$ s^{-1})	7.1	E_a (kJ/mol)	80.3
$t_{1/2}$ (s)	325658	138642	63117	$t_{1/2}$ (d)	113	ln$A$	15.9

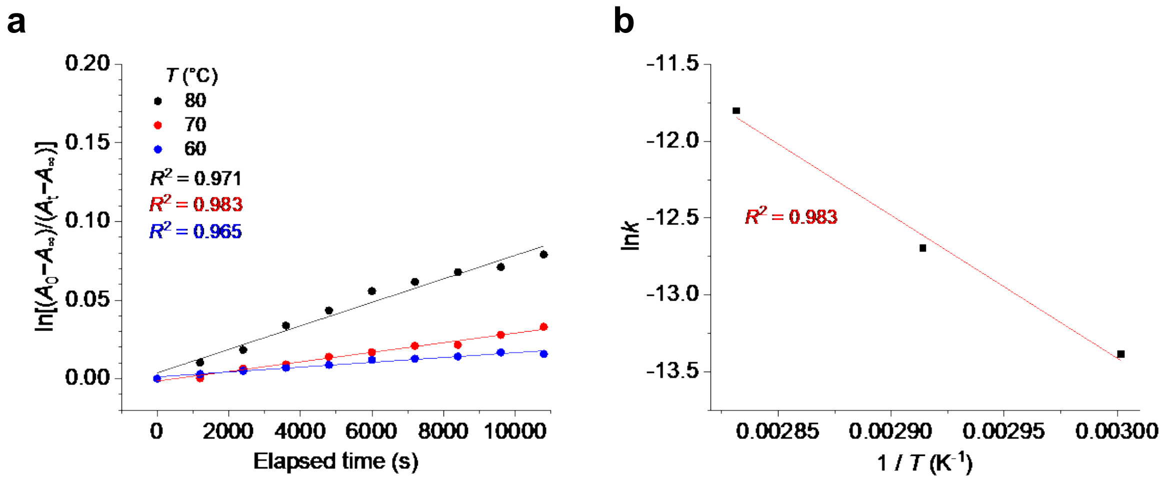

Figure S10 (a) Kinetic analysis of **e7** in DMSO solution (5.0×10^{-5} M). Absorption change at 354.5 nm was monitored and fitted with first-order kinetics to obtain the rate constant of *Z*-to-*E* thermal relaxation. (b) Arrhenius plot for thermal relaxation of **e7** in DMSO.

Table S6 Thermal relaxation kinetics results of **e7** in DMSO.

	Experimental			Calculated			
	60 °C	70 °C	80 °C		25 °C		
k ($\times10^{-6}$ s^{-1})	1.5	3.1	7.5	k ($\times10^{-8}$ s^{-1})	5.6	E_a (kJ/mol)	77.3
$t_{1/2}$ (s)	451575	227174	92742	$t_{1/2}$ (d)	144	ln$A$	14.5

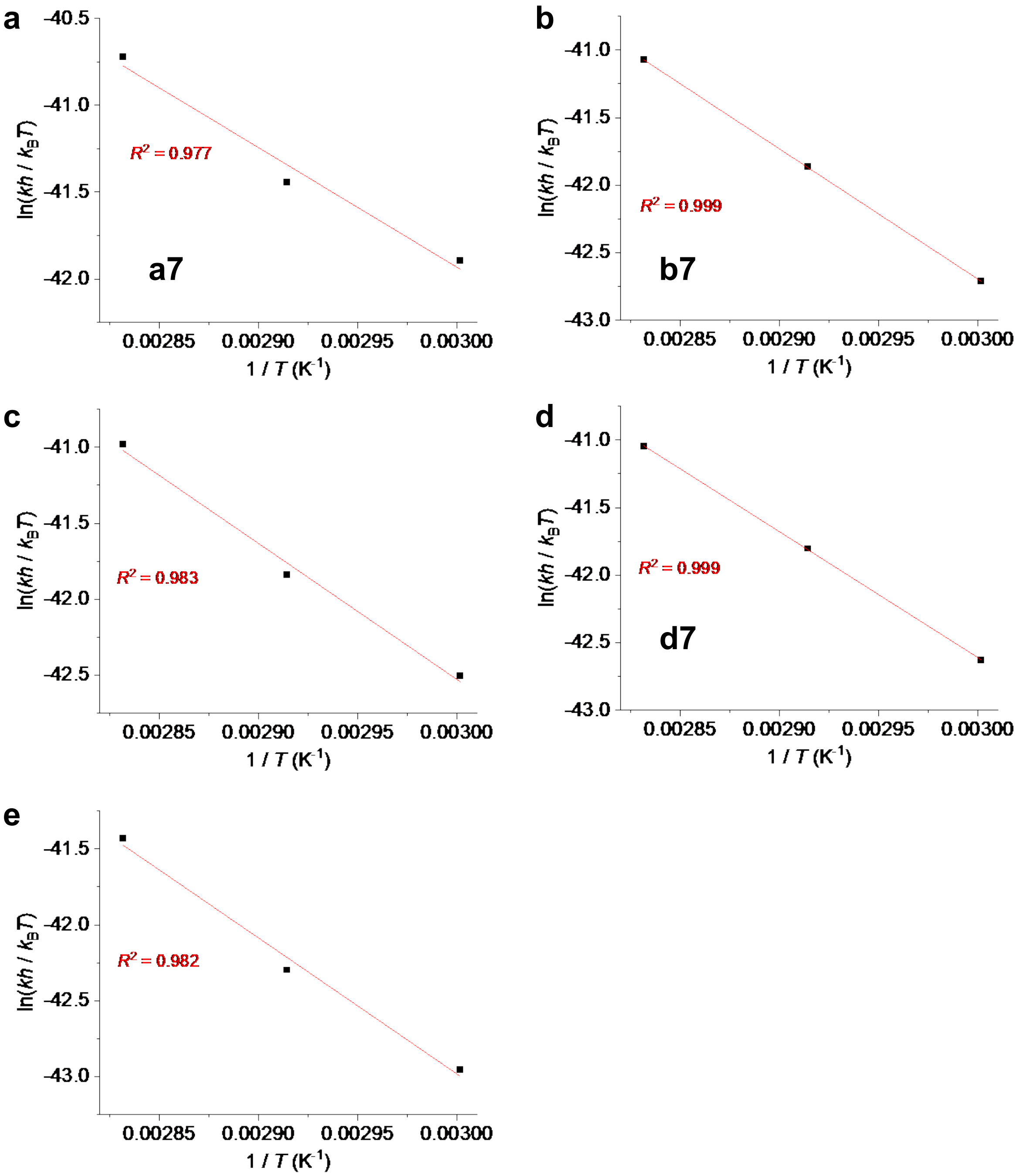

Figure S11 (a) Eyring plot of thermal *Z*-to-*E* relaxation for acylhydrazones in DMSO.

6 Quantum yields of photoisomerization

The differential rate equation of $E \rightarrow Z$ photoisomerization is as following[8–11]:

$$\frac{dc_t}{dt} = k_1(c_0 - c_t) - k_{-1}c_t$$

$$k_1 = \frac{I \cdot l \cdot \left(1 - 10^{-A(t)}\right) \cdot \Phi_{E \rightarrow Z} \cdot \epsilon_E}{V \cdot A(t)}$$

$$k_{-1} = \frac{I \cdot l \cdot \left(1 - 10^{-A(t)}\right) \cdot \Phi_{Z \rightarrow E} \cdot \epsilon_Z}{V \cdot A(t)}$$

where k_1 and k_{-1} are the rate constants at the excitation wavelength of $E \rightarrow Z$ and $Z \rightarrow E$ isomerization, respectively; $c_0 = [E]_0$ is the initial concentration of E isomer; $c_t = [Z]_t$ is the concentration of Z isomer at time; I is the photon flux of the excitation light; l is the beam path length through quartz cuvette; $A(t)$ is the time dependent absorbance at the excitation wavelength; $\Phi_{E \rightarrow Z}$ and $\Phi_{Z \rightarrow E}$ are the quantum yields of $E \rightarrow Z$ and $Z \rightarrow E$ isomerization at the excitation wavelength, respectively; ε_E and ε_Z are the molar absorption coefficients of the E and Z isomer at the excitation wavelength, respectively; V is the volume of the irradiated solution. The thermal back reaction was neglected due to the long half-life. At the photostationary state, the concentrations of both isomers do not change, namely $\frac{dc_t}{dt} = 0$, resulting in $\frac{\Phi_{E \rightarrow Z}}{\Phi_{Z \rightarrow E}} = \frac{c_\infty \cdot \epsilon_Z}{(c_0 - c_\infty) \cdot \epsilon_E}$. where $c_\infty = [Z]_\infty$ is the concentration of Z isomer at the PSS. Defining the fraction of Z isomer as $y = c_t / c_0$ (calculated from UV-Vis spectra), the equations depicted above are combined as

$$\ln\left(\frac{y_\infty - y}{y_\infty - y_0}\right) = -\frac{I \cdot l \cdot \Phi_{E \rightarrow Z} \cdot \epsilon_E}{V \cdot y_\infty} \int_{t_0}^{t} \frac{1 - 10^{-A(t)}}{A(t)}\, dt$$

where $y_\infty = c_\infty / c_0$ is the fraction of Z isomer at the PSS. The value of y_∞ was estimated by fitting the time-dependent change in absorbance to a single-exponential model. The parameter B and the integrated photokinetic factor $x(t)$ were defined as follows:

$$B = \frac{I \cdot l \cdot \Phi_{E \rightarrow Z} \cdot \epsilon_E}{V \cdot y_\infty}$$

$$x(t) = \int_{t_0}^{t} \frac{1 - 10^{-A(t)}}{A(t)}\, dt$$

Then, the equation can be modified as follows:

$$y = (y_0 - y_\infty) \cdot \exp[-B \cdot x(t)] + y_\infty$$

Plotting y against $x(t)$, followed by exponential fitting, the B and y_∞ are obtained. The quantum yield is allowed to be calculated as $\Phi_{E \rightarrow Z} = \frac{B \cdot V \cdot y_\infty}{I \cdot l \cdot \epsilon_E}$.

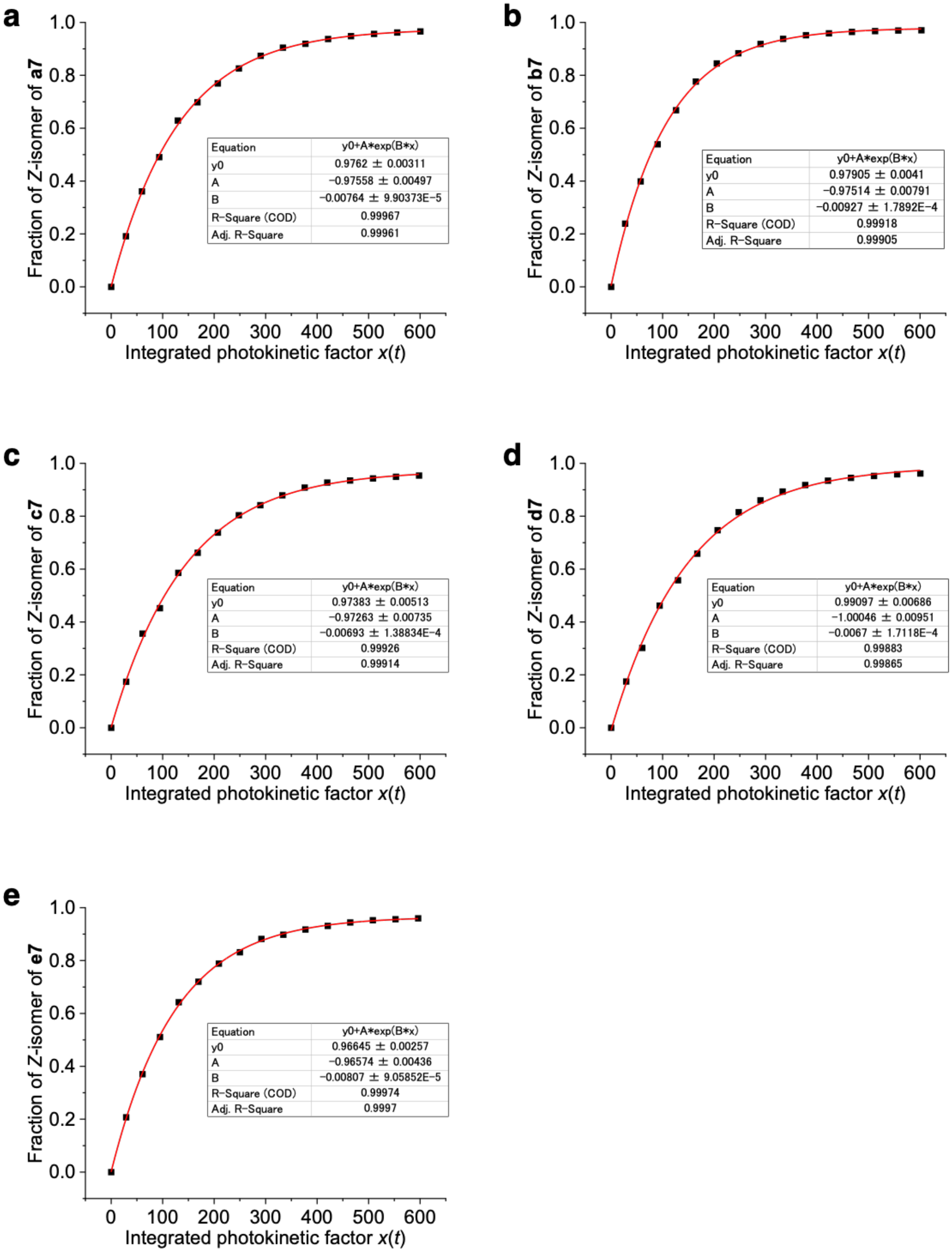

Equation	y0+A*exp(B*x)
y0	0.9762 ± 0.00311
A	−0.97558 ± 0.00497
B	−0.00764 ± 9.90373E−5
R−Square (COD)	0.99967
Adj. R−Square	0.99961

Equation	y0+A*exp(B*x)
y0	0.97905 ± 0.0041
A	−0.97514 ± 0.00791
B	−0.00927 ± 1.7892E−4
R−Square (COD)	0.99918
Adj. R−Square	0.99905

Equation	y0+A*exp(B*x)
y0	0.97383 ± 0.00513
A	−0.97263 ± 0.00735
B	−0.00693 ± 1.38834E−4
R−Square (COD)	0.99926
Adj. R−Square	0.99914

Equation	y0+A*exp(B*x)
y0	0.99097 ± 0.00686
A	−1.00046 ± 0.00951
B	−0.0067 ± 1.7118E−4
R−Square (COD)	0.99883
Adj. R−Square	0.99865

Equation	y0+A*exp(B*x)
y0	0.96645 ± 0.00257
A	−0.96574 ± 0.00436
B	−0.00807 ± 9.05852E−5
R−Square (COD)	0.99974
Adj. R−Square	0.9997

Figure S12 Exponential fitting of the fraction of *Z* isomer (generated by 365 nm of light) for (a) **a7**, (b) **b7**, (c) **c7**, (d) **d7**, and (e) **e7** against the integrated photokinetic factor.

7 Determination of Photon Flux

We used reported procedure for the determination of photon flux[8,12,13]. A solution of $K_3[Fe(C_2O_4)_3]\cdot 3H_2O$ (30 mM in 0.2 N H_2SO_4, 2 mL, V_1) was irradiated by 365 nm light under stirring conditions. After irradiation, a sample of the irradiated ferrioxalate solution (V_2, 0.5 mL) was taken for analysis. This sample was mixed with a buffer solution (1.2 M NaOAc + 0.72 N H_2SO_4, 1 mL) and phenanthroline (6 mM in H_2O, 2 mL). The mixture was then diluted with water to a final volume of 25 mL (V_3) and left to react for one hour. After the reaction period, the absorbance at 510 nm of the tris-phenanthroline complex was measured ($\varepsilon_{510\mathrm{nm}}$ = 11100 M^{-1} cm^{-1}). This procedure was repeated for different irradiation times (0 s, 200 s, 400 s, 600 s, and 800 s), and a plot of absorbance versus irradiation time was collected. The slope of this plot was used to calculate the photon flux (I). The parameters used in this procedure were as follows: path length (l) = 1 cm, V_1 = 2 mL, V_2 = 0.5 mL, V_3 = 25 mL, Φ = 1.21[12] (for 365 nm), and ε = 11100 M^{-1} cm^{-1}.

$$I = \frac{V_1 \cdot V_3 \cdot slope}{V_2 \cdot \epsilon_{510\mathrm{nm}} \cdot l \cdot \phi}$$

According to the following fitting, the photon flux of 365 nm light source was calculated to be 5.57×10^{-9} mol s^{-1}.

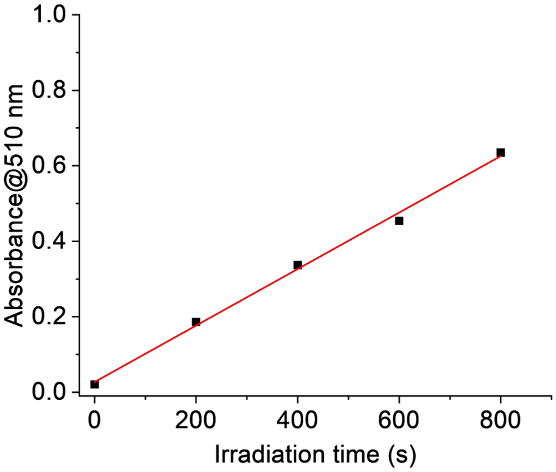

Figure S13 Absorbance of the tris-phenanthroline iron (II) complex as a function of irradiation time of potassium ferrioxalate (black squares). The red line shows a linear fit, which is used to calculate the photon flux.

8 Crystallographic data

Table S7 Crystallographic data for the *E*-isomer crystal.

	a7 (*A*-type)	**b7 (*S*-type)**	**c7 (*S*-type)**	**c7 (*A*-type)**	**d7 (*S*-type)**	**d7 (*A*-type)**	**e7 (*S*-type)**	**e7 (*A*-type)**
Space group	$P2_12_12_1$ (#19)	$P2_1/c$ (#14)	$P2_1/c$ (#14)	$P2_1/n$ (#14)	$P2_1/c$ (#14)	$P2_1/c$ (#14)	$P2_1$ (#4)	$P2_1/n$ (#14)
a / Å	4.88890(10)	11.0009(9)	10.8189(8)	11.2171(9)	12.1158(7)	27.00(2)	14.3138(8)	11.0325(4)
b / Å	12.1565(3)	6.1674(7)	6.0464(5)	4.8288(3)	5.2152(3)	4.853(2)	4.9630(3)	4.8266(2)
c / Å	29.4745(7)	33.376(3)	33.609(2)	38.442(3)	33.911(3)	15.832(10)	14.9598(9)	39.7434(11)
α / deg								
β / deg		98.601(9)	98.370(7)	92.782(8)	93.589(6)	96.16(8)	90.559(5)	92.711(3)
γ / deg								
V / Å^3	1751.73(7)	2239.0(4)	2175.1(3)	2079.8(3)	2138.5(2)	2062(2)	1062.68(11)	2113.95(13)
D_calc / g cm^{-3}	1.238	1.135	1.174	1.228	1.238	1.283	1.245	1.252
Z	4	4	4	4	4	4	2	4
T / K	93(2)	100(2)	100(2)	100(2)	100(2)	100(2)	100(2)	93(2)
R	0.0313	0.1867	0.1449	0.1579	0.1288	0.2653	0.1045	0.0572
R_w	0.0809	0.5497	0.4199	0.4341	0.3701	0.6375	0.3139	0.1645
R_int	0.0369	0.1019	0.0793	0.1255	0.0785	0.219	0.0609	0.0541
θ_max	72.476	72.065	70.737	71.928	67.53	70.826	72.079	72.531
μ (Cu-Kα) / mm^{-1}	0.632	0.561	0.615	0.644	0.684	0.704	0.673	0.691
Reflections measured	17421	10265	8960	19328	20657	11390	8771	18530
Reflections unique	3429	4258	4054	4144	4172	4033	3348	4131
CCSD number	2286121	2431296	2431297	2431298	2431299	2431295	2431293	2431300

Table S8 Crystallographic data for the *Z*-isomer crystal.

	a7	**b7**	**c7**	**d7**	**e7**
Space group	$P2_1/n$ (#14)	P-1 (#2)	$P2_1/c$ (#14)	P-1 (#2)	$P2_12_12_1$ (#19)
a / Å	12.7940(5)	8.1719(2)	18.5994(9)	8.2378(4)	8.1133(2)
b / Å	8.3129(3)	18.6119(4)	13.5295(6)	13.9123(4)	13.2489(3)
c / Å	33.0603(12)	28.8584(9)	8.1978(4)	18.4427(6)	40.4914(13)
α / deg		95.236(2)		87.269(2)	
β / deg	98.150(3)	90.111(2)	94.826(4)	81.750(3)	
γ / deg		96.1650(18)		88.914(3)	
V / Å^3	3480.6(2)	4345.3(2)	2055.59(17)	2089.25(14)	4352.5(2)
D_{calc} / g cm^{-3}	1.246	1.169	1.242	1.267	1.216
Z	8	8	4	4	8
T / K	93(2)	100(2)	100(2)	100(2)	100(2)
R	0.1332	0.1095	0.0642	0.0581	0.1315
R_{w}	0.3865	0.3673	0.1948	0.1712	0.3548
R_{int}	0.0696	0.0638	0.0422	0.0523	0.1623
θ_{max}	72.099	72.46	72.195	72.319	71.235
μ (Cu-Kα) / mm^{-1}	0.636	0.58	0.648	0.692	0.671
Reflections measured	19963	46790	10300	23125	50190
Reflections unique	6772	16558	3963	8010	8344
CCSD number	2286117	2431302	2431294	2431301	2431303

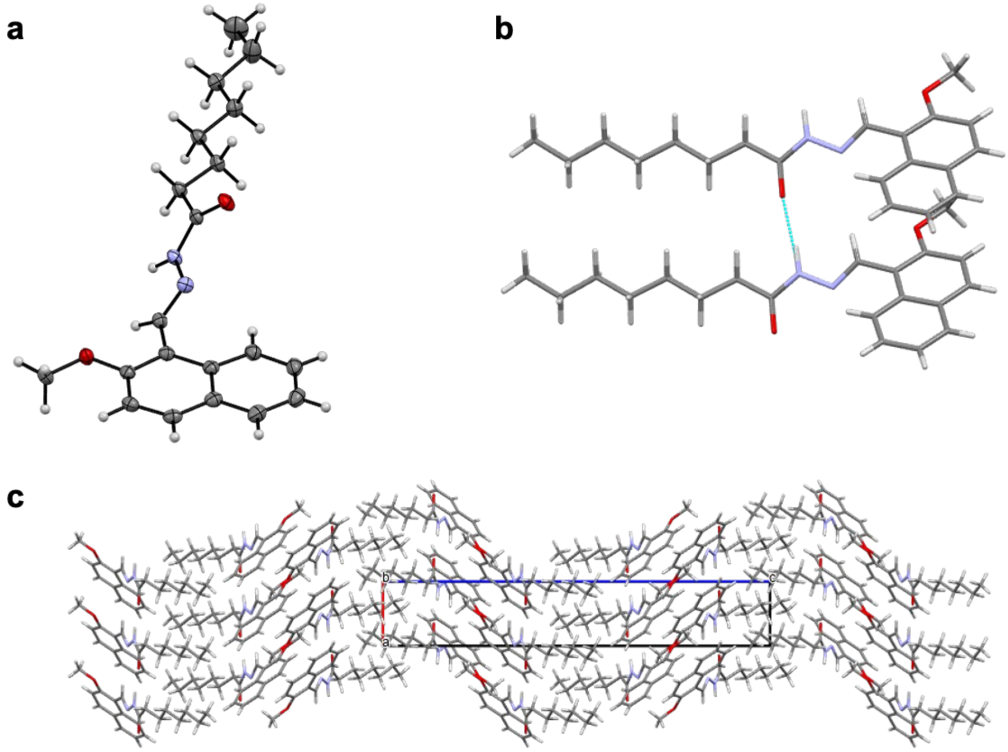

Figure S14 (a) Oak Ridge thermal ellipsoid plot (ORTEP) view of *E* isomer of **a7** (*A*-type) (50% probability level). (b) Short contact with an adjacent molecule. (c) The crystal structure of *E* isomer of **a7** (*A*-type) along with *b* axis.

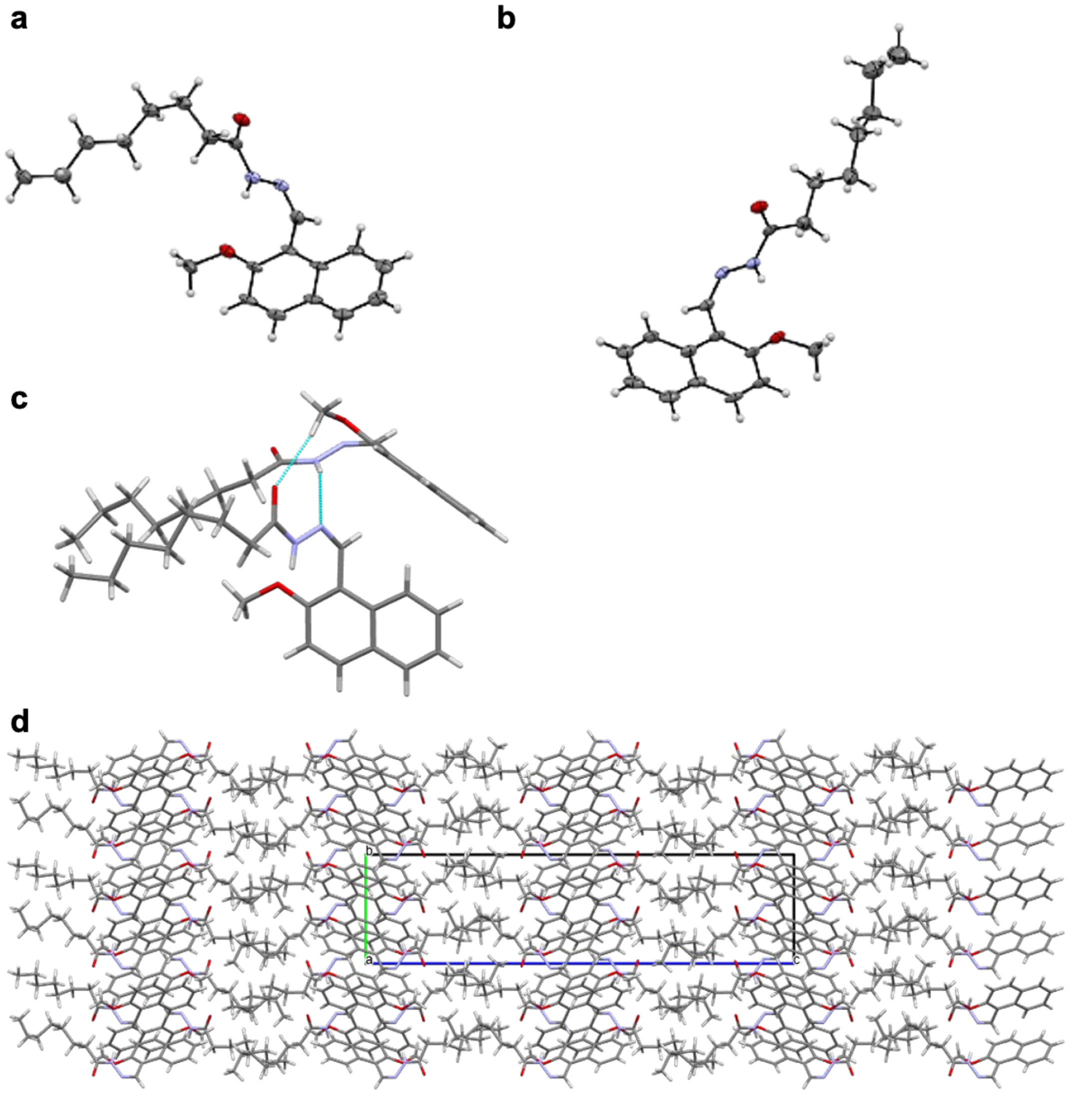

Figure S15 (a, b) ORTEP views of two asymmetric units for *Z* isomer of **a7** (50% probability level). (c) Short contact with an adjacent molecule. (d) The crystal structure of *Z* isomer of **a7** along with *a* axis.

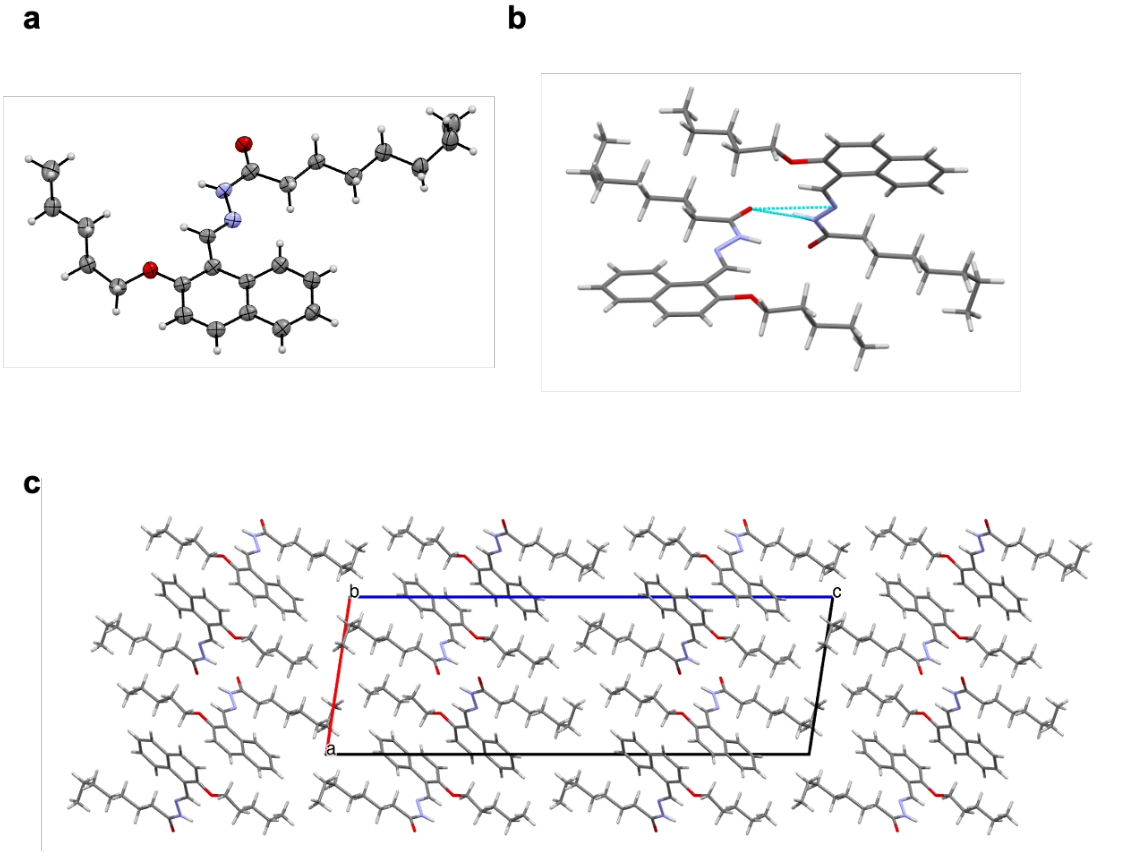

Figure S16 (a) ORTEP view of *E* isomer of **b7** (*S*-type) (50% probability level). (b) Short contact with an adjacent molecule. (c) The crystal structure of *E* isomer of **b7** (*S*-type) along with *b* axis.

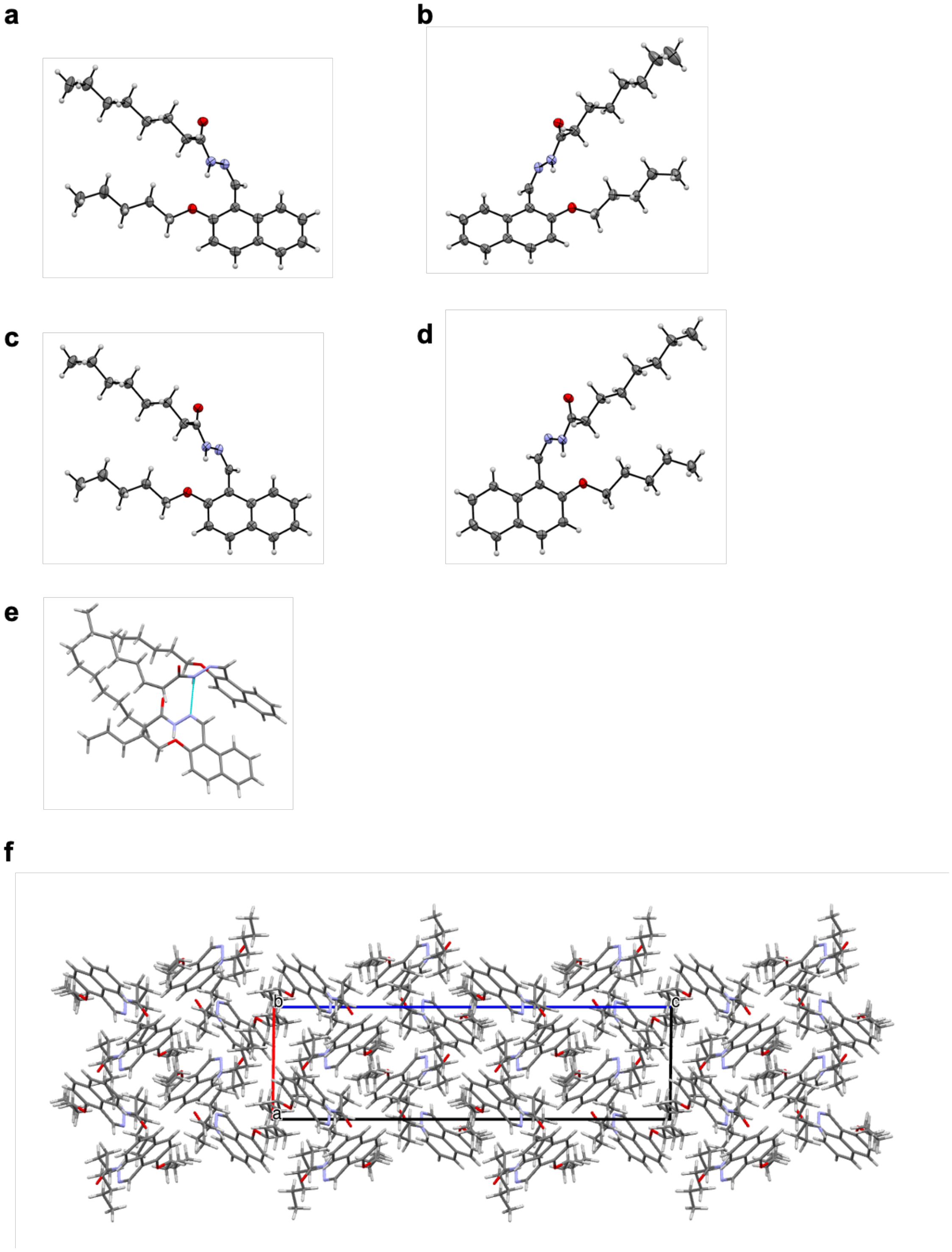

Figure S17 (a, b, c, d) ORTEP views of four asymmetric units for *Z* isomer of **b7** (50% probability level). (e) Short contact with an adjacent molecule. (f) The crystal structure of *Z* isomer of **b7** along with *b* axis.

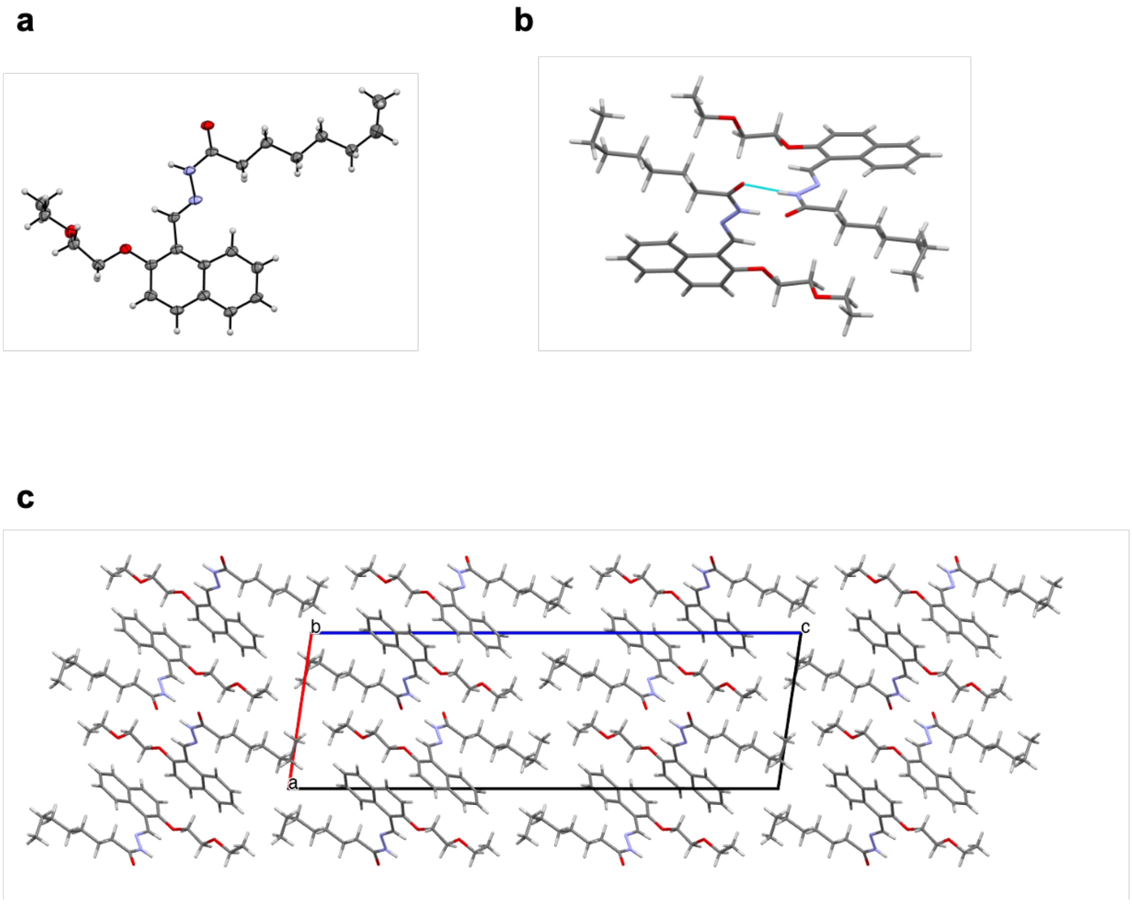

Figure S18 (a) ORTEP view of *E* isomer of **c7** (*S*-type) (50% probability level). (b) Short contact with an adjacent molecule. (c) The crystal structure of *E* isomer of **c7** (*S*-type) along with *b* axis.

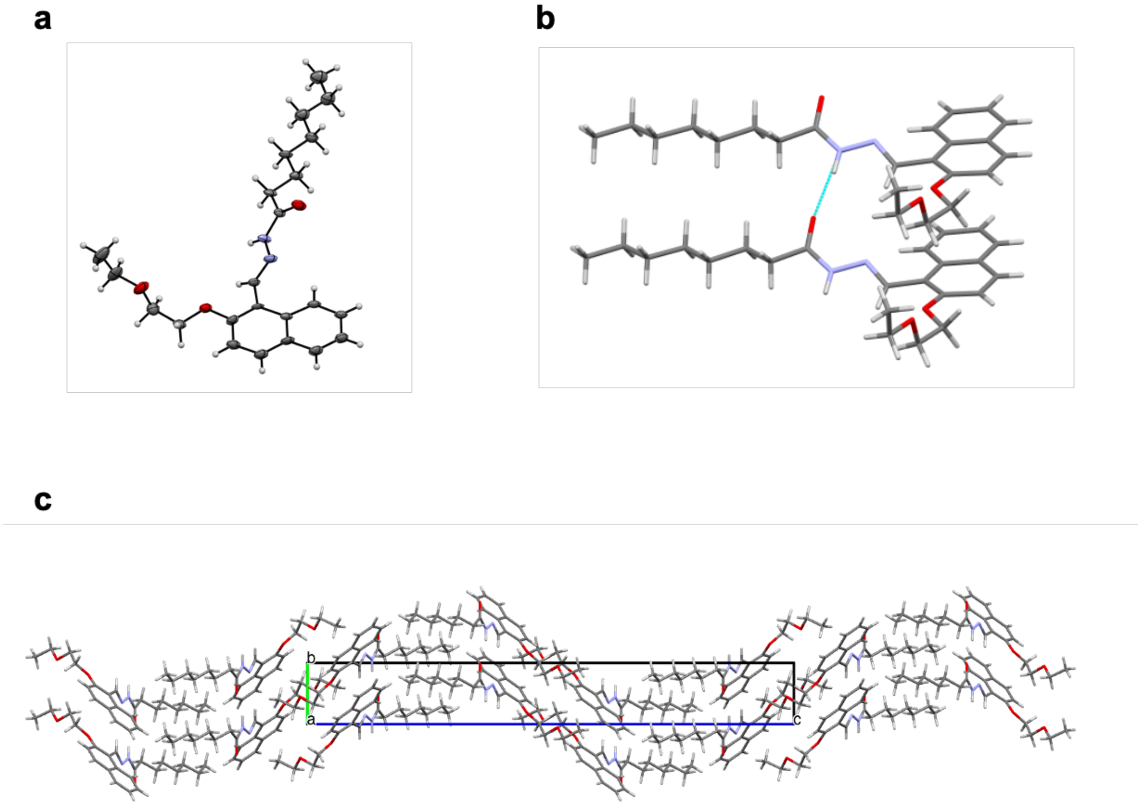

Figure S19 (a) ORTEP view of *E* isomer of **c7** (*A*-type) (50% probability level). (b) Short contact with an adjacent molecule. (c) The crystal structure of *E* isomer of **c7** (*A*-type) along with *a* axis.

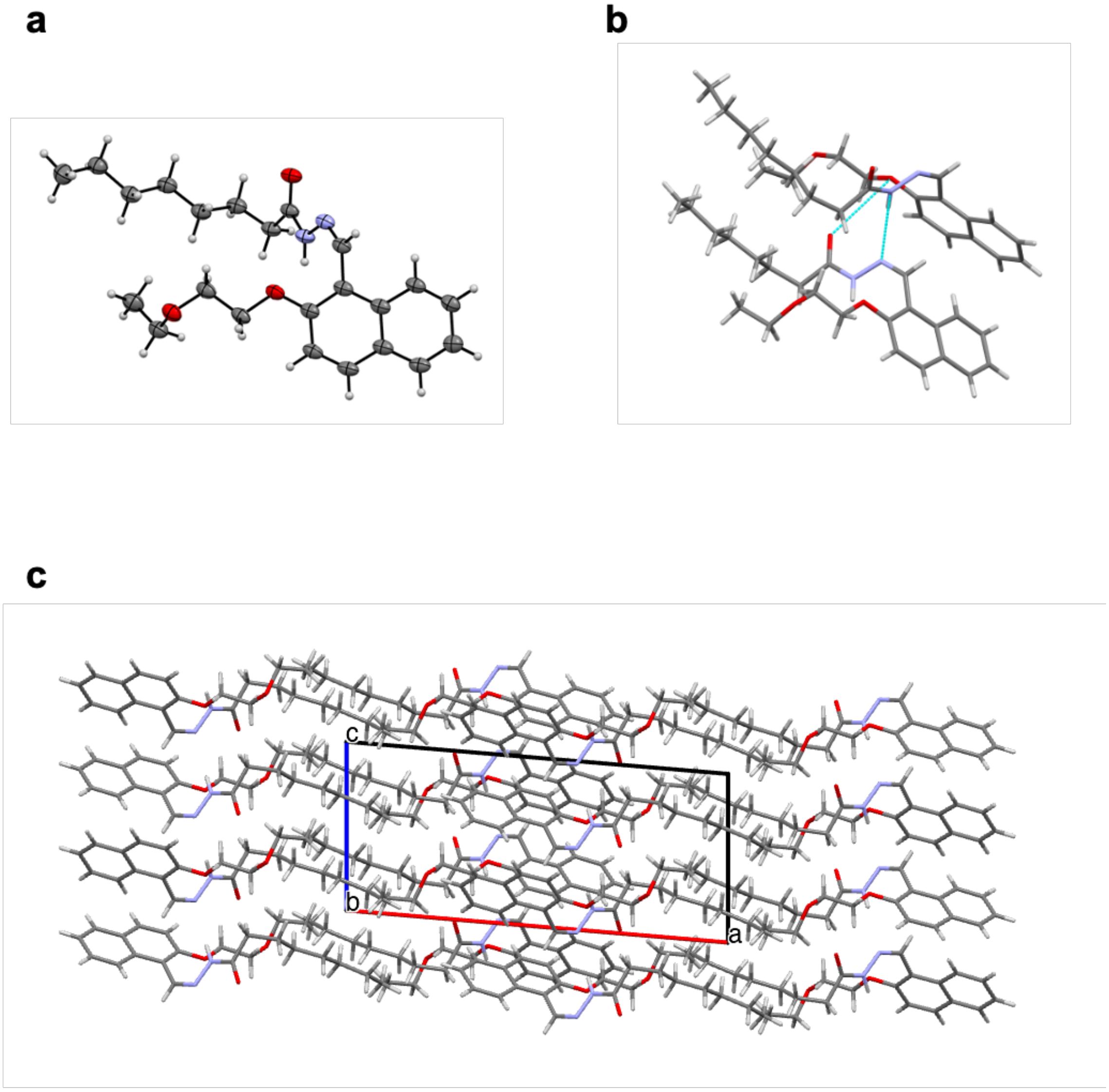

Figure S20 (a) ORTEP view of *Z* isomer of **c7** (50% probability level). (b) Short contact with an adjacent molecule. (c) The crystal structure of *Z* isomer of **c7** along with *b* axis.

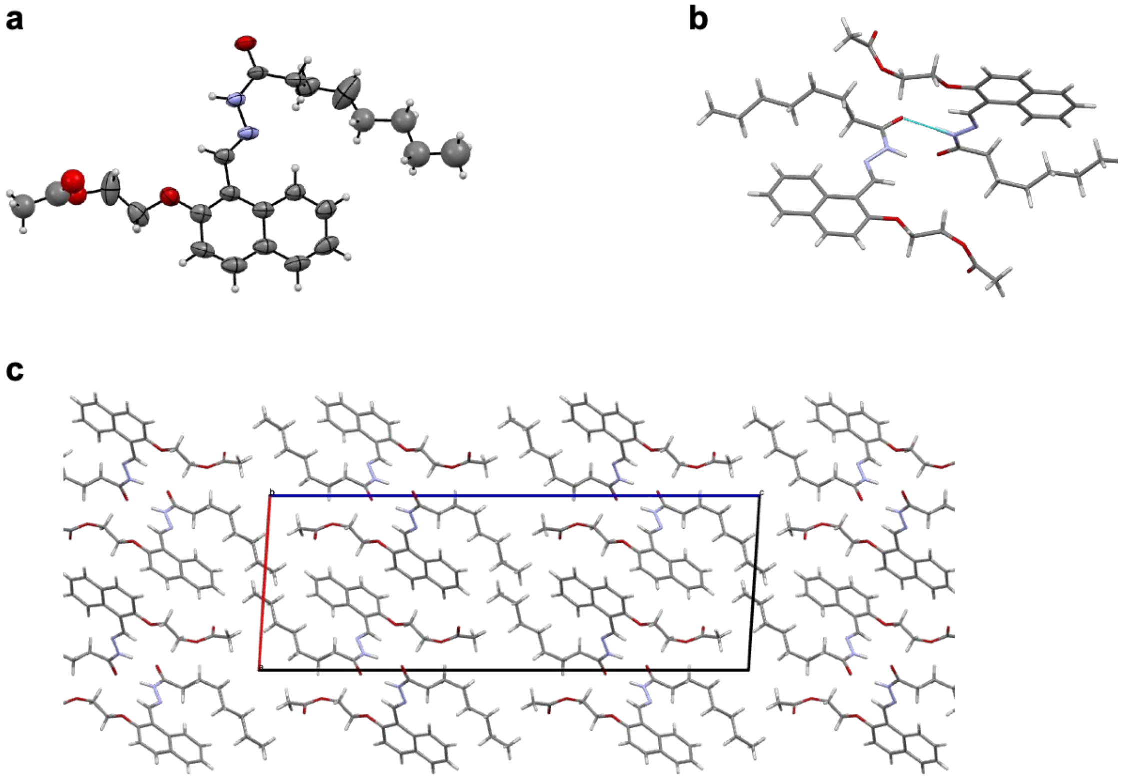

Figure S21 (a) ORTEP view of *E* isomer of **d7** (*S*-type) (50% probability level). (b) Short contact with an adjacent molecule. (c) The crystal structure of *E* isomer of **d7** (*S*-type) along with *b* axis. The disorder parts were removed for clarity.

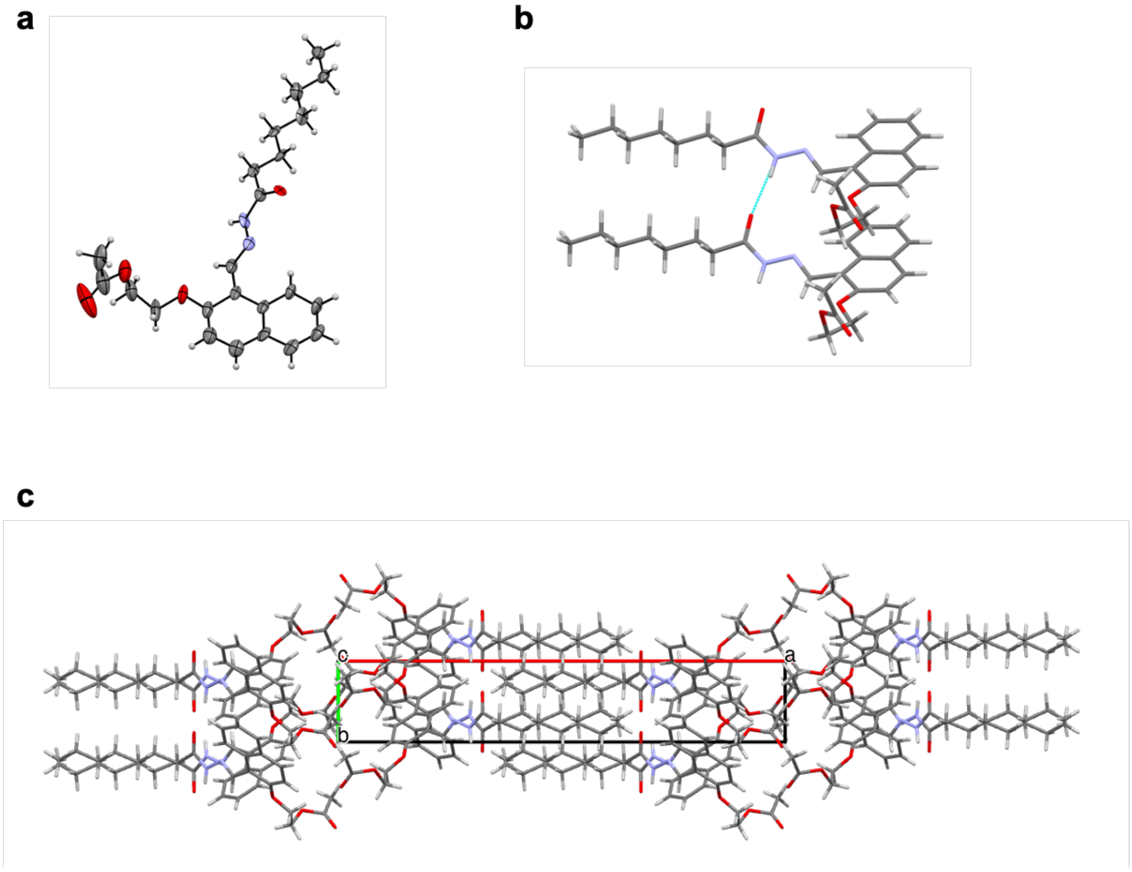

Figure S22 (a) ORTEP view of *E* isomer of **d7** (*A*-type) (50% probability level). (b) Short contact with an adjacent molecule. (c) The crystal structure of *E* isomer of **d7** (*A*-type) along with *c* axis.

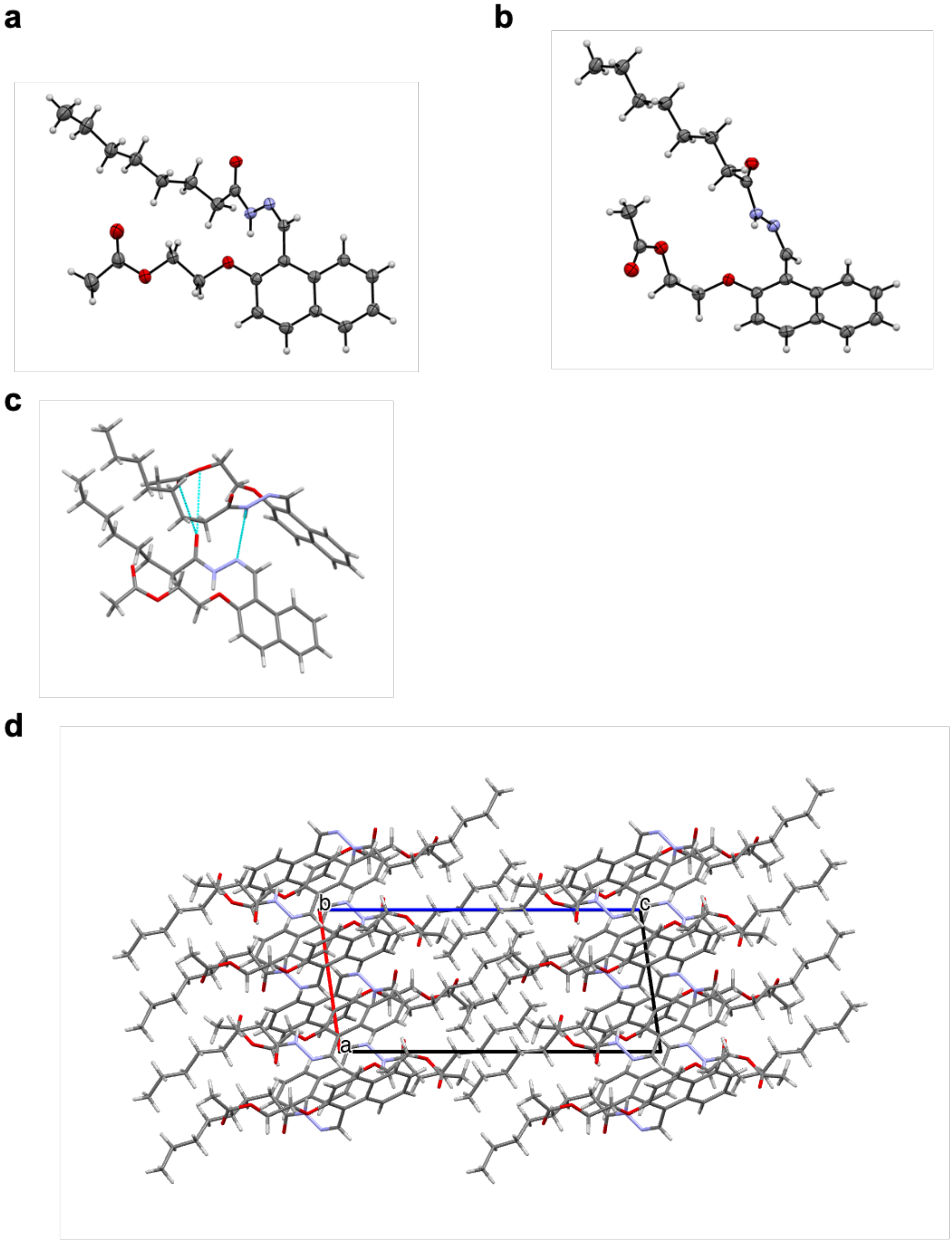

Figure S23 (a, b) ORTEP views of two asymmetric units for *Z* isomer of **d7** (50% probability level). (c) Short contact with an adjacent molecule. (d) The crystal structure of *Z* isomer of **d7** along with *b* axis.

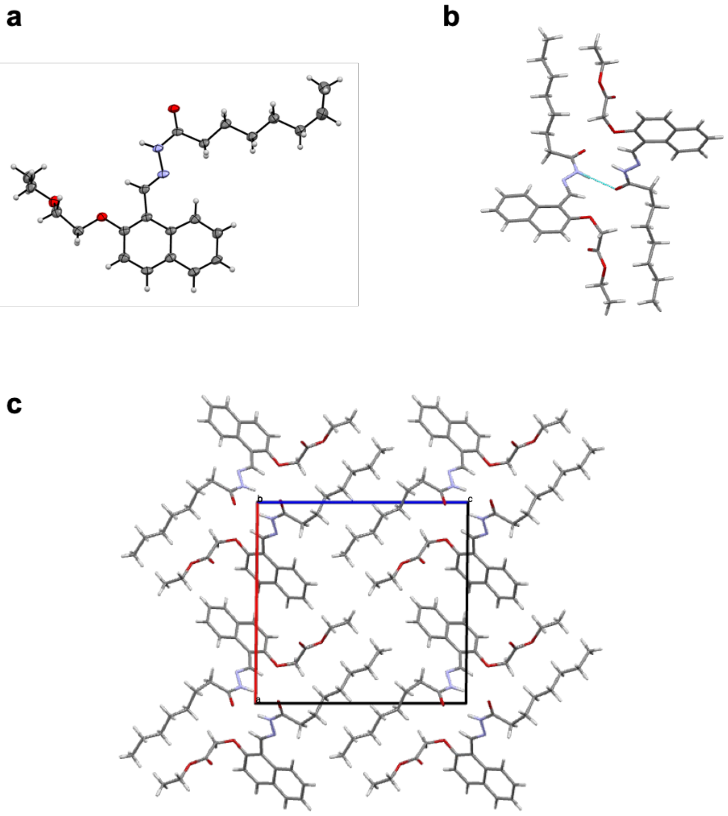

Figure S24 (a) ORTEP view of *E* isomer of **e7** (*S*-type) (50% probability level). (b) Short contact with an adjacent molecule. (c) The crystal structure of *E* isomer of **e7** (*S*-type) along with *b* axis. The disorder parts were removed for clarity.

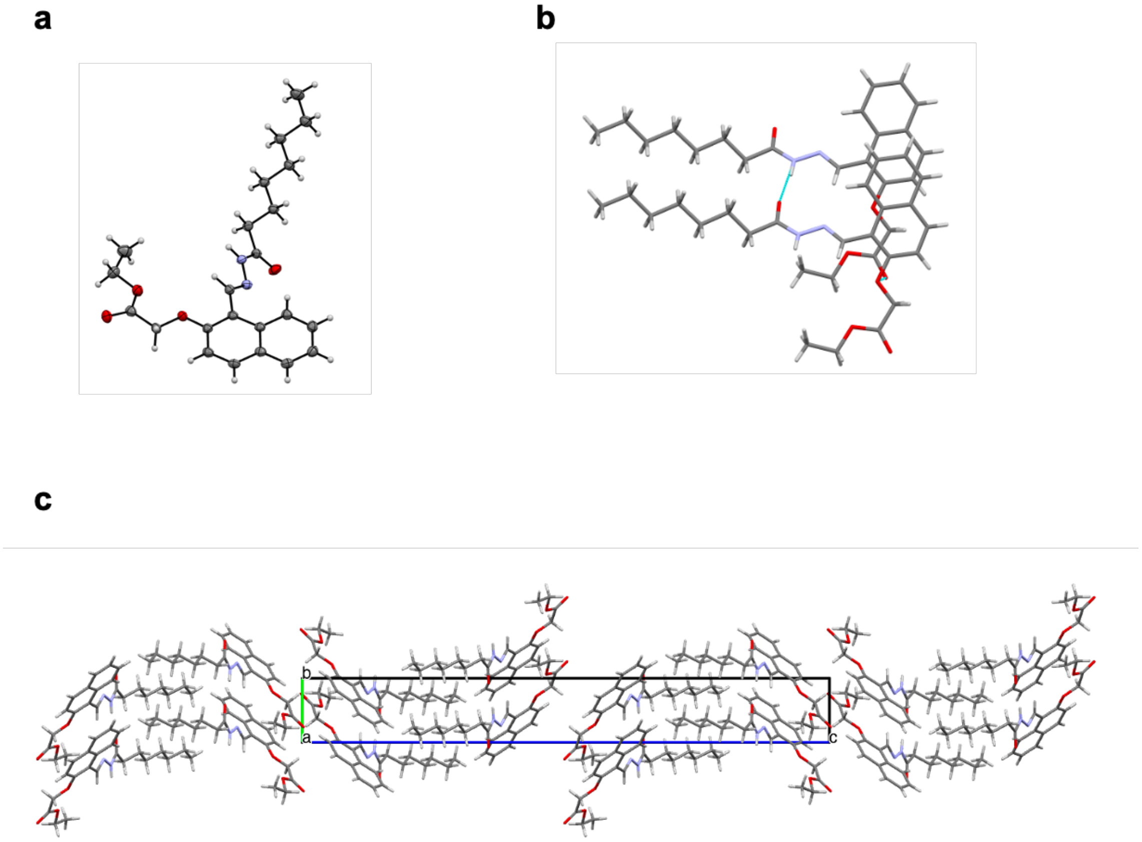

Figure S25 (a) ORTEP view of *E* isomer of **e7** (*A*-type) (50% probability level). (b) Short contact with an adjacent molecule. (c) The crystal structure of *E* isomer of **e7** (*A*-type) along with *a* axis.

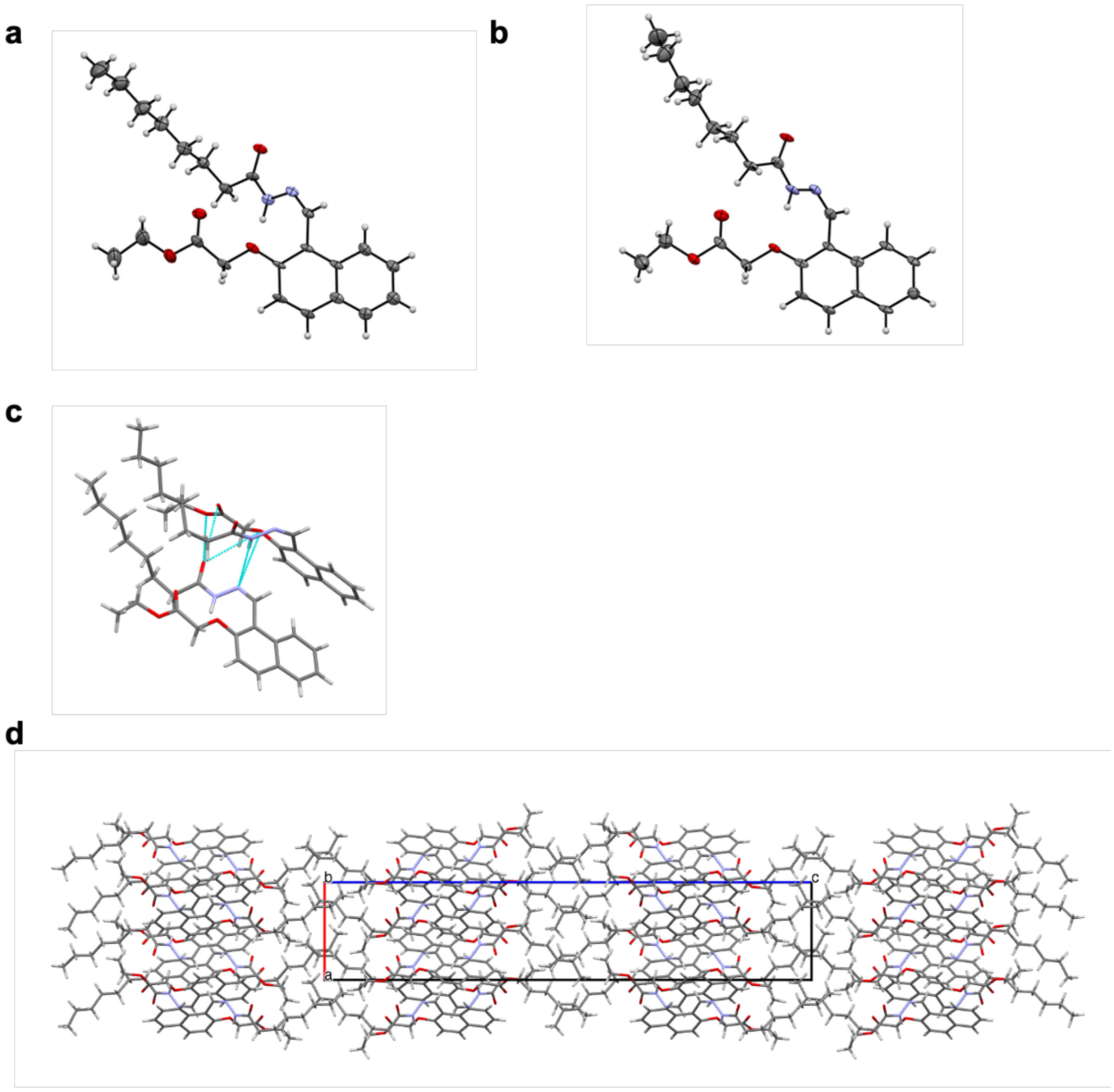

Figure S26 (a, b) ORTEP views of two asymmetric units for *Z* isomer of **e7** (50% probability level). (c) Short contact with an adjacent molecule. (d) The crystal structure of *Z* isomer of **e7** along with *b* axis.

9 Thermal analysis

9.1 Preparation of crystalline film for the microscopic observations

The crystalline films used for microscopic observations were prepared by placing 0.01 mmol of the *E* isomer onto a cover glass, melting it by heating, and then sandwiching it between another glass slide to form a crystalline film.

9.2 Preparation of eutectic mixture for DSC measurement

The *E*/*Z* binary mixture was prepared by mixing crystalline *E* and *Z* isomers at a specific ratio, heating them on a hot stage to the melting point of the *E* isomer, maintaining the molten state for a few seconds to ensure mixing, and then cooling to room temperature to obtain the solid mixture. The collected samples were left at room temperature for 2 days to allow sufficient time for nucleation before being used for DSC measurement.

Table S9 Summary of thermal properties obtained by DSC: T_m as the onset of melting peaks observed by DSC, ΔH_m as melting enthalpy, and ΔS_m as melting entropy. The thermal properties of the *Z*-isomer sample were obtained from the first heating cycle to minimize the influence of the thermal reversion.

	E isomer						*Z* isomer		
	S-type			*A*-type					
	T_m (°C)	ΔH_m (kJ/mol)	ΔS_m (J/mol K)	T_m (°C)	ΔH_m (kJ/mol)	ΔS_m (J/mol K)	T_m (°C)	ΔH_m (kJ/mol)	ΔS_m (J/mol K)
a7	-[1]	-[1]	-[1]	137.4	38.7	94.3	111.9	33.7	87.6
b7	124.6	29.8	75.0	-[1]	-[1]	-[1]	86.8	32.9	91.3
c7	111.0	30.0	78.1	-[2]	-[2]	-[2]	73.8	31.3	93.9
d7	102.1	24.4	64.9	116.2	49.1	126.1	60.1	35.1	104.4
e7	108.1	29.6	77.7	119.9	49.4	125.6	89.2	34.2	94.4

[1] Crystal structure was not obtained.

[2] *A*-type crystal exhibited phase transition to *S*-type crystal upon heating.

Table S10 Melting enthalpies for compounds **a7**–**e7** presented in molar (kJ/mol), gravimetric (J/g), and volumetric (J/cm^3) units.

	E isomer						*Z* isomer		
	S-type			*A*-type					
	ΔH_m (kJ/mol)	ΔH_m (J/g)	ΔH_m[1] (J/cm^3)	ΔH_m (kJ/mol)	ΔH_m (J/g)	ΔH_m[1] (J/cm^3)	ΔH_m (kJ/mol)	ΔH_m (J/g)	ΔH_m[1] (J/cm^3)
a7	-[2]	-[2]	-[2]	38.7	118.6	146.8	33.7	103.3	128.7
b7	29.8	78.0	88.5	-[2]	-[2]	-[2]	32.9	85.9	100.4
c7	30.0	78.0	91.6	-[3]	-[3]	-[3]	31.3	81.4	101.1
d7	24.4	61.1	75.6	49.1	123.2	158.1	35.1	88.1	111.6
e7	29.6	74.3	92.5	49.4	123.8	155.0	34.2	85.8	104.3

[1] The density value in the X-ray data (Table S7 and S8) was used to calculate ΔH_m (J/cm^3).

[2] Crystal structure was not obtained.

[3] *A*-type crystal exhibited phase transition to *S*-type crystal upon heating.

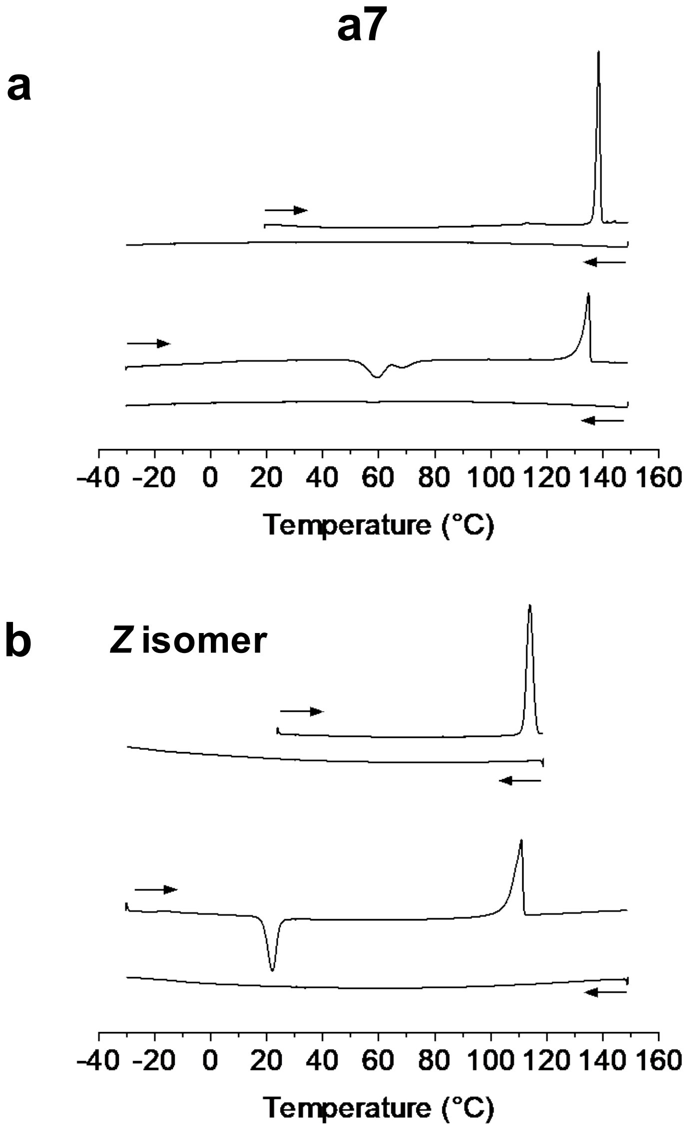

Figure S27 DSC curves (endothermic: upward) of **a7** measured at 5 °C/min: (a) the *E*-isomer crystal and (b) the *Z*-isomer crystal.

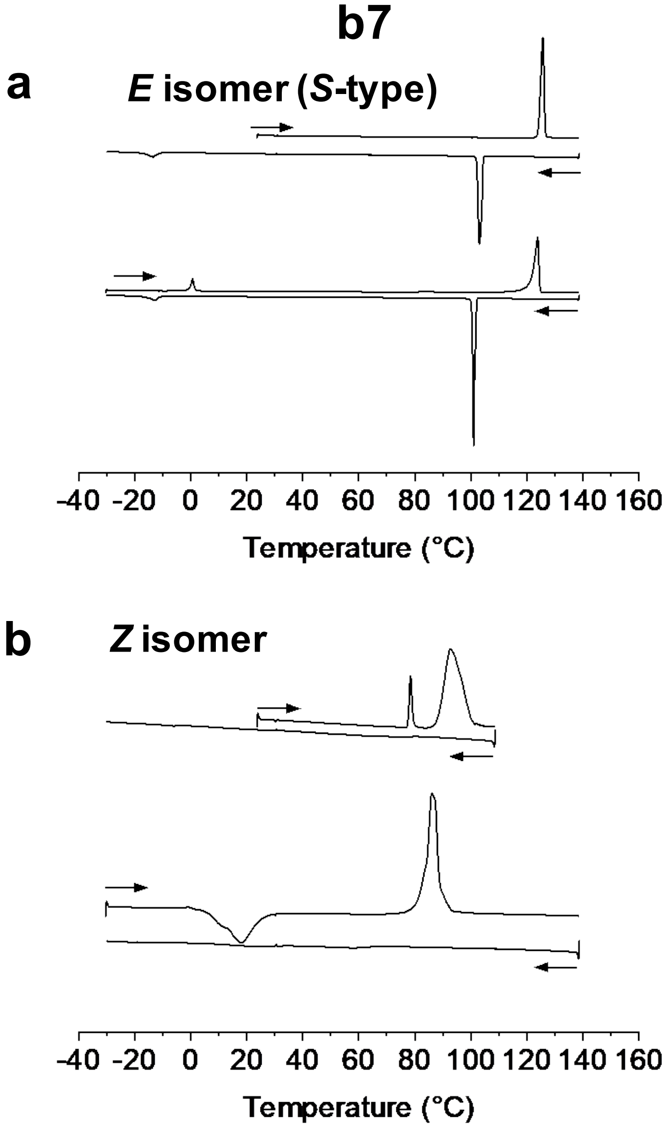

Figure S28 DSC curves (endothermic: upward) of **b7** measured at 5 °C/min: (a) the *E*-isomer crystal and (b) the *Z*-isomer crystal.

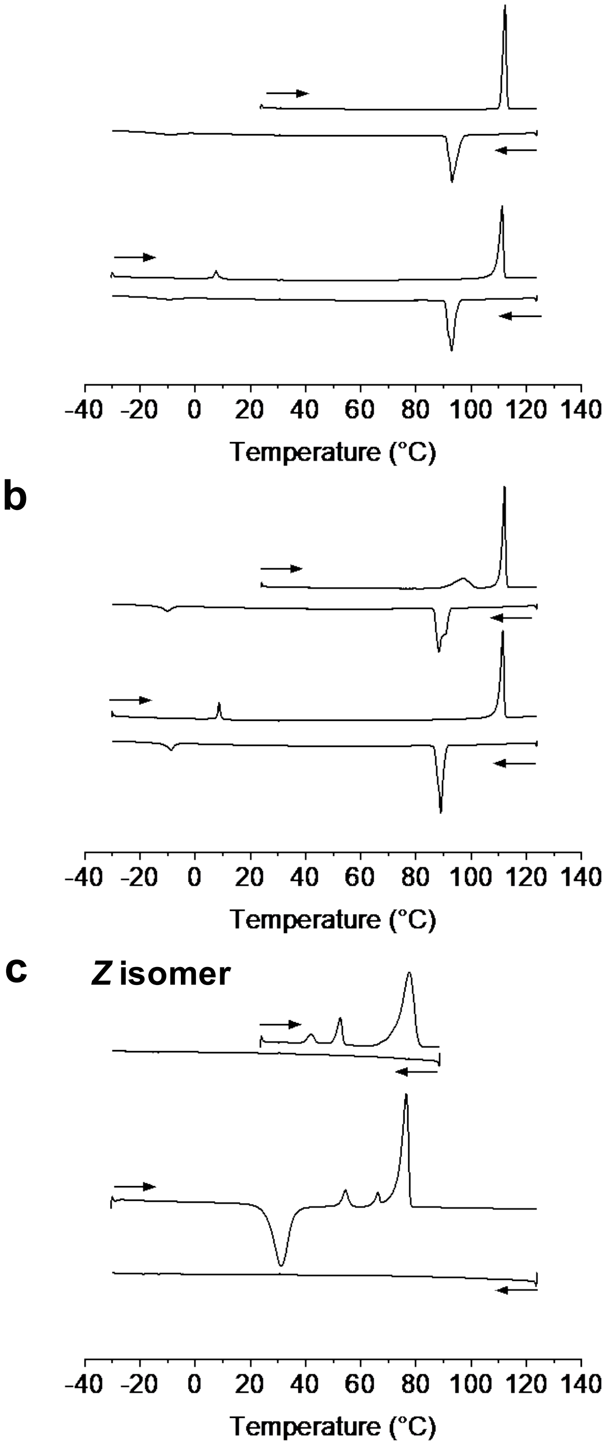

Figure S29 DSC curves (endothermic: upward) of **c7** measured at 5 °C/min: (a) the *S*-type and (b) the *A*-type conformational polymorphs of the *E*-isomer, and (c) the *Z*-isomer crystal.

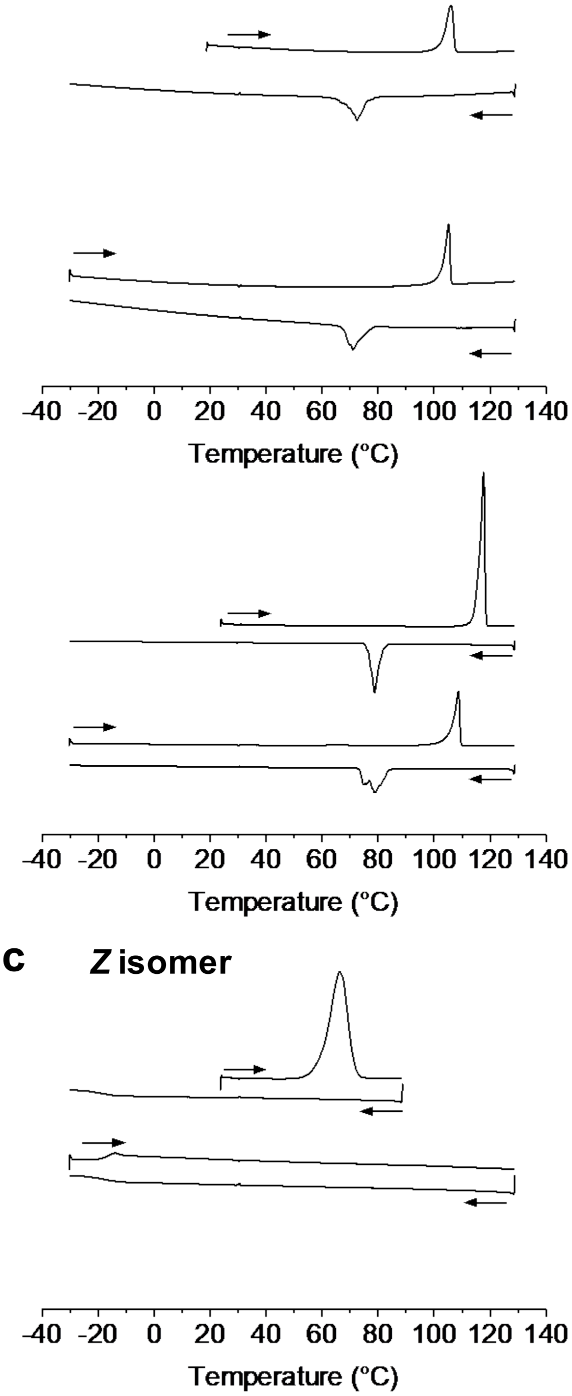

Figure S30 DSC curves (endothermic: upward) of **d7** measured at 5 °C/min: (a) the *S*-type and (b) the *A*-type conformational polymorphs of the *E*-isomer, and (c) the *Z*-isomer crystal.

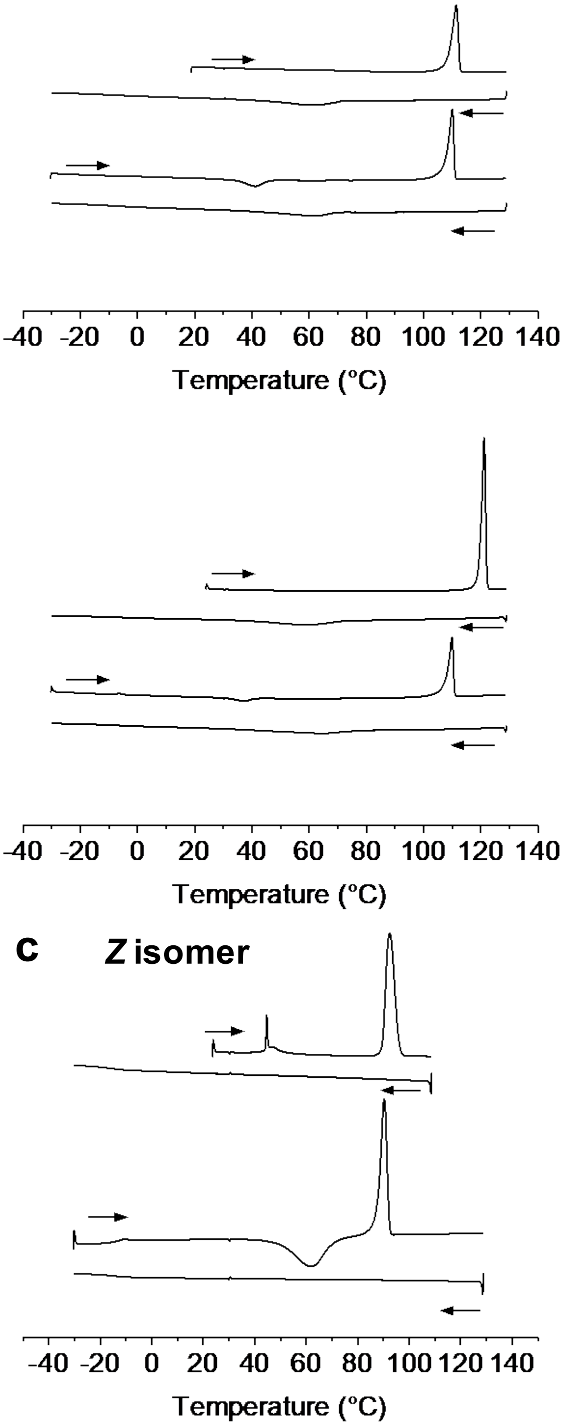

Figure S31 DSC curves (endothermic: upward) of **e7** measured at 5 °C/min: (a) the *S*-type and (b) the *A*-type conformational polymorphs of the *E*-isomer, and (c) the *Z*-isomer crystal

9.3 Le Chatelier-Schröder equation

In a binary component phase diagram, the Le Chatelier-Schröder equation can be used to theoretically calculate the melting point depression curves and the eutectic point.[14–16] The theoretical estimation of the eutectic point is determined from the intersection of the melting point depression curves of each component, calculated using the values obtained from the DSC measurements:

$$\ln(x_{\mathrm{A}}) = \frac{\Delta H_{\mathrm{f}}^{\mathrm{A}}}{R}\left(\frac{1}{T_{\mathrm{m}}^{\mathrm{A}}} - \frac{1}{T}\right)$$

$$\ln(1 - x_{\mathrm{A}}) = \frac{\Delta H_{\mathrm{f}}^{\mathrm{B}}}{R}\left(\frac{1}{T_{\mathrm{m}}^{\mathrm{B}}} - \frac{1}{T}\right)$$

where

x_{A} : molar fraction of component A in the mixture,

$\Delta H_{\mathrm{f}}^{\mathrm{A}}$: enthalpy of fusion of component A obtained by DSC measurement,

$\Delta H_{\mathrm{f}}^{\mathrm{B}}$: enthalpy of fusion of component B obtained by DSC measurement,

R : gas constant,

$T_{\mathrm{m}}^{\mathrm{A}}$: melting point of component A obtained by DSC measurement,

$T_{\mathrm{m}}^{\mathrm{B}}$: melting point of component B obtained by DSC measurement,

T : melting point of the mixture;

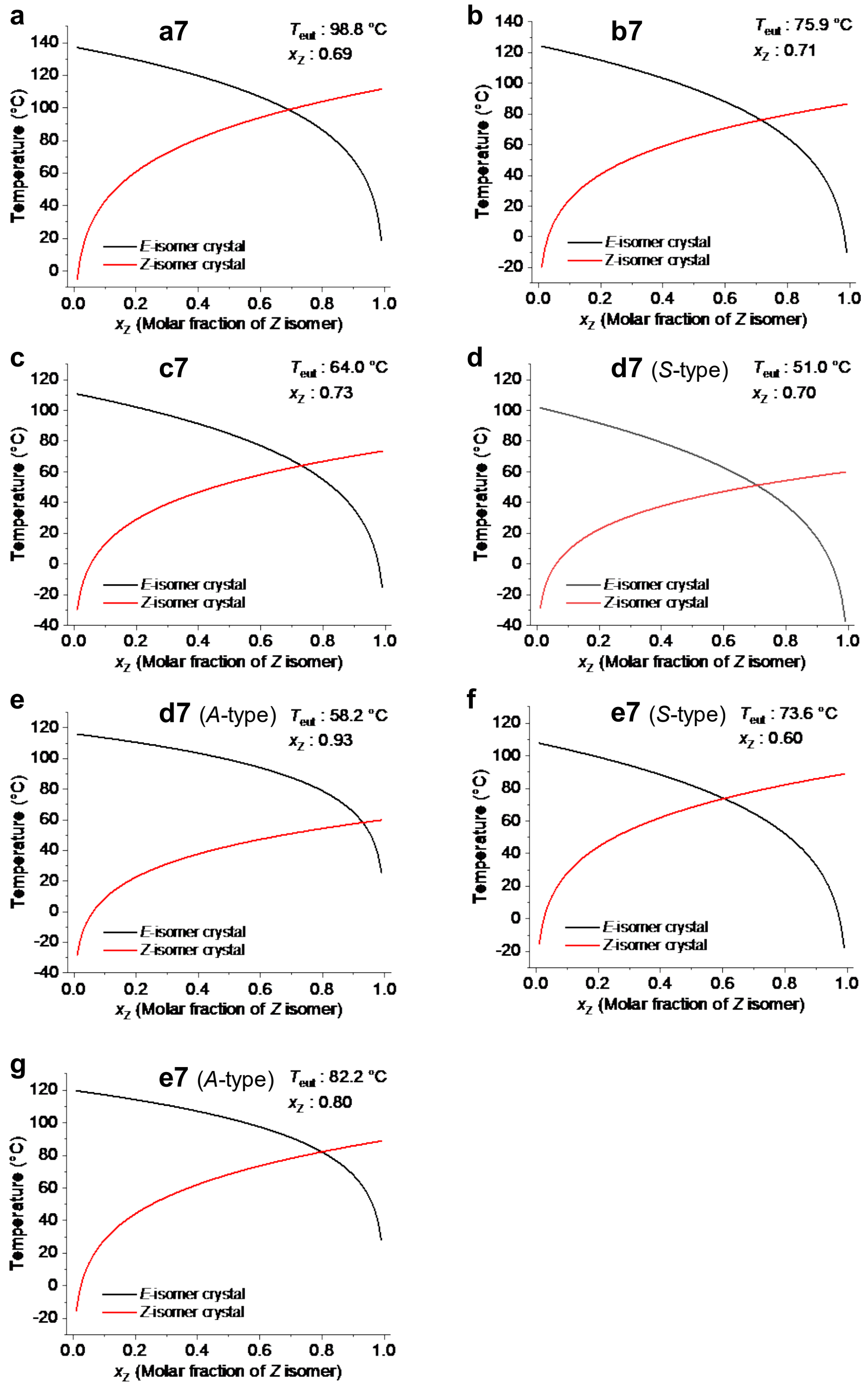

Figure S32 The melting point depression curve based on the Le Chatelier-Schröder equation, calculated from the melting points and melting enthalpies obtained by the DSC measurement of the *E*- and *Z*-isomer crystals. The curves of the individual components intersect at the eutectic point (T_{eut}), as described in the graph. The T_{eut} of **c7** was calculated using the thermal parameters of the *S*-type crystal due to the phase transition.

9.4 Thermal analysis of eutectic mixtures

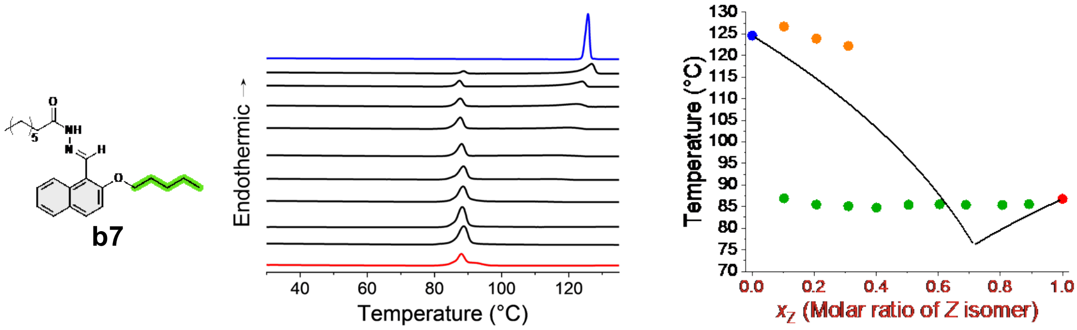

Figure S33 (a) The DSC curves of *E* and *Z* isomers of **b7** and their mixture during the first heating process. (b) Temperature–composition (*T*–*x*) phase diagram for the binary system of **b7**, where the green symbols indicate the onset temperatures of the melting of the eutectic mixture and orange symbols indicate the peak top of the melting of the pure solid. The meanings of the lines, symbols are the same as given in Figures 2(b–c).

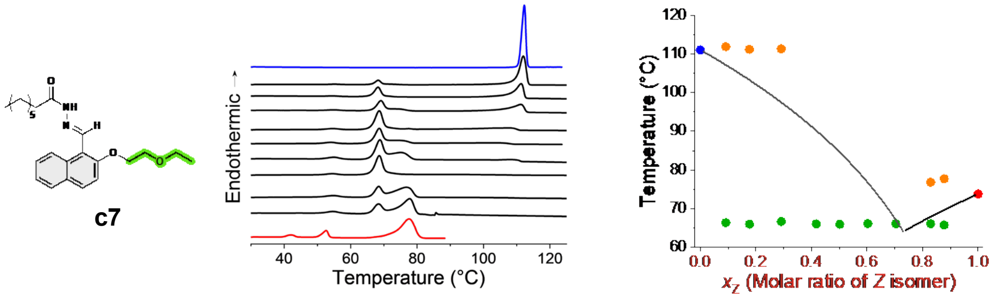

Figure S34 (a) The DSC curves of *E* and *Z* isomers of **c7** and their mixture during the first heating process. (b) Temperature–composition (*T*–*x*) phase diagram for the binary system of **c7**, where the green symbols indicate the onset temperatures of the melting of the eutectic mixture and orange symbols indicate the peak top of the melting of the pure solid. The meanings of the lines, symbols are the same as given in Figures 2(b–c).

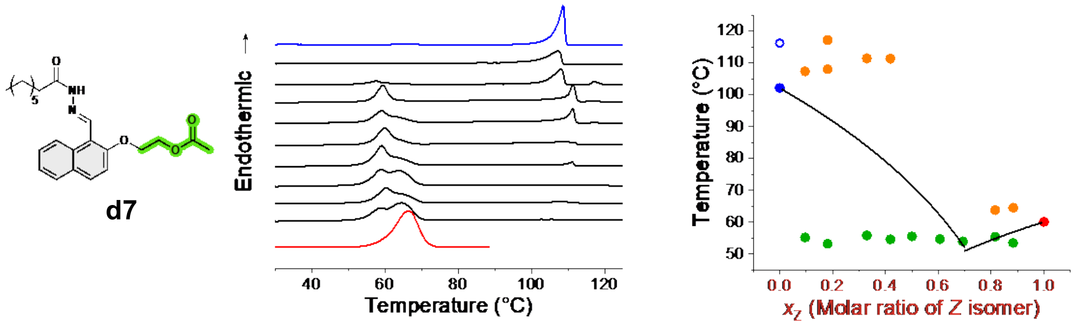

Figure S35 (a) The DSC curves of *E* and *Z* isomers of **d7** and their mixture during the first heating process. (b) Temperature–composition (*T*–*x*) phase diagram for the binary system of **d7**, where the green symbols indicate the onset temperatures of the melting of the eutectic mixture and orange symbols indicate the peak top of the melting of the pure solid. The blue filled plot represents the melting point of the *S*-type crystal, while the blue empty plot represents the melting point of the *A*-type crystal. The meanings of the lines, symbols are the same as given in Figures 2(b–c).

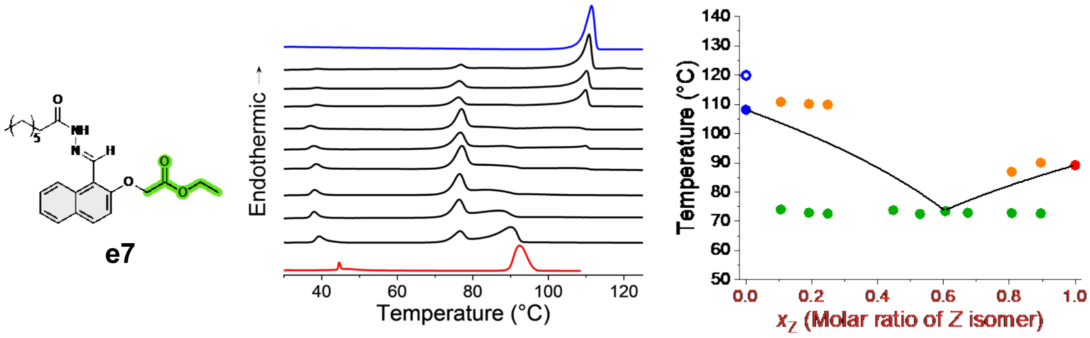

Figure S36 (a) The DSC curves of *E* and *Z* isomers of **e7** and their mixture during the first heating process. (b) Temperature–composition (*T*–*x*) phase diagram for the binary system of **e7**, where the green symbols indicate the onset temperatures of the melting of the eutectic mixture and orange symbols indicate the peak top of the melting of the pure solid. The blue filled plot represents the melting point of the *S*-type crystal, while the blue empty plot represents the melting point of the *A*-type crystal. The meanings of the lines, symbols are the same as given in Figures 2(b–c).

10 Microscopy images of PCLT

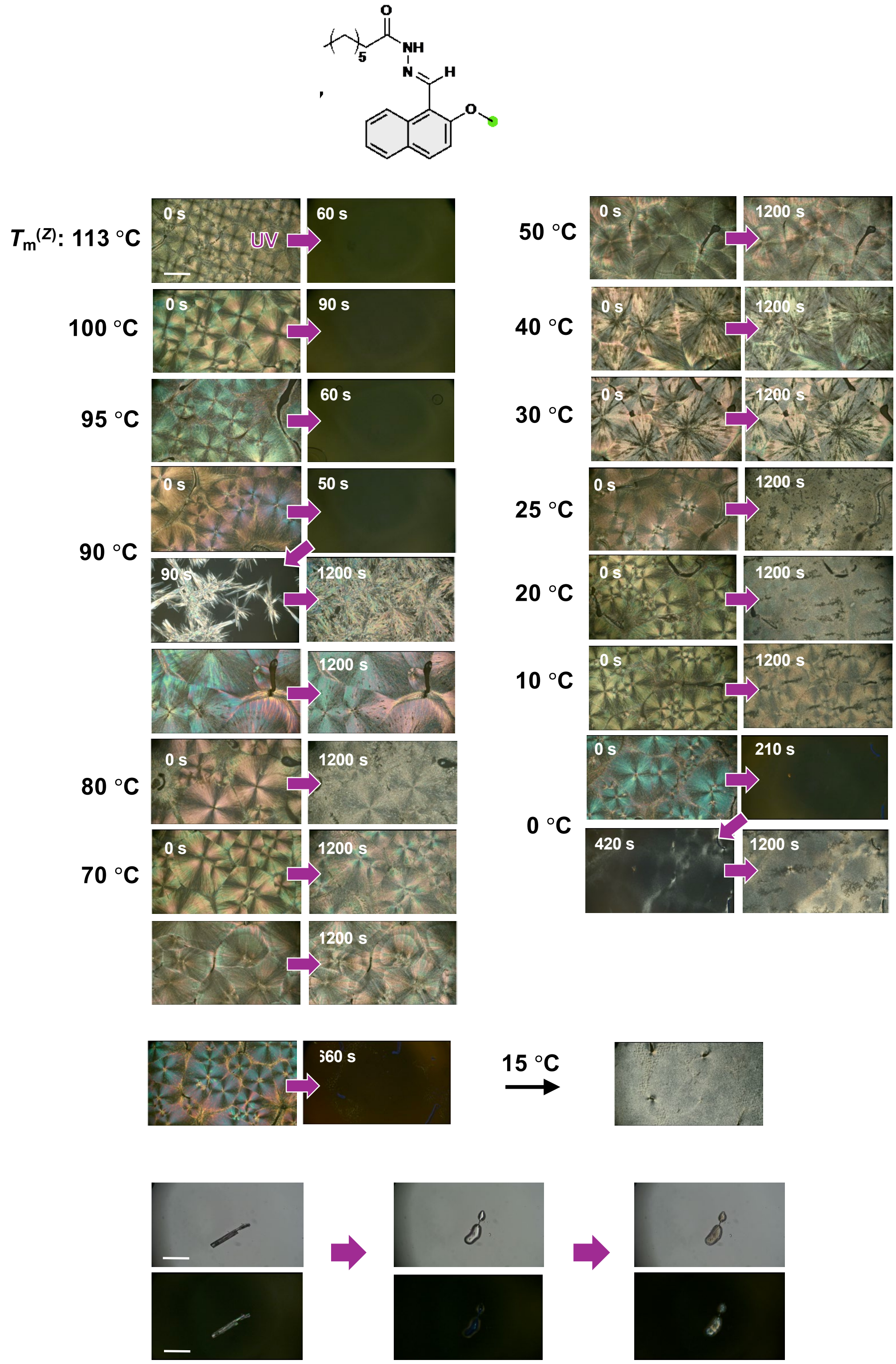

Figure S37 (a) Microscopy images of the PCLT observation for **a7** recorded under cross-Nicole condition at different temperatures. (b) Further observations of cold PCLT in bulk samples under bright-field and cross-Nicole conditions at 0 °C.

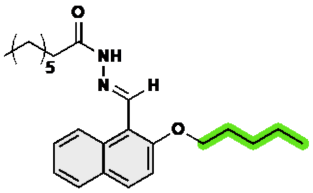

b7

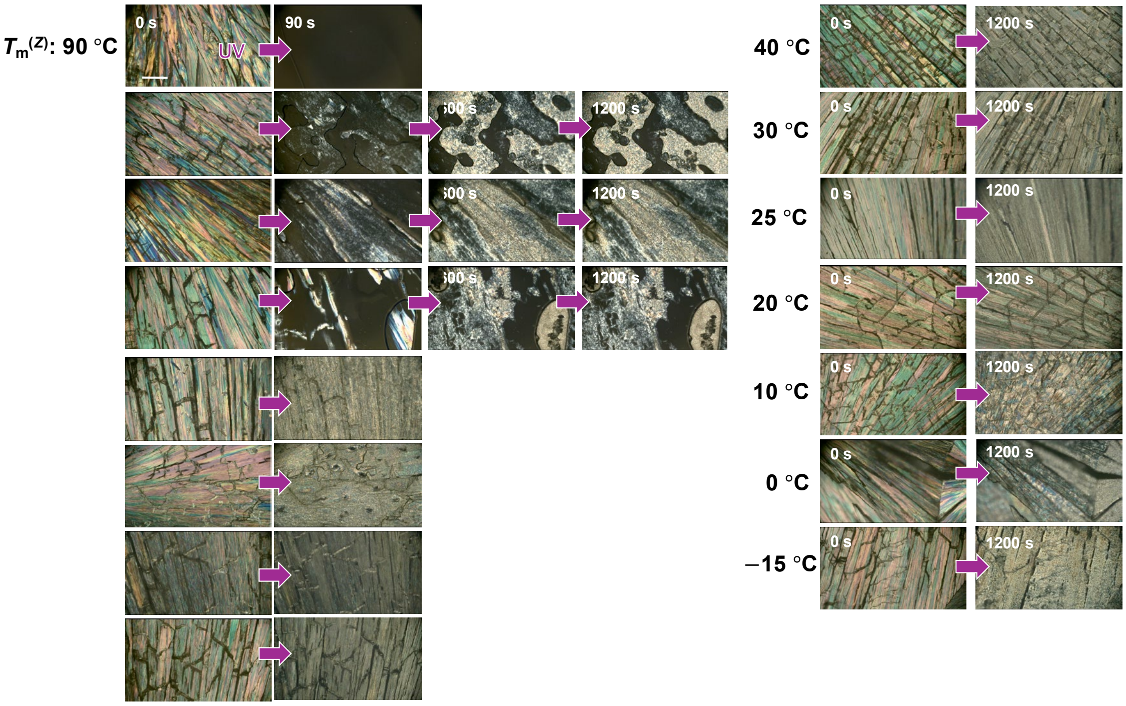

Figure S38 Microscopy images of the PCLT observation for **b7** recorded under cross-Nicole condition at different temperatures.

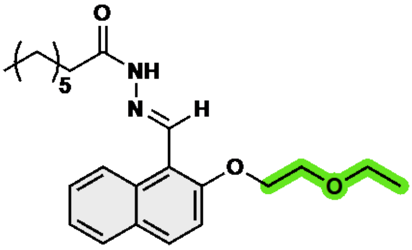

c7

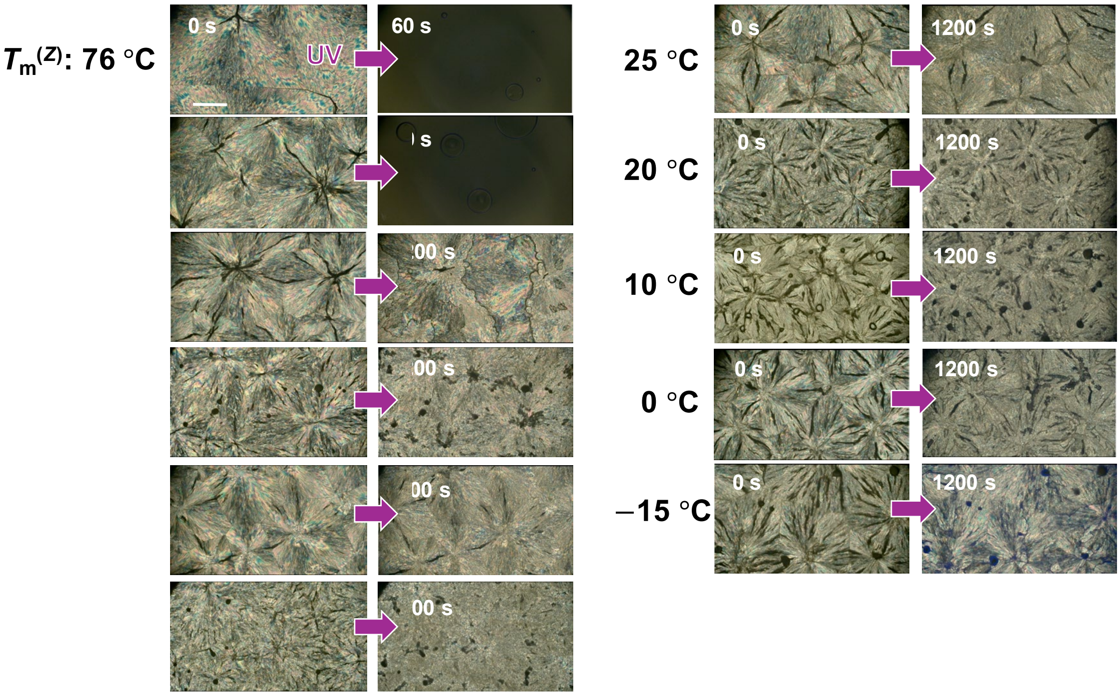

Figure S39 Microscopy images of the PCLT observation for **c7** recorded under cross-Nicole condition at different temperatures.

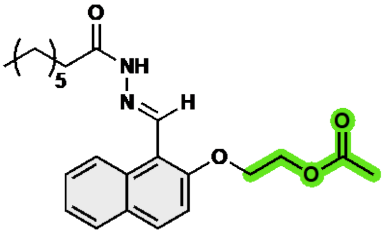

d7

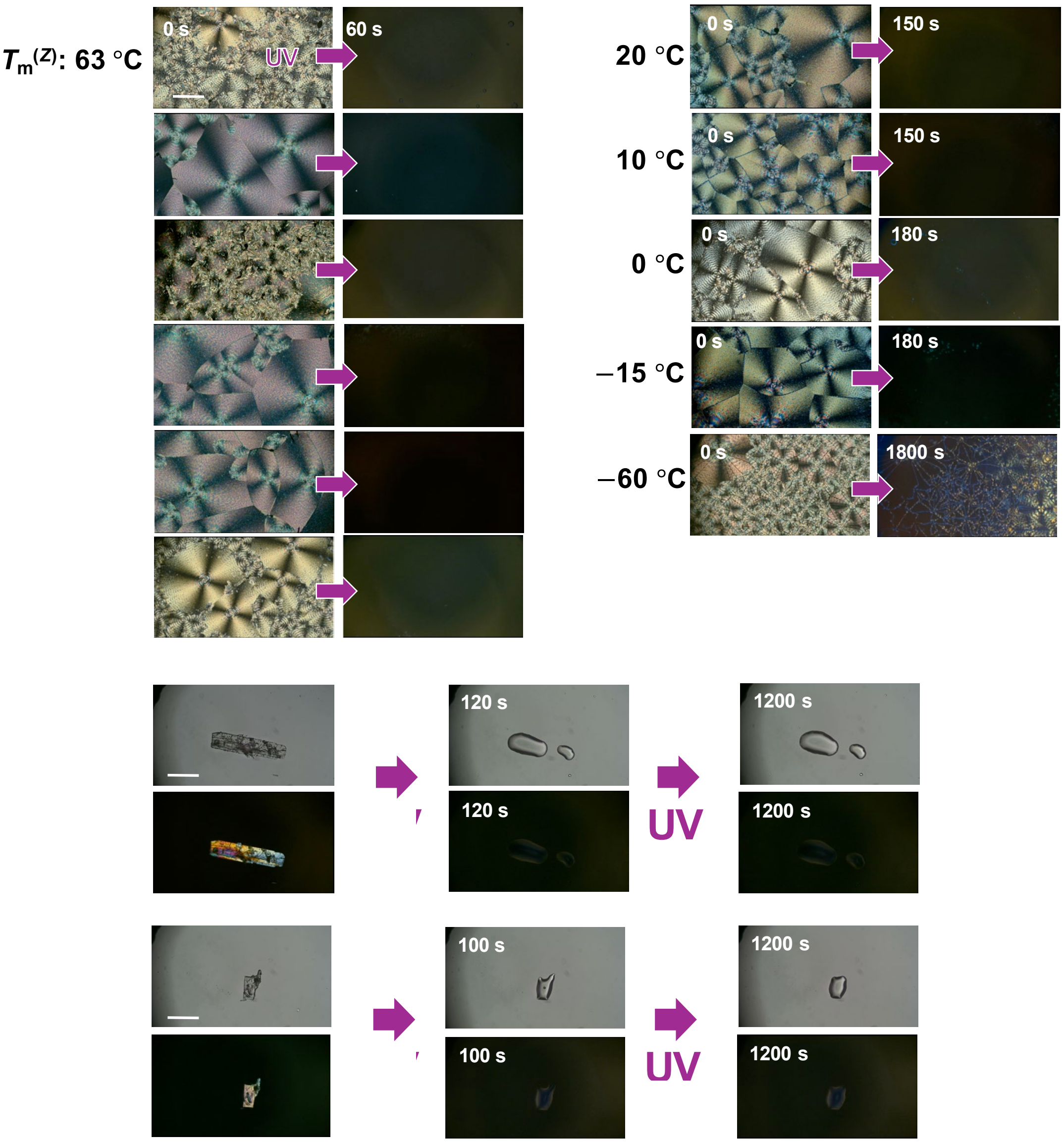

Figure S40 (a) Microscopy images of the PCLT observation for **d7** recorded under cross-Nicole condition at different temperatures. (b) Further observations of cold PCLT in bulk samples under bright-field and cross-Nicole conditions at 0 °C and 25 °C.

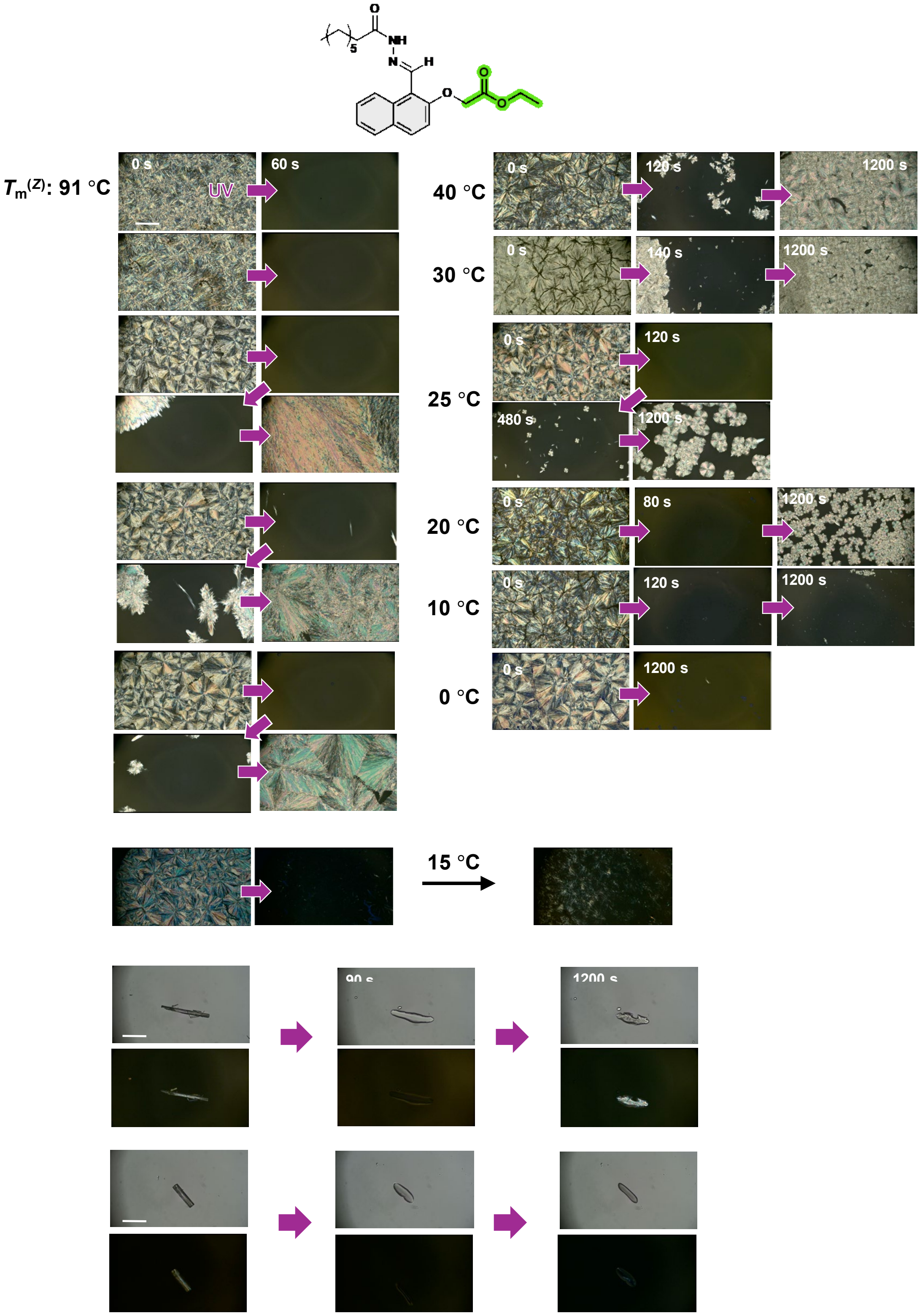

Figure S41 (a) Microscopy images of the PCLT observation for **e7** recorded under cross-Nicole condition at different temperatures. (b) Further observations of cold PCLT in bulk samples under bright-field and cross-Nicole conditions at 0 °C and 25 °C.

11 IR spectroscopy

11.1 Comparison between E and Z isomer

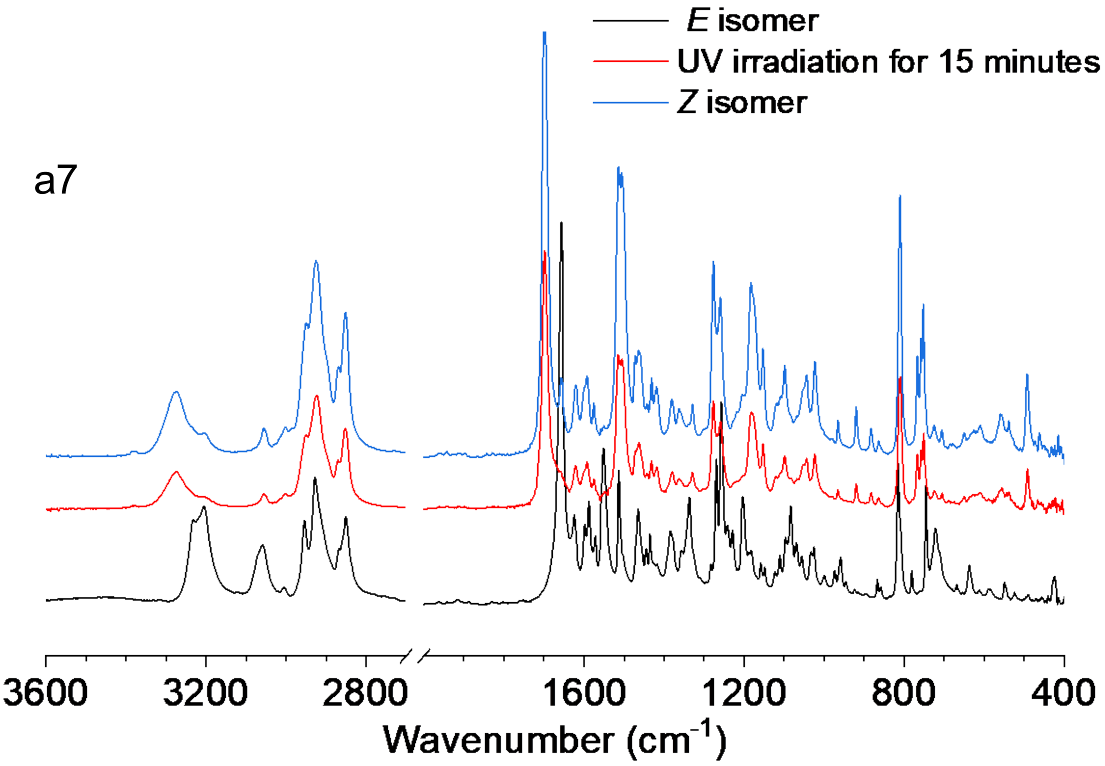

Figure S42 IR spectra of **a7**: *E*-isomer crystal (black), *Z*-isomer crystal (red), and *E*-isomer crystal irradiated with UV light for 15 minutes (blue).

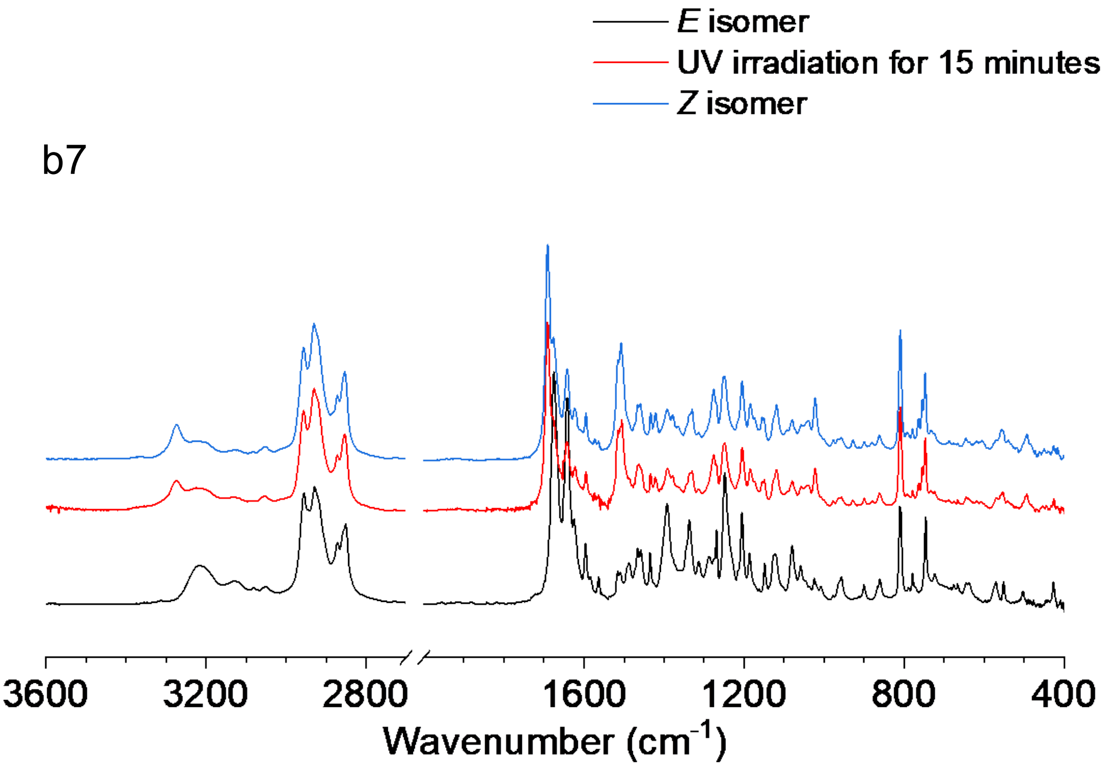

Figure S43 IR spectra of **b7**: *E*-isomer crystal (black), *Z*-isomer crystal (red), and *E*-isomer crystal irradiated with UV light for 15 minutes (blue).

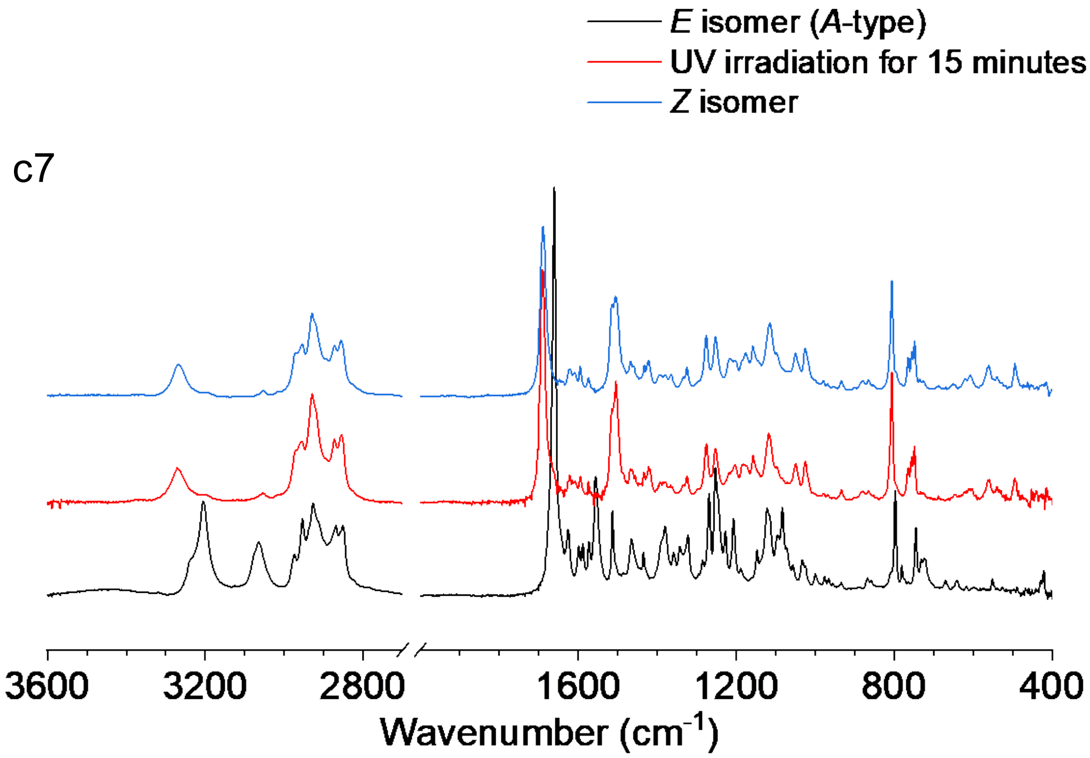

Figure S44 IR spectra of **c7** (*A*-type): *E*-isomer crystal (black), *Z*-isomer crystal (red), and *E*-isomer crystal irradiated with UV light for 15 minutes (blue).

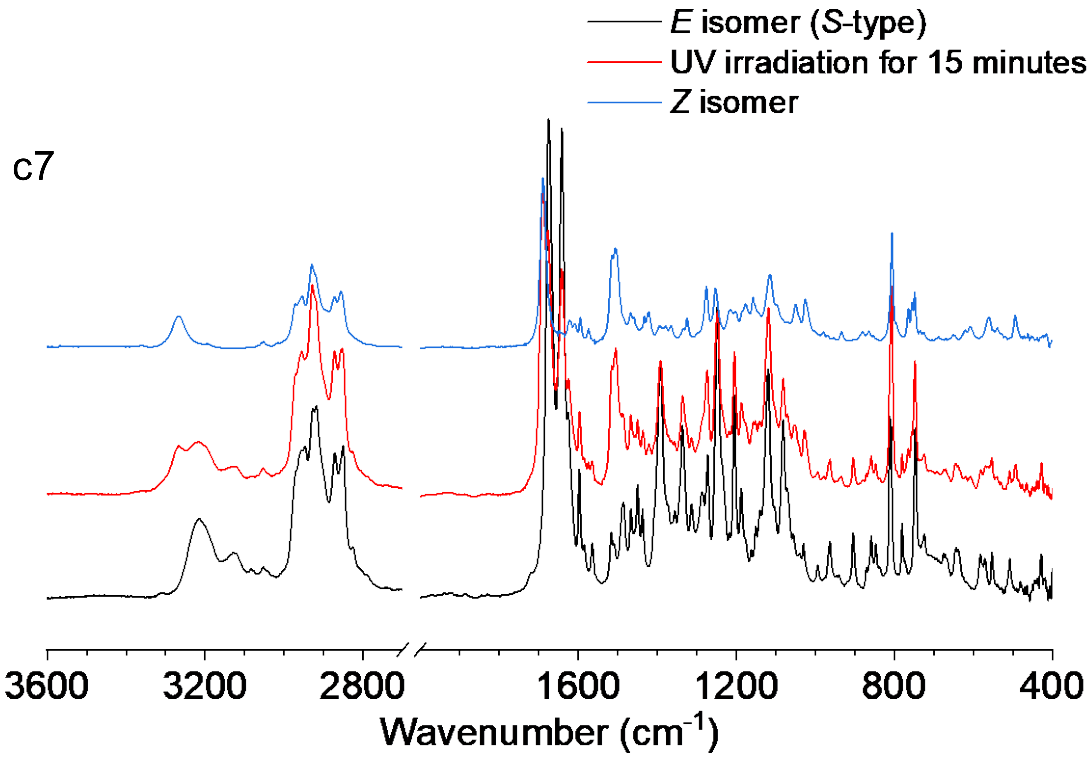

Figure S45 IR spectra of **c7** (*S*-type): *E*-isomer crystal (black), *Z*-isomer crystal (red), and *E*-isomer crystal irradiated with UV light for 15 minutes (blue).

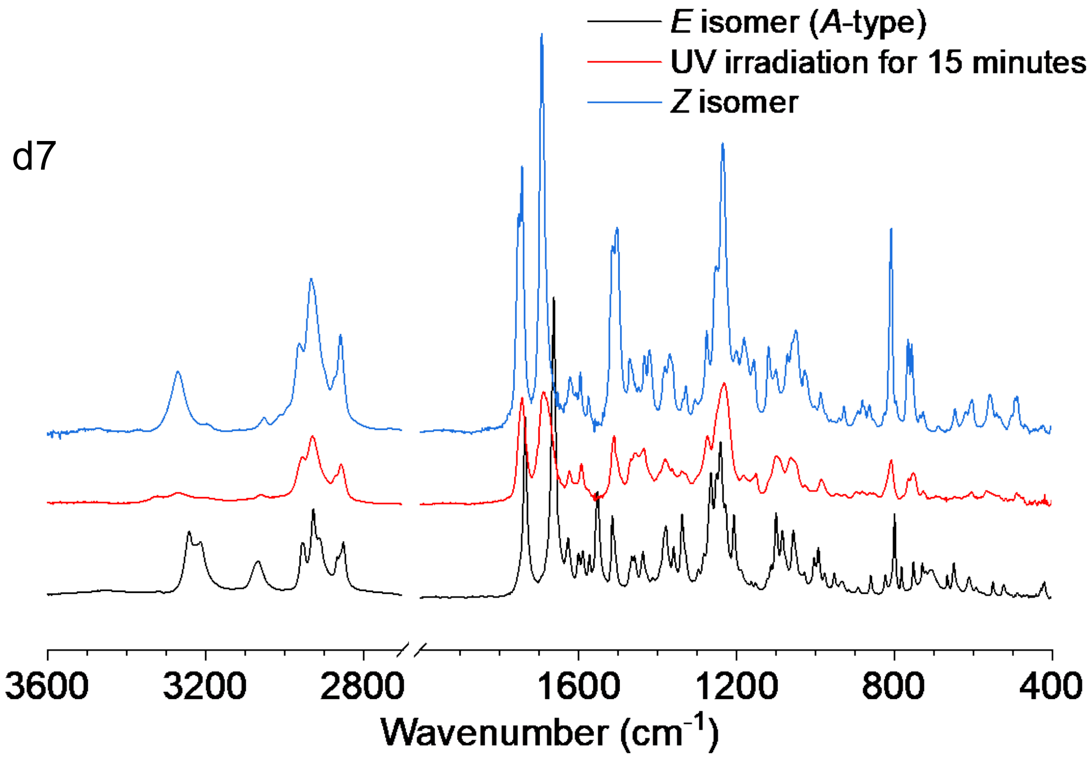

Figure S46 IR spectra of **d7** (*A*-type): *E*-isomer crystal (black), *Z*-isomer crystal (red), and *E*-isomer crystal irradiated with UV light for 15 minutes (blue).

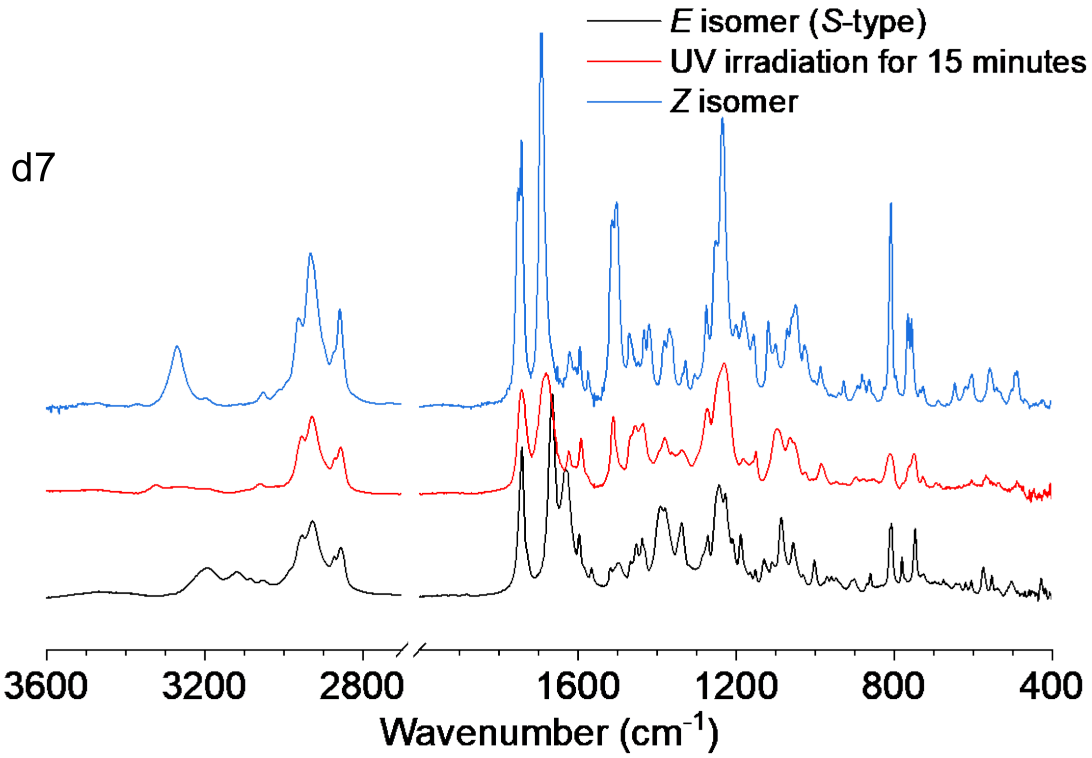

Figure S47 IR spectra of **d7** (*S*-type): *E*-isomer crystal (black), *Z*-isomer crystal (red), and *E*-isomer crystal irradiated with UV light for 15 minutes (blue).

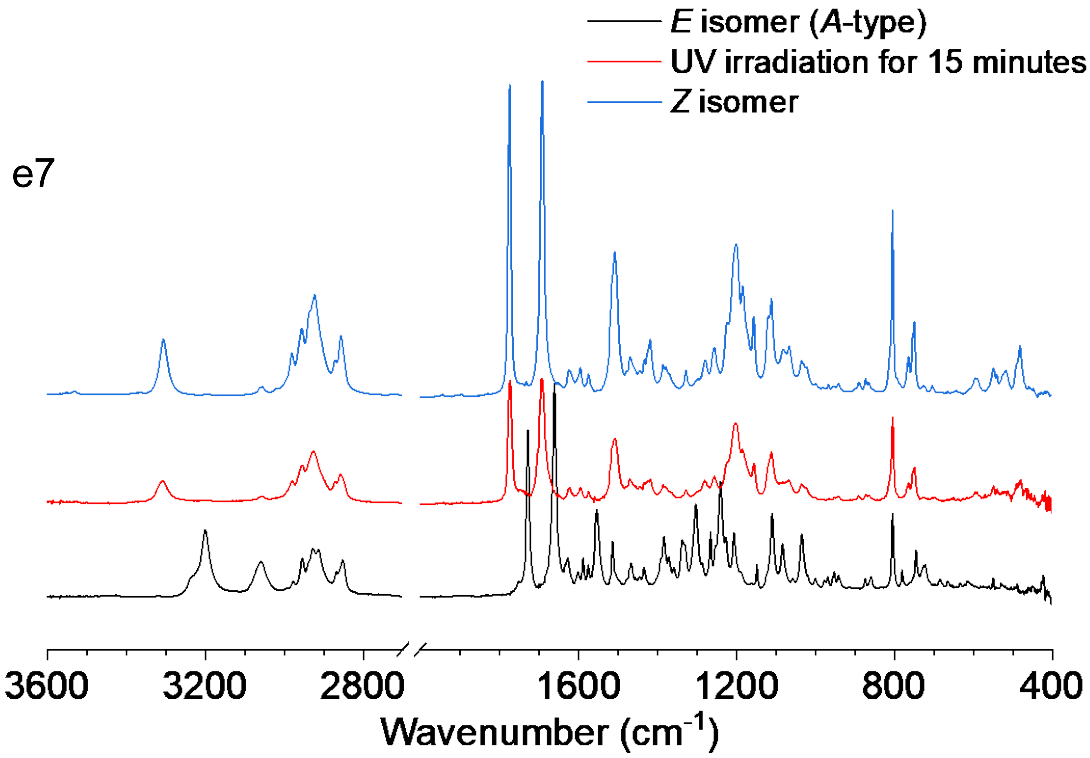

Figure S48 IR spectra of **e7** (*A*-type): *E*-isomer crystal (black), *Z*-isomer crystal (red), and *E*-isomer crystal irradiated with UV light for 15 minutes (blue).

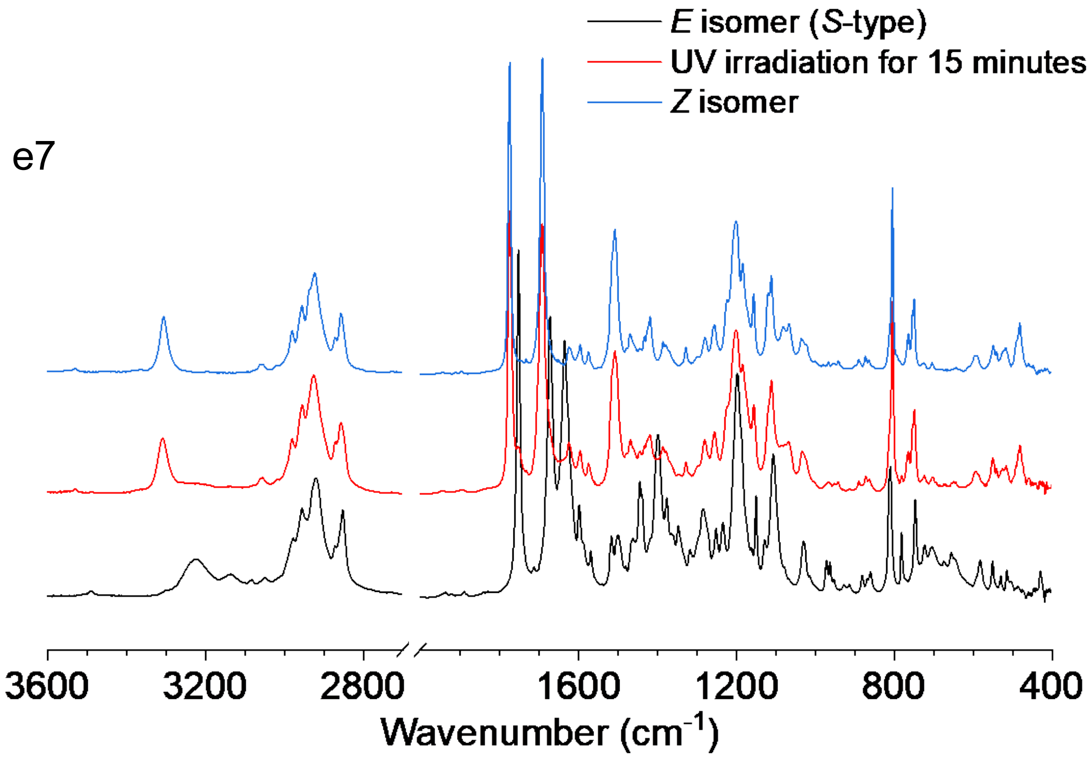

Figure S49 IR spectra of **e7** (*S*-type): *E*-isomer crystal (black), *Z*-isomer crystal (red), and *E*-isomer crystal irradiated with UV light for 15 minutes (blue).

11.2 Time-dependent change with respect to irradiation time

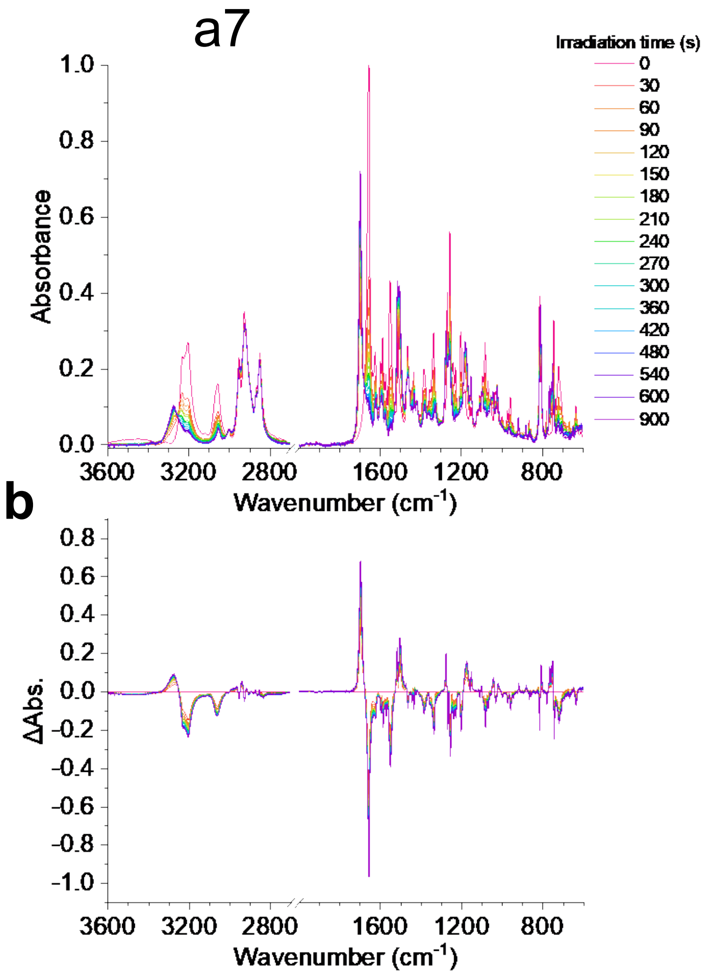

Figure S50 (a) IR spectra of the *E* isomer of **a7** as a function of UV irradiation time: the color of the lines indicates the UV irradiation time. (b) Difference spectra relative to the spectra at 0 s irradiation.

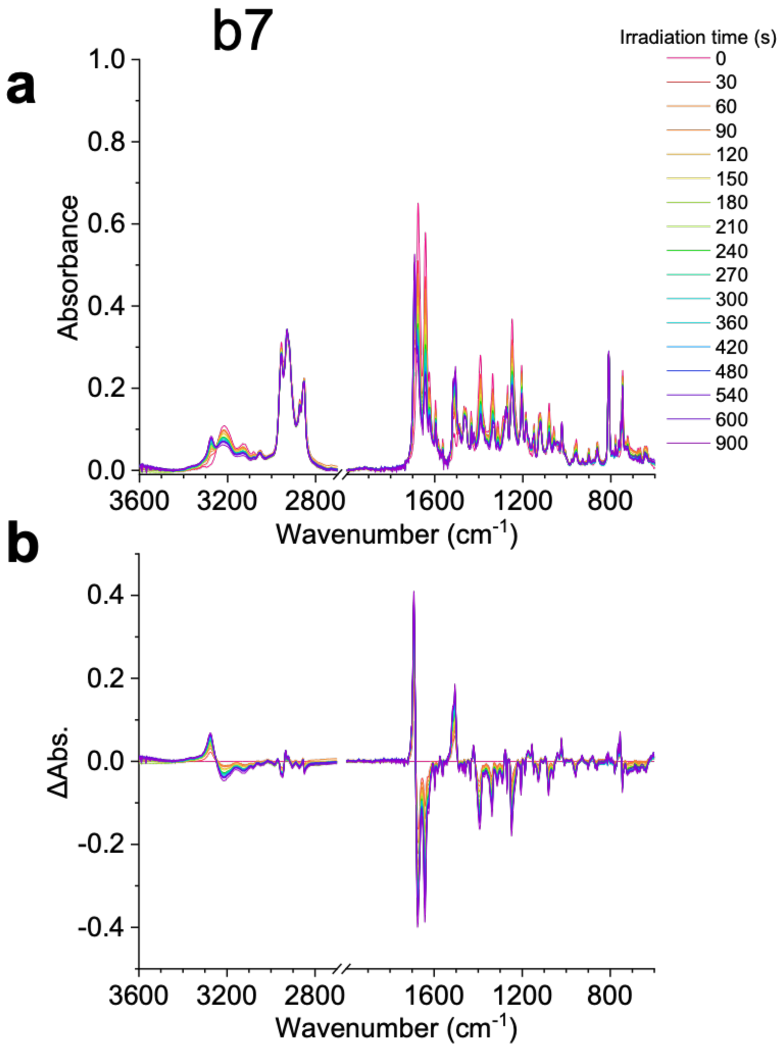

Figure S51 (a) IR spectra of the *E* isomer of **b7** as a function of UV irradiation time: the color of the lines indicates the UV irradiation time. (b) Difference spectra relative to the spectra at 0 s irradiation.

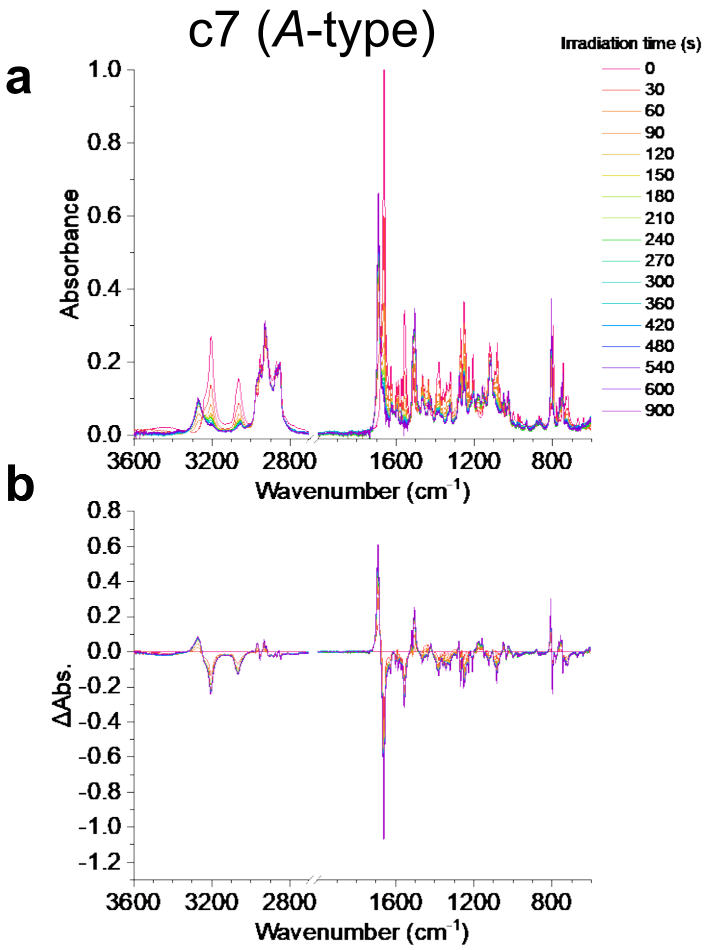

Figure S52 (a) IR spectra of the *E* isomer of **c7 (*A*-type)** as a function of UV irradiation time: the color of the lines indicates the UV irradiation time. (b) Difference spectra relative to the spectra at 0 s irradiation.

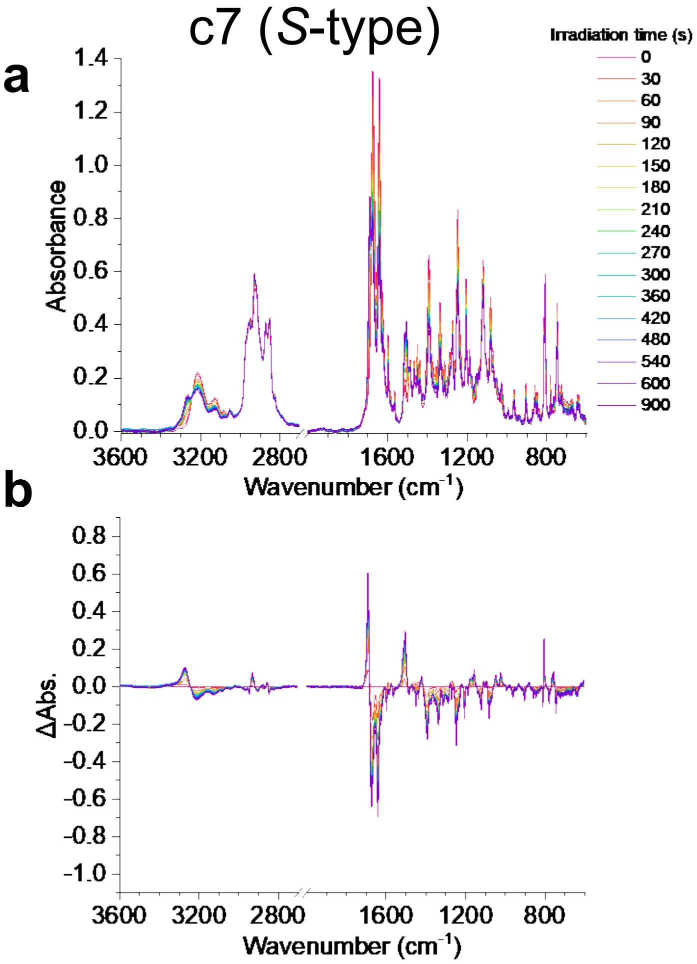

Figure S53 (a) IR spectra of the *E* isomer of **c7 (*S*-type)** as a function of UV irradiation time: the color of the lines indicates the UV irradiation time. (b) Difference spectra relative to the spectra at 0 s irradiation.

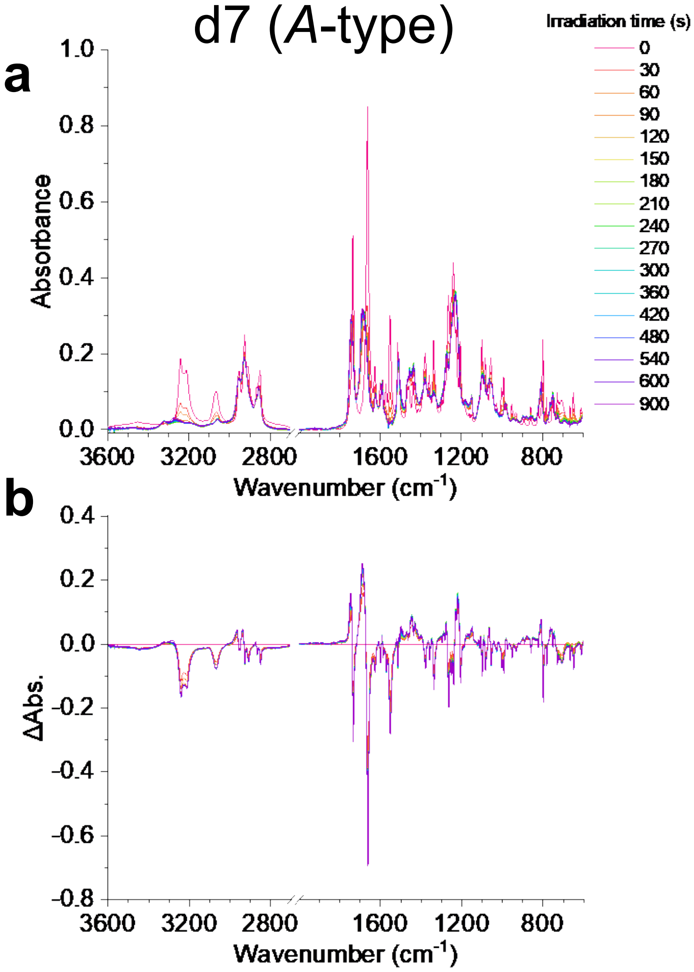

Figure S54 (a) IR spectra of the *E* isomer of **d7 (*A*-type)** as a function of UV irradiation time: the color of the lines indicates the UV irradiation time. (b) Difference spectra relative to the spectra at 0 s irradiation.

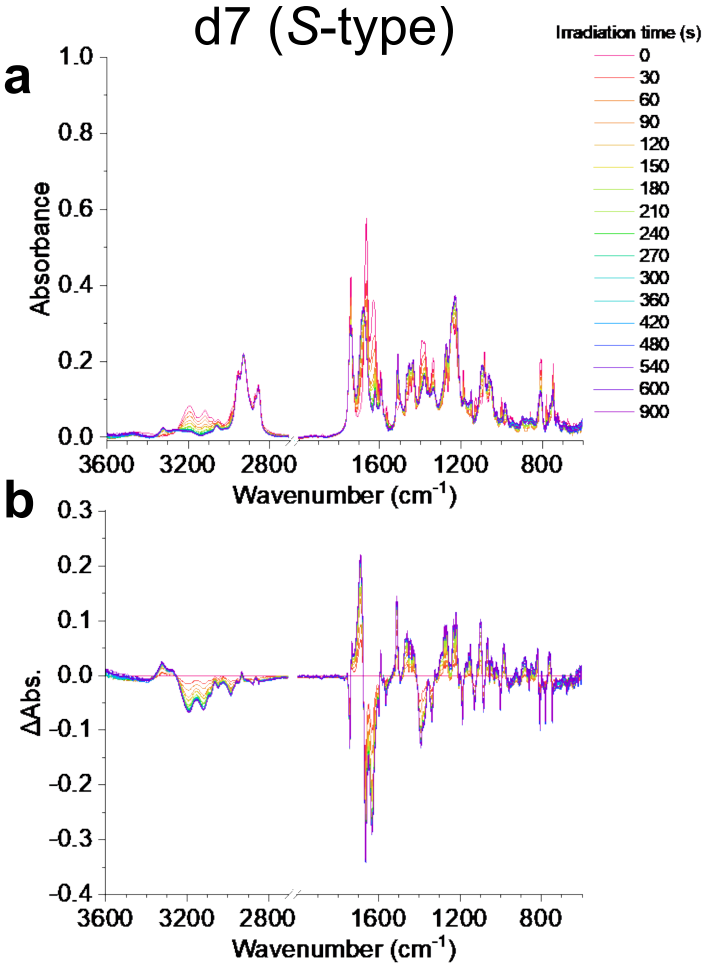

Figure S55 (a) IR spectra of the *E* isomer of **d7 (*S*-type)** as a function of UV irradiation time: the color of the lines indicates the UV irradiation time. (b) Difference spectra relative to the spectra at 0 s irradiation.

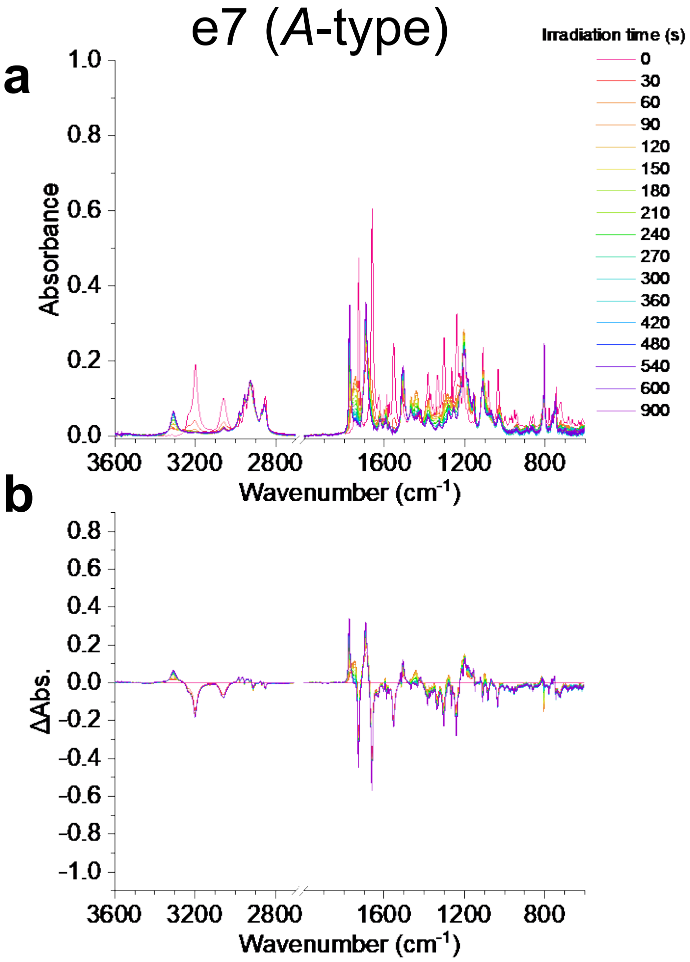

Figure S56 (a) IR spectra of the *E* isomer of **e7 (*A*-type)** as a function of UV irradiation time: the color of the lines indicates the UV irradiation time. (b) Difference spectra relative to the spectra at 0 s irradiation.

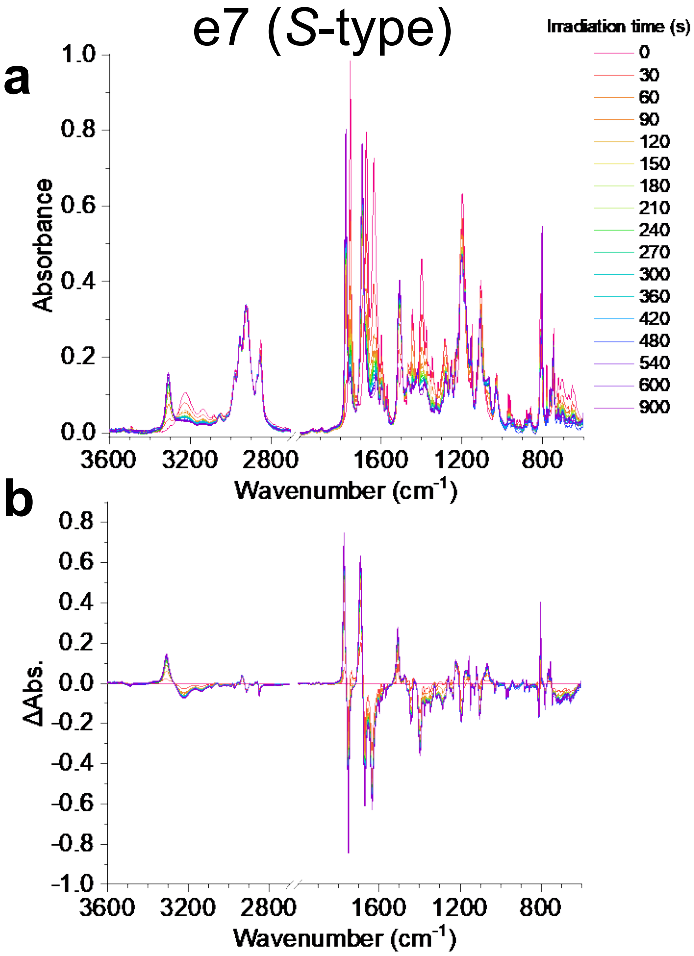

Figure S57 (a) IR spectra of the *E* isomer of **e7 (*S*-type)** as a function of UV irradiation time: the color of the lines indicates the UV irradiation time. (b) Difference spectra relative to the spectra at 0 s irradiation.

11.3 Tracking the transient state

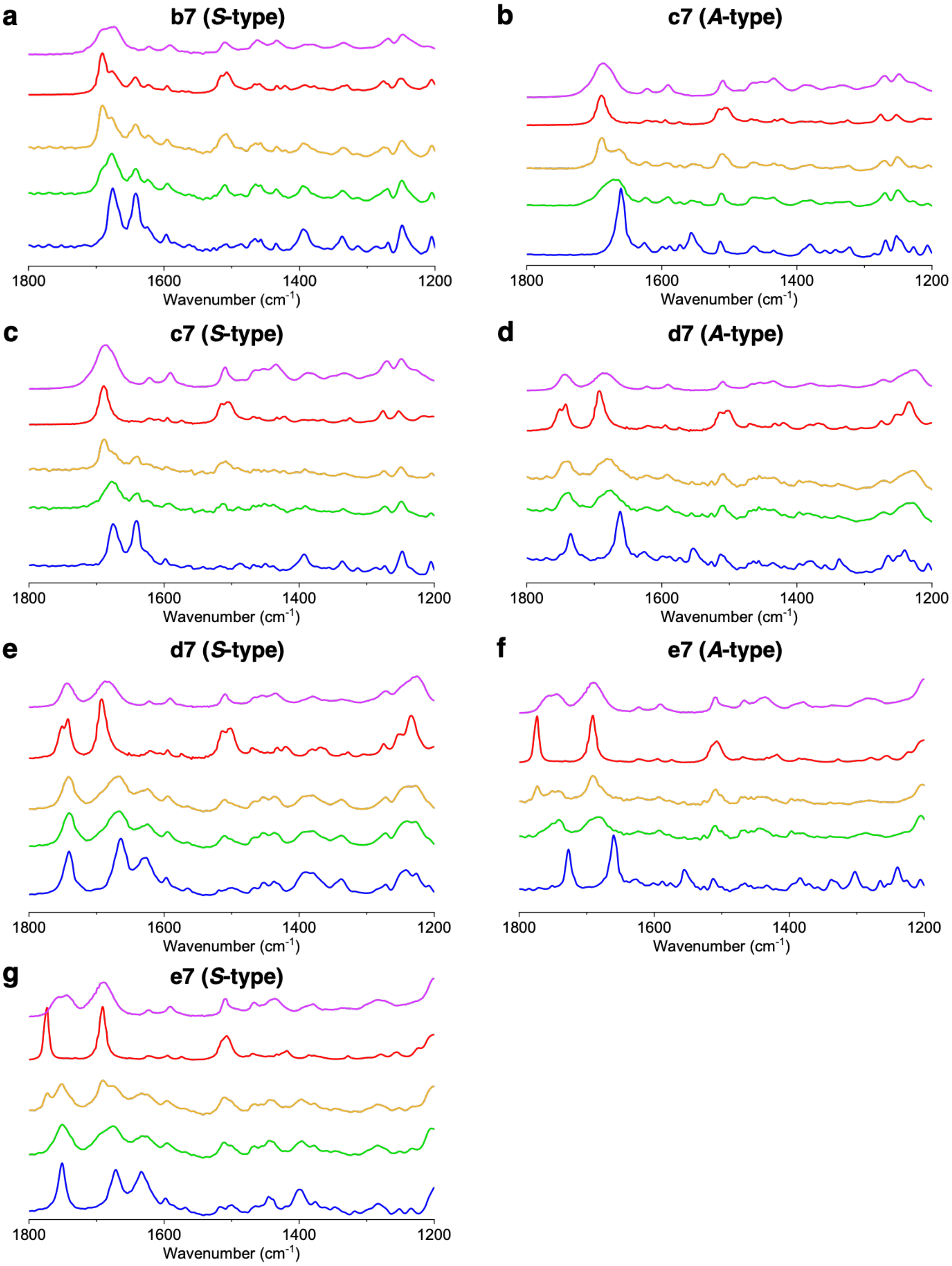

Figure S58 IR spectra of *E*-isomer (blue) and *Z*-isomer (red) crystals of (a) **b7** (*S*-type), (b) **c7** (*A*-type), (c) **c7** (*S*-type), (d) **d7** (*A*-type), (e) **d7** (*S*-type), (f) **e7** (*A*-type), and (a) **e7** (*S*-type) under various conditions: irradiation of the *E*-isomer crystal with 365 nm light at −15 °C for 2 minutes (green), subsequent heating of the irradiated crystal to 25 °C at a rate of 20 K/min (yellow), and heating of the *Z*-isomer crystal to its melting point under the observation of the VT-IR (purple).

12 Computational details

12.1 Optimization procedure of the crystal structure

For the calculation using QE, the Perdew-Burke-Ernzerhof (PBE) exchange correlational functional was employed to solve the Kohn-Sham equations under the periodic boundary conditions.[17] The dispersion force effect was incorporated by the semiempirical Grimme's D3BJ dispersion correction scheme.[18] The convergence threshold for self-consistency was set to 1×10^{-8}. For the atomic optimization of Compounds 1-3, the kinetic energy cutoff for wavefunctions (ecutwfc) and charge density (ecutrho) were set to 30 and 270 Ry, respectively. The setting of *k*-point was determined according to the crystal structure of each crystal: 2 × 1 × 1 for *Z* isomer of **b7**, **d7** and **e7**; 1 × 2 × 1 for *E* isomer of **b7**, **c7** (*S*-type and *A*-type), and *Z* isomer of **a7**; 1 × 1 × 2 for *Z* isomer of **c7**; 1 × 1 × 2 for *Z* isomer of **c7**; 3 × 1 × 1 for *E* isomer of **a7**; 1 × 3 × 1 for *E* isomer of **d7** (*A*-type) and **e7** (*S*-type and *A*-type). The convergence threshold on total energy (etot_conv_thr) and force (forc_conv_thr) were 1×10^{-4} Ry and 1×10^{-3} Ry Bohr^{-1}, respectively. After the atomic optimization of the crystal structure, a single-point SCF calculation was carried out. The ecutwfc and ecutrho were set to 64 and 576 Ry, respectively. The *k*-point was set to 3 × 3 × 3. The etot_conv_thr and forc_conv_thr were 3×10^{-5} Ry and 3×10^{-4} Ry Bohr^{-1}, respectively. The calculation protocol of the lattice energy is described in our previous report.[19]

12.2 *Calculation procedure of* $\boldsymbol{E_{conf}^{cry}}$ *and* $\boldsymbol{S_{conf}^{cry}}$

A minimal molecular cluster mimicking the crystal structure was constructed using the structure optimized by QE. This molecular cluster consists of a central embedded molecule and its surrounding molecules, with the number of surrounding molecules determined based on the literature.[20] To compare the energy values with those of an isolated molecule, the central molecule was optimized under ONIOM(ωB97X-D/6-311G:HF/STO-3G) conditions. The energy of the optimized central molecule obtained through this procedure was used as $E_{\mathrm{conf}}^{\mathrm{cry}}$ in eq. 3. The configurational entropy in the crystal, $S_{\mathrm{conf}}^{\mathrm{cry}}$, was approximated as zero based on the literature.[21]

12.3 Calculation procedure of $\boldsymbol{E_{conf}^{iso}}$ *and* $\boldsymbol{S_{conf}^{iso}}$

The stable conformations in the isolated state were explored by varying the structure of the modifier under ωB97X-D/6-31G conditions. The resulting multiple structures were further optimized using ωB97X-D/6-311G* conditions, and their energy values were compared. Among these, the energy of the most stable conformer was determined as $E_{\mathrm{conf}}^{\mathrm{iso}}$. Similarly, the energies of other locally stable conformers were calculated and used to derive $S_{\mathrm{conf}}^{\mathrm{iso}}$. The value of $S_{\mathrm{conf}}^{\mathrm{iso}}$ was calculated as follows[21,22]:

$$S_{\mathrm{conf}}^{\mathrm{iso}} = -R \sum_{\mathrm{i}} p_{\mathrm{i}} \ln p_{\mathrm{i}}$$

$$p_i = \frac{e^{-\frac{E_i}{kT}}}{Z}$$

$$Z = \sum_i e^{-\frac{E_i}{kT}}$$

Here, p_i represents the probability of the i-th conformer, E_i is the energy of the i-th conformer, Z is the partition function, R is the gas constant, k is the Boltzmann constant, and T is temperature and set to 298.15 K in this study. The number of conformers used to calculate $S_{\mathrm{conf}}^{\mathrm{iso}}$ was determined such that the increase in $S_{\mathrm{conf}}^{\mathrm{iso}}$ calculated using the i-th and (i+1)-th conformers was less than 1% (Figure S71).

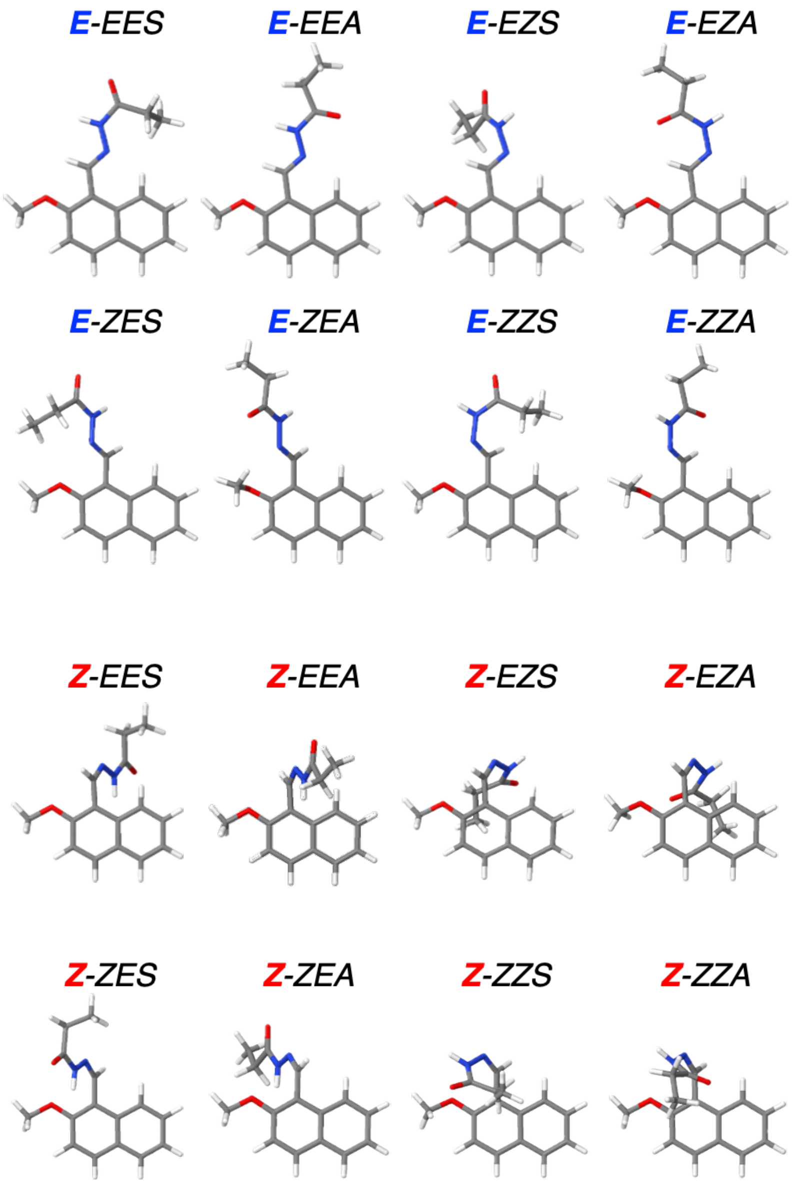

E-*EES* *E*-*EEA* *E*-*EZS* *E*-*EZA*

E-*ZES* *E*-*ZEA* *E*-*ZZS* *E*-*ZZA*

Z-*EES* *Z*-*EEA* *Z*-*EZS* *Z*-*EZA*

Z-*ZES* *Z*-*ZEA* *Z*-*ZZS* *Z*-*ZZA*

Figure S59 Sixteen structures generated by three single-bond rotations in the acylhydrazone moiety. Geometry optimizations for all ground-state structures in **a2** were performed at the ωB97X-D/6-311G** level.

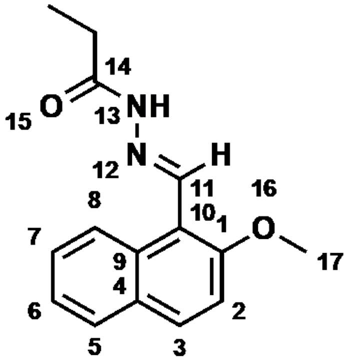

Figure S60 Numbering of atoms in **a2**.

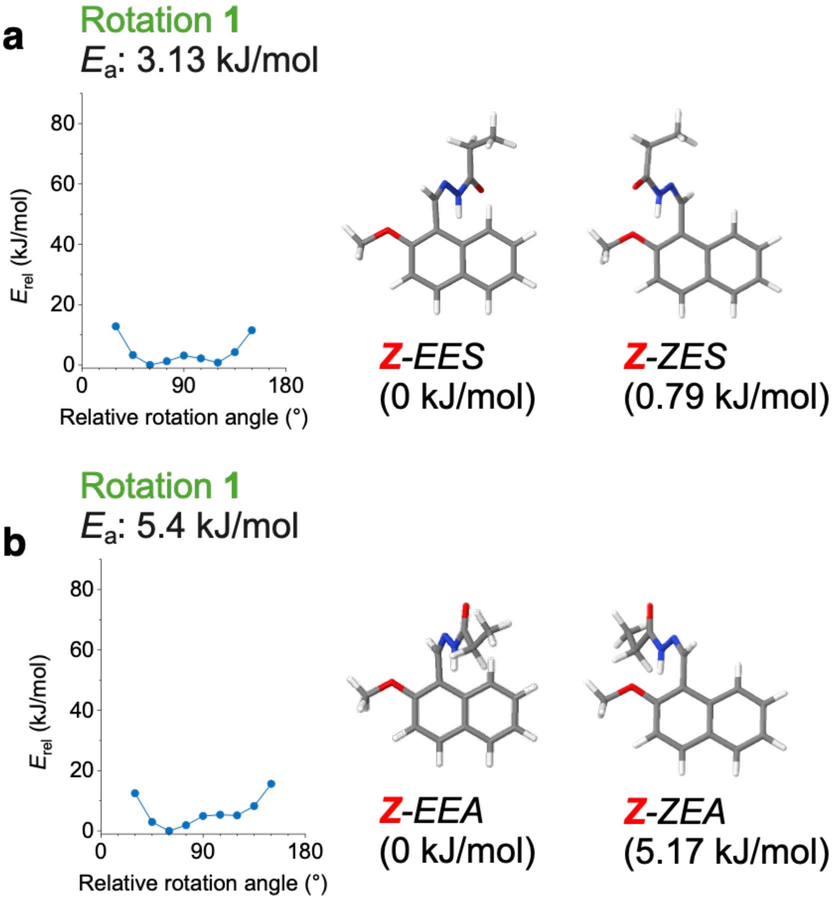

Figure S61 The PES scan of isolated **a2** along the rotation of C1–C10–C11–N12 starting from (a) *Z-EES* and (b) *Z-EEA* structures calculated at the ωB97X-D/6-311G** level with a step of 15°. E_a indicates the rotational barrier. The values in parentheses indicate the relative energy from the minimum energy structure in the PES. Please refer to Figure S60 for the atomic number.

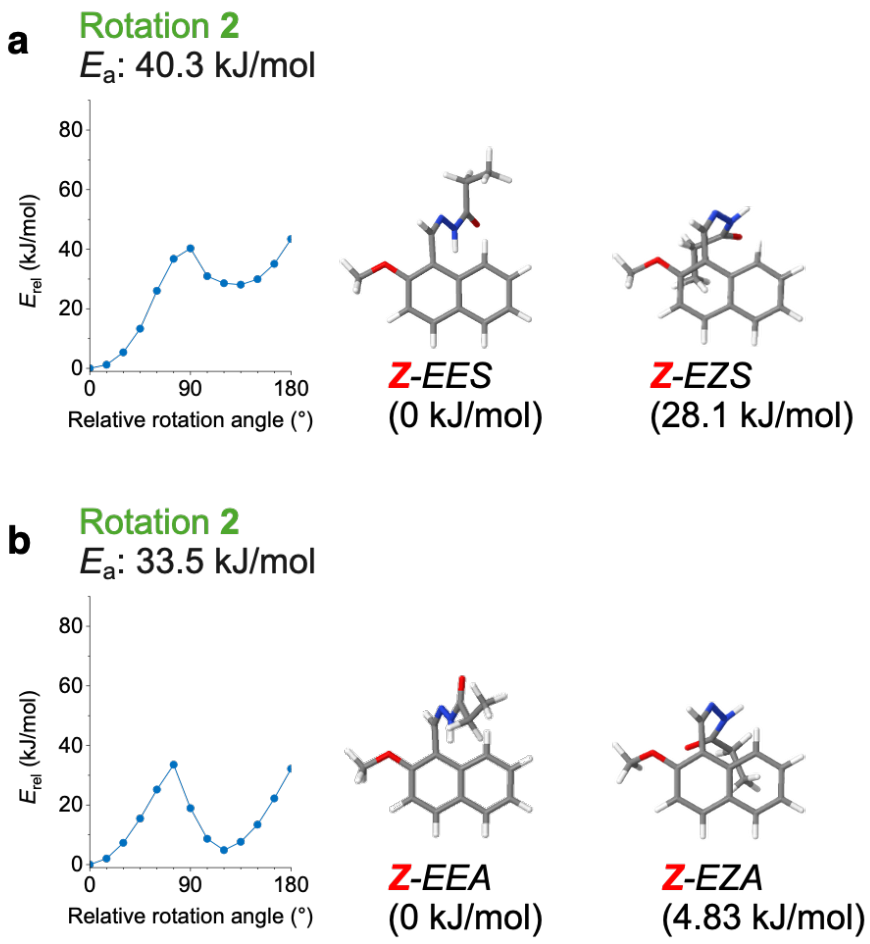

Figure S62 The PES scan of isolated **a2** along the rotation of C11–N12–N13–C14 starting from (a) *Z-EES* and (b) *Z-EEA* structures calculated at the ωB97X-D/6-311G** level with a step of 15°. E_a indicates the rotational barrier. The values in parentheses indicate the relative energy from the minimum energy structure in the PES. Please refer to Figure S60 for the atomic number.

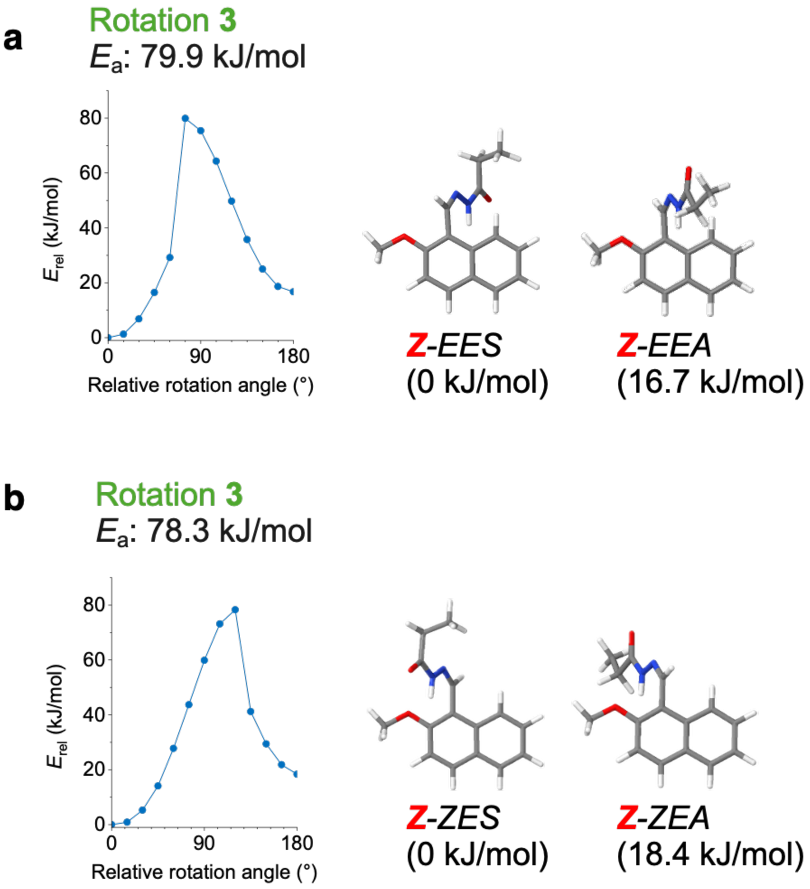

Figure S63 The PES scan of isolated **a2** along the rotation of N12–N13–C14–O15 starting from (a) *Z-EES* and (b) *Z-ZES* structures calculated at the ωB97X-D/6-311G** level with a step of 15°. E_a indicates the rotational barrier. The values in parentheses indicate the relative energy from the minimum energy structure in the PES. Please refer to Figure S60 for the atomic number.

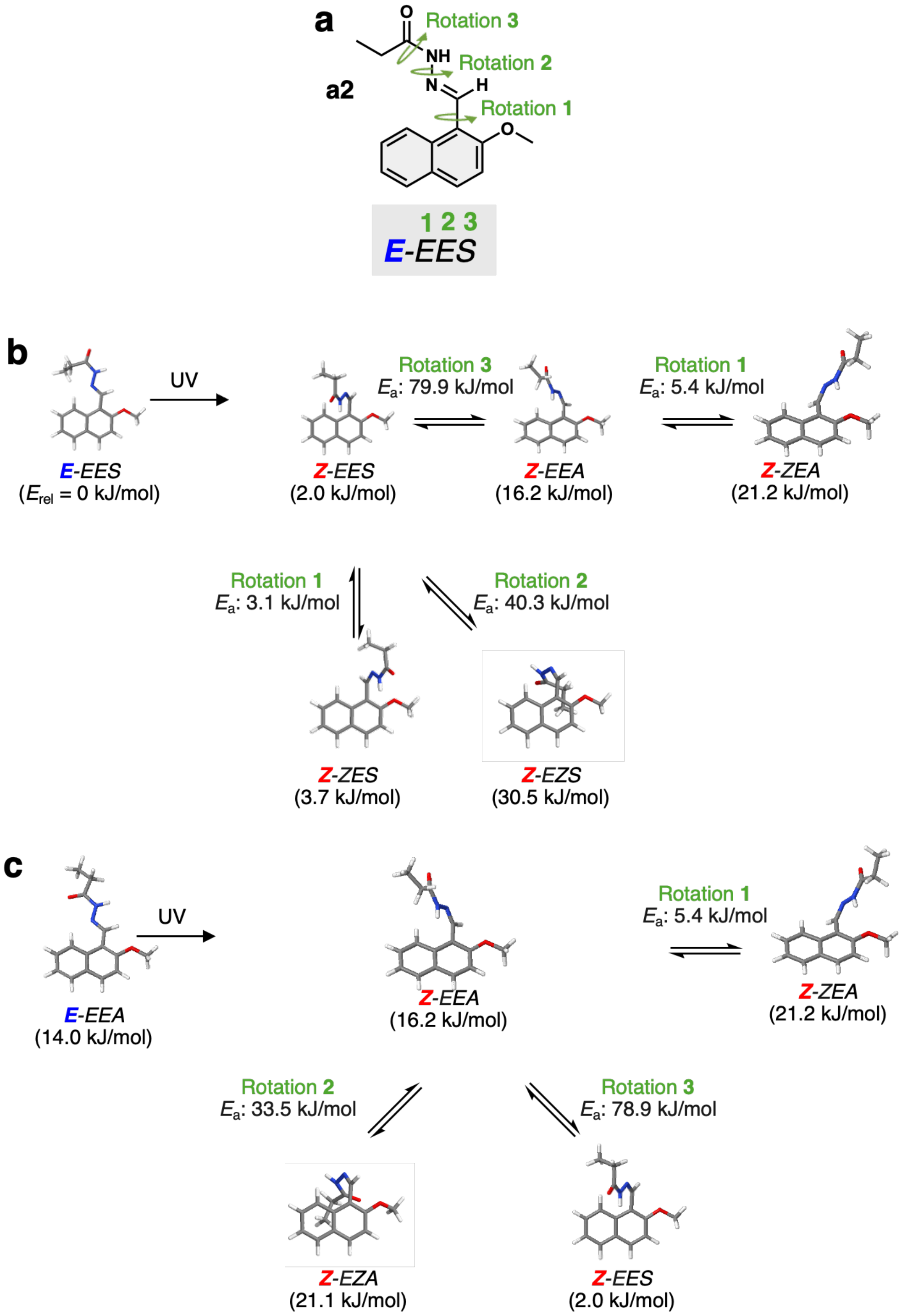

Figure S64 The reaction pathway from (a) *E-EES* and (b) *E-EEA* to *Z-ZEA*. The values in parentheses represent relative energies with respect to *E-EES* (ωB97X-D/6-311G**). The transient conformer here includes those generated by a single-bond rotation from *Z-EES* or *Z-EEA*.

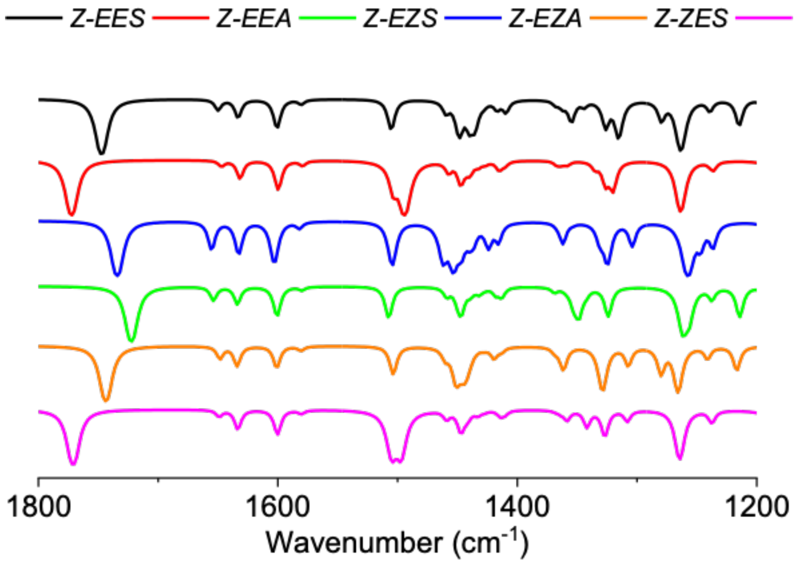

Figure S65 Simulated (bottom) IR spectra for isolate **a2** molecules calculated with the ωB97X-D/6-311G** condition. The strong peaks at ~1750 cm-1 were assigned to the C=O stretching vibration.

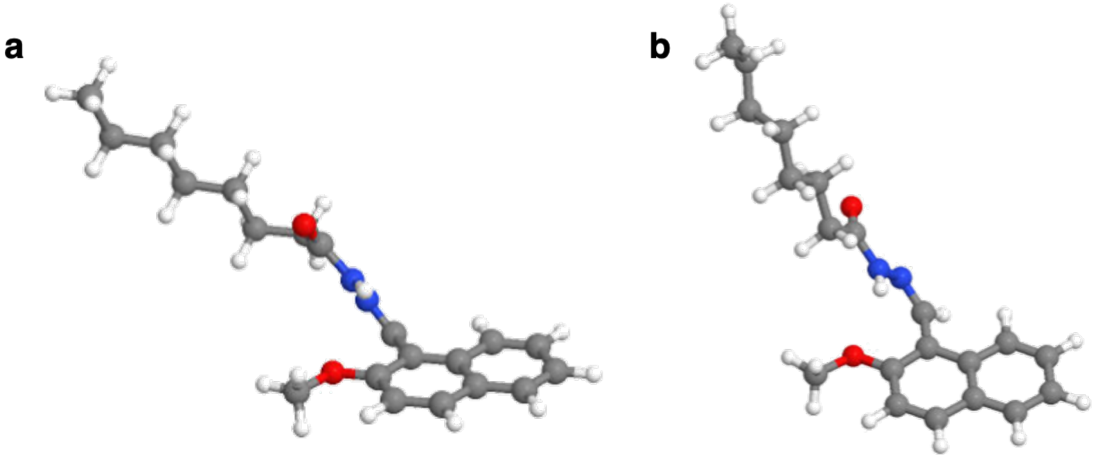

Figure S66 Comparison of (a) conformations in the isolated state (WC) and (b) conformations in the crystal (RC) for **a7**.

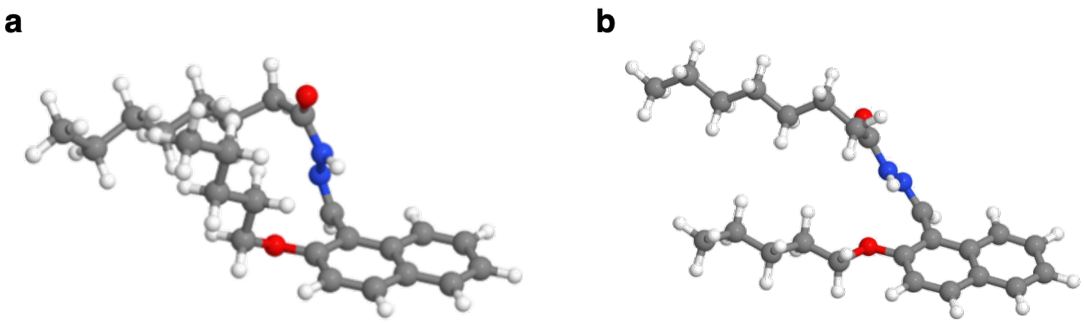

Figure S67 Comparison of (a) conformations in the isolated state (WC) and (b) conformations in the crystal (RC) for **b7**.

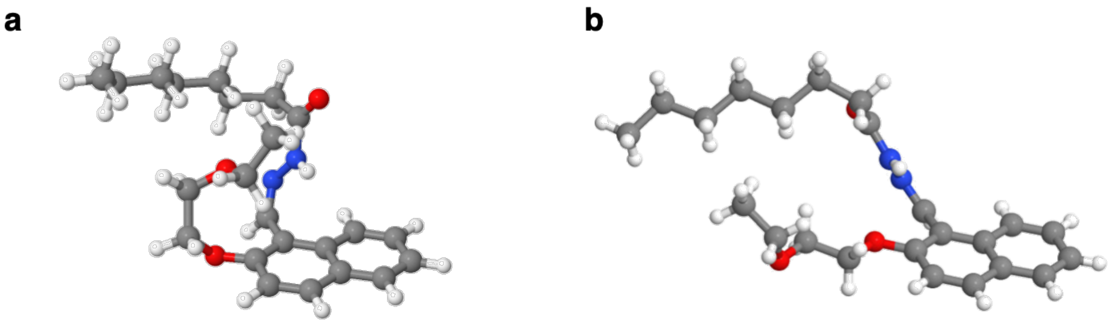

Figure S68 Comparison of (a) conformations in the isolated state (WC) and (b) conformations in the crystal (RC) for **c7**.

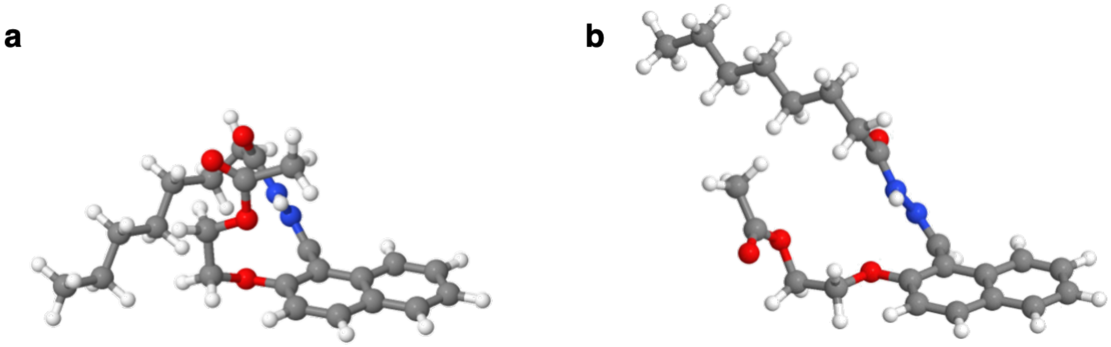

Figure S69 Comparison of (a) conformations in the isolated state (WC) and (b) conformations in the crystal (RC) for **d7**.

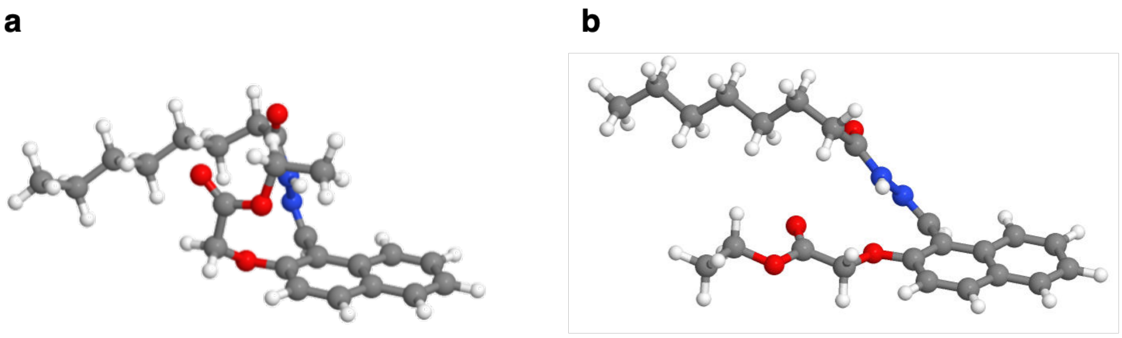

Figure S70 Comparison of (a) conformations in the isolated state (WC) and (b) conformations in the crystal (RC) for **e7**.

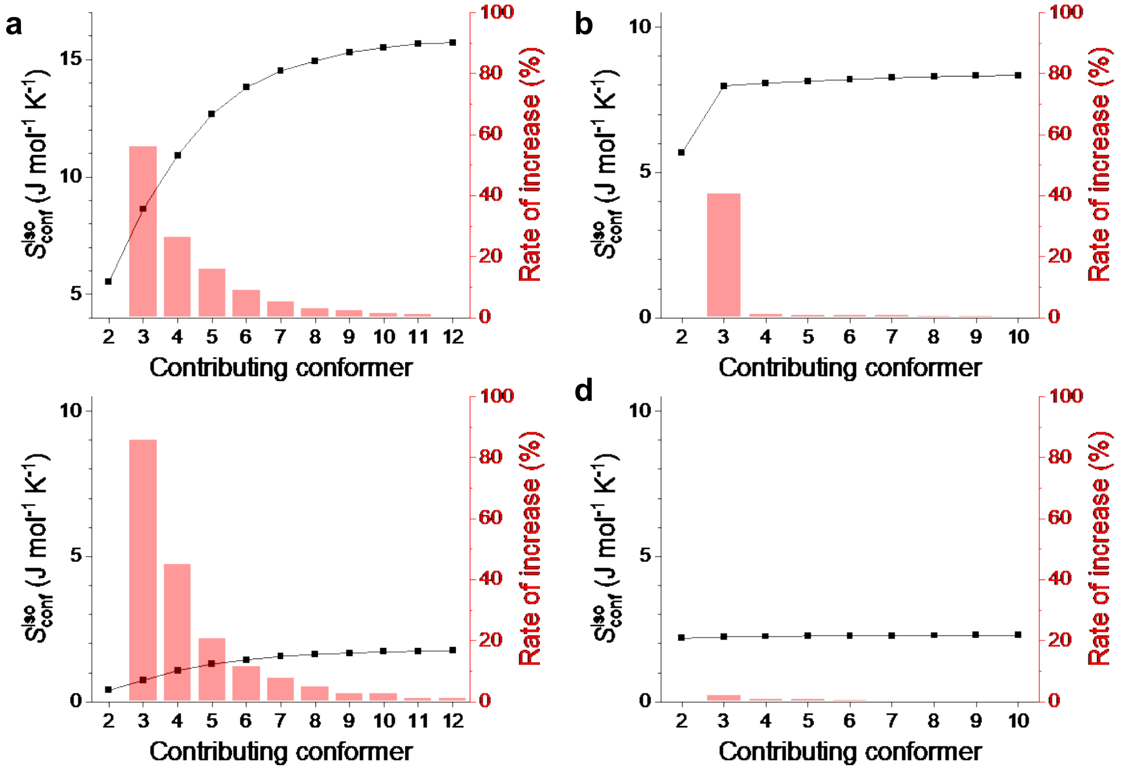

Figure S71 Transition of $S^{\mathrm{iso}}_{\mathrm{conf}}$ (black plot, left axis) with respect to the number of contributing conformers for (a) **b7**, (b) **c7**, (c) **d7**, and (d) **e7**. The rate of increase (red bars, right axis) indicates the percentage increase in $S^{\mathrm{iso}}_{\mathrm{conf}}$ as additional conformers are included.

Table S11 Comparison of lattice energy for each compound.

	E isomer		*Z* isomer
	S-type	*A*-type	
a7	-[1]	−198.8	−190.5
b7	−199.8	-[1]	−206.7
c7	−199.8	−221.0	−210.9
d7	-[2]	−231.8	−215.1
e7	−203.5	−230.3	−213.5

[1] Crystal structure was not obtained.

[2] Not calculated due to insufficient quality of crystal data.

13 Reference

1 R. Koibuchi, I. Yoshikawa and H. Houjou, *J. Phys. Chem. A*, 2022, **126**, 4164–4175.

2 G. M. Sheldrick, *Acta Crystallogr. A*, 2008, **64**, 112–122.

3 G. M. Sheldrick, *Acta Crystallogr. A Found. Adv.*, 2015, **71**, 3–8.

4 G. M. Sheldrick, *Acta Crystallogr. C Struct. Chem.*, 2015, **71**, 3–8.

5 Kabuto C., Akine S., Nemoto T. and Kwon E., *Nihon Kessho Gakkaishi*, 2009, **51**, 218–224.

6 R. Koibuchi, K. Omasa, I. Yoshikawa and H. Houjou, *J. Phys. Chem. Lett.*, 2023, **14**, 8320–8326.

7 Z.-Y. Zhang, Y. He, Y. Zhou, C. Yu, L. Han and T. Li, *Chemistry*, 2019, **25**, 13402–13410.

8 Y. He, Z. Shangguan, Z.-Y. Zhang, M. Xie, C. Yu and T. Li, *Angew. Chem. Int. Ed Engl.*, 2021, **60**, 16539–16546.

9 C. Knie, M. Utecht, F. Zhao, H. Kulla, S. Kovalenko, A. M. Brouwer, P. Saalfrank, S. Hecht and D. Bléger, *Chemistry*, 2014, **20**, 16492–16501.

10 G. Zimmerman, L.-Y. Chow and U.-J. Paik, 1958, **80**, 14. DOI:10.1021/ja01547a010.

11 Y. Yan, X. Wang, J. I. L. Chen and D. S. Ginger, *J. Am. Chem. Soc.*, 2013, **135**, 8382–8387.

12 C. A. Parker, *Proc. R. Soc. Lond.*, 1953, **220**, 104–116.

13 K. Stranius and K. Börjesson, *Sci. Rep.*, 2017, **7**, 41145.

14 K. Karunakaran, *J. Solution Chem.*, 1981, **10**, 431–435.

15 H. Matsunaga, K. Katoh, H. Habu, M. Noda and A. Miyake, *J. Therm. Anal. Calorim.*, 2019, **135**, 2677–2685.

16 K. M. Kenges, A. A. Krasilin and E. A. Tugova, *Heliyon*, 2024, **10**, e29056.

17 J. P. Perdew, K. Burke and M. Ernzerhof, *Phys. Rev. Lett.*, 1996, **77**, 3865–3868.

18 S. Grimme, S. Ehrlich and L. Goerigk, *J. Comput. Chem.*, 2011, **32**, 1456–1465.

19 C. Raju, Z. Sun, R. Koibuchi, J. Y. Choi, S. Chakraborty, J. Park, H. Houjou, K. Schmidt-Rohr and G. G. D. Han, *J. Mater. Chem. A Mater. Energy Sustain.*, 2024, **12**, 26678–26686. DOI:10.1039/d4ta05282j.

20 R. Koibuchi, I. Yoshikawa, Y. Shigemitsu and H. Houjou, *Cryst. Growth Des.*, 2024, **24**, 238–251.

21 T. Endo, K. Sunada, H. Sumida and Y. Kimura, *Chem. Sci.*, 2022, **13**, 7560–7565.

22 K. A. Sharp, *Methods Enzymol.*, 2019, **615**, 1–41.

14 Synthesis Characterization

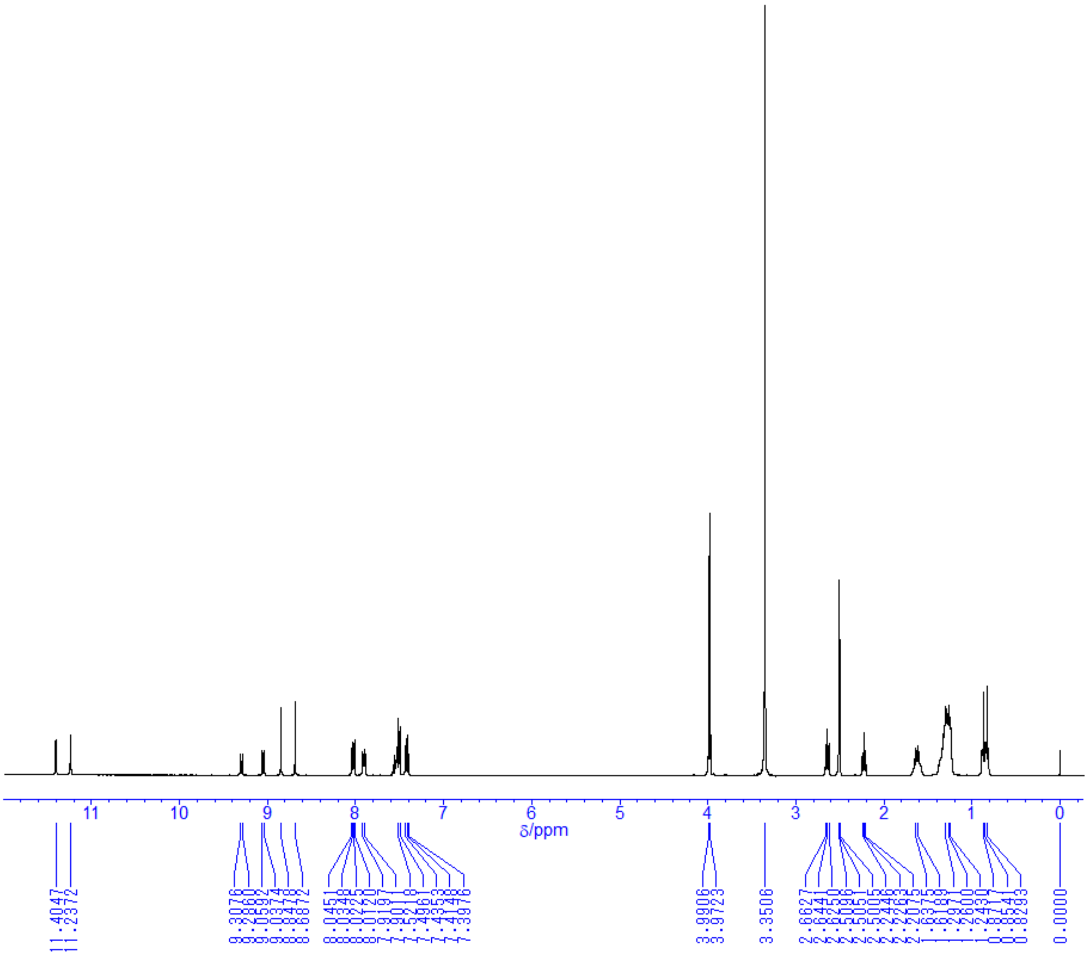

Figure S72 ^{1}H NMR (400 MHz, DMSO-d_6) spectrum of **a7** (as prepared).

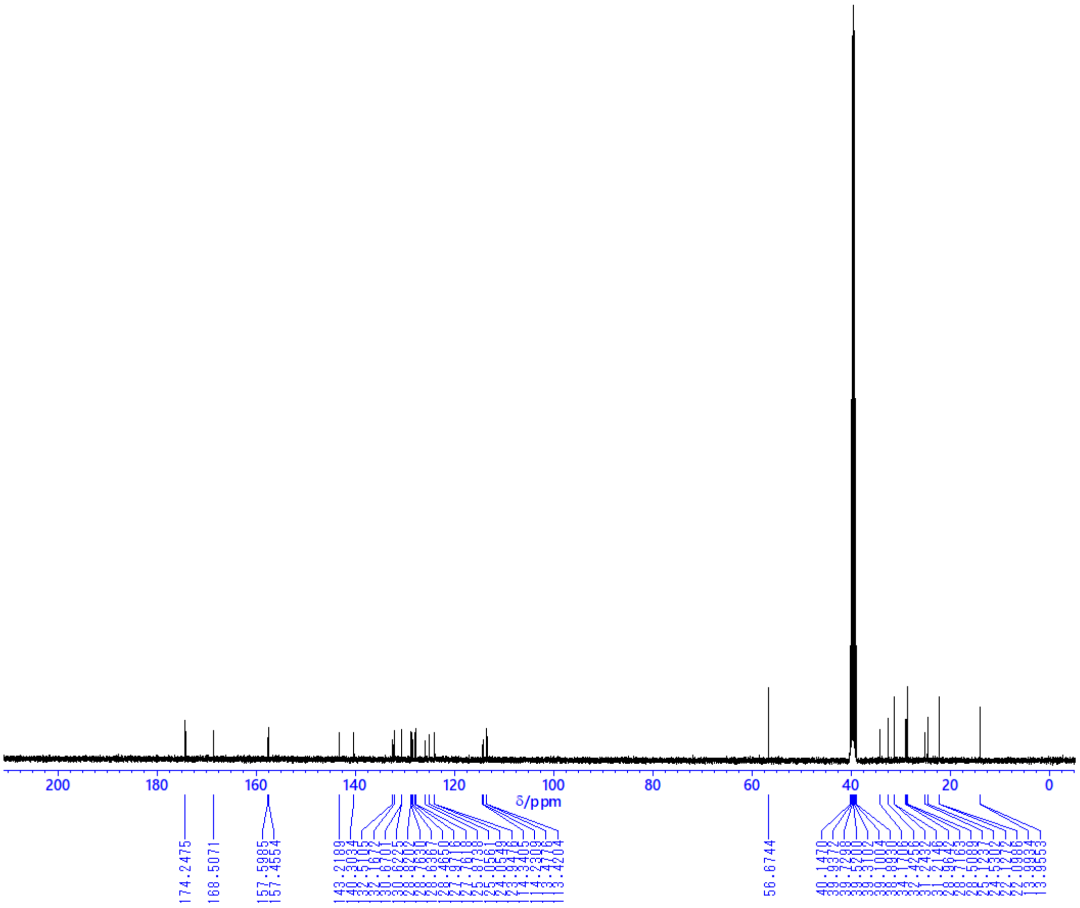

Figure S73 ^{13}C NMR (100 MHz, DMSO-d_6) spectrum of **a7** (as prepared).

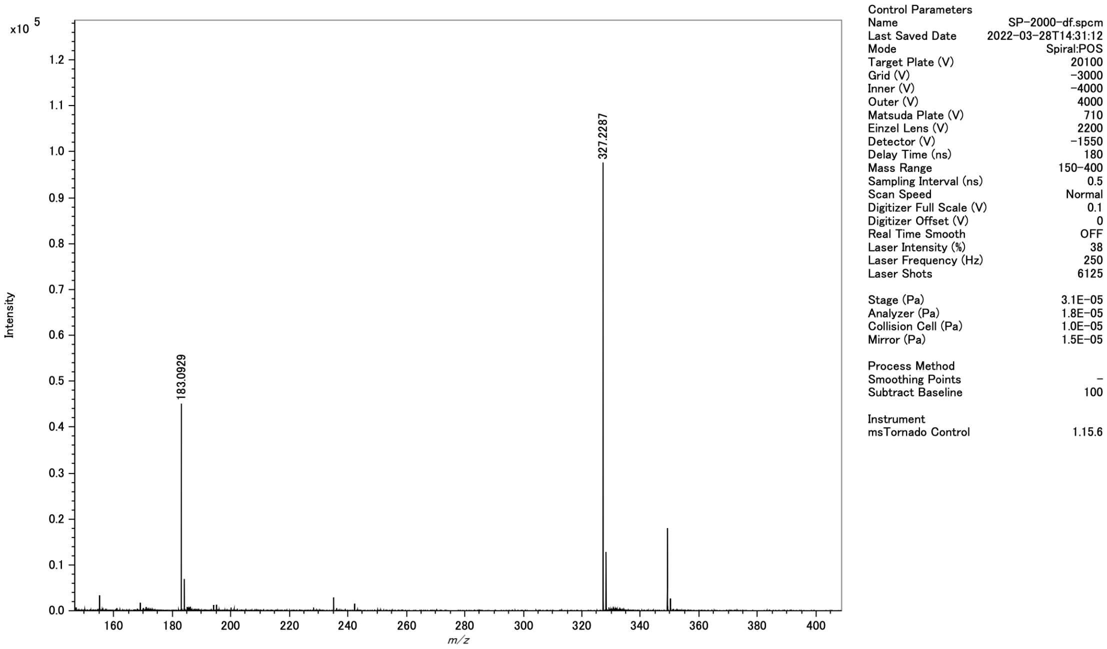

Control Parameters	
Name	SP-2000-df.spcm
Last Saved Date	2022-03-28T14:31:12
Mode	Spiral:POS
Target Plate (V)	20100
Grid (V)	-3000
Inner (V)	-4000
Outer (V)	4000
Matsuda Plate (V)	710
Einzel Lens (V)	2200
Detector (V)	-1550
Delay Time (ns)	180
Mass Range	150-400
Sampling Interval (ns)	0.5
Scan Speed	Normal
Digitizer Full Scale (V)	0.1
Digitizer Offset (V)	0
Real Time Smooth	OFF
Laser Intensity (%)	38
Laser Frequency (Hz)	250
Laser Shots	6125
Stage (Pa)	3.1E-05
Analyzer (Pa)	1.8E-05
Collision Cell (Pa)	1.0E-05
Mirror (Pa)	1.5E-05
Process Method	
Smoothing Points	-
Subtract Baseline	100
Instrument	
msTornado Control	1.15.6

Figure S74 MALDI-TOF-MS spectra of **a7** (as prepared).

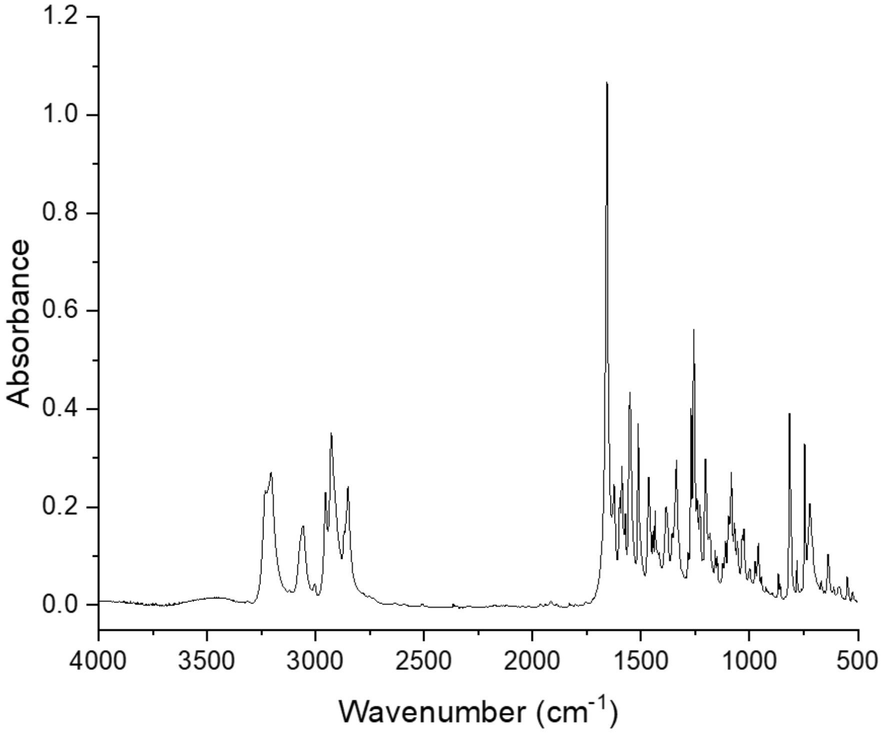

Figure S75 FT-IR spectra of **a7** (as prepared) in KBr.

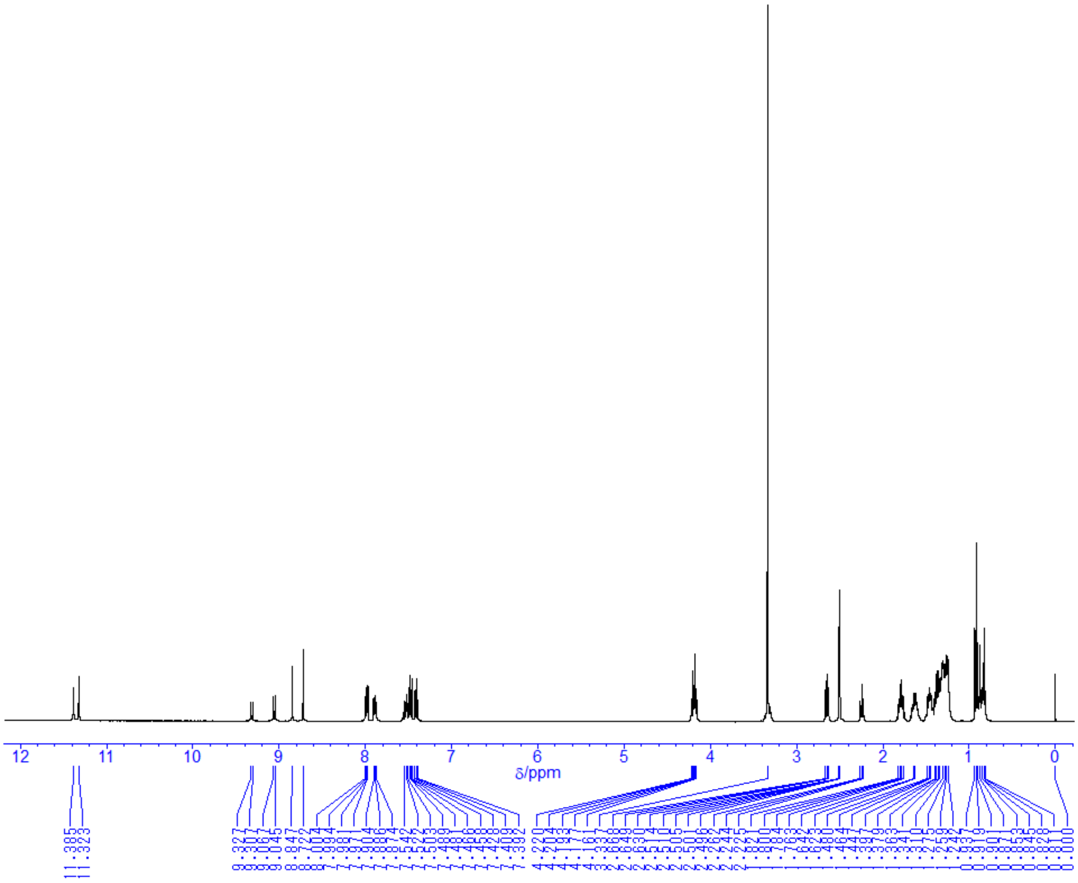

Figure S76 ^{1}H NMR (400 MHz, DMSO-d_6) spectrum of **b7** (as prepared).

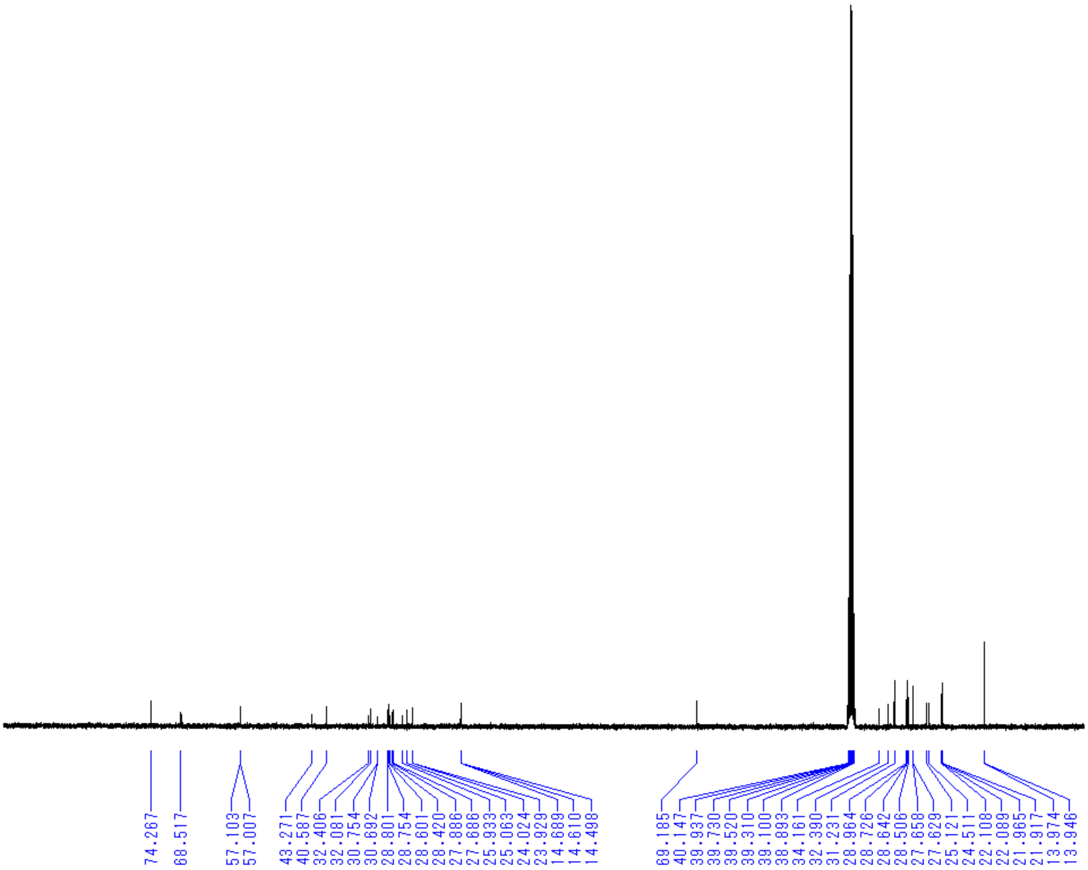

Figure S77 ^{13}C NMR (100 MHz, DMSO-d_6) spectrum of **b7** (as prepared).

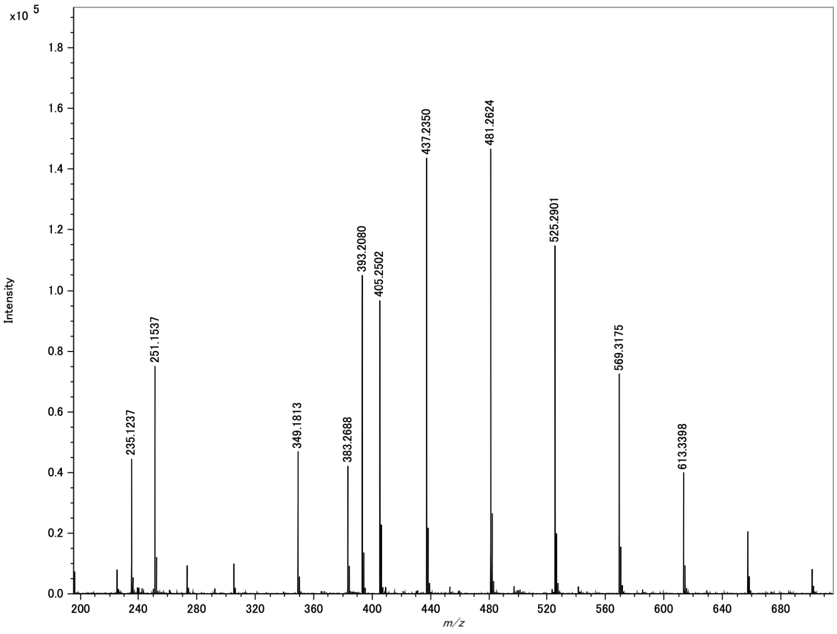

Control Parameters	
Name	SP-2000-df.spcm
Last Saved Date	2022-03-28T14:31:12
Mode	Spiral:POS
Target Plate (V)	20100
Grid (V)	-3000
Inner (V)	-4000
Outer (V)	4000
Matsuda Plate (V)	710
Einzel Lens (V)	2200
Detector (V)	-1550
Delay Time (ns)	160
Mass Range	200-700
Sampling Interval (ns)	0.5
Scan Speed	Normal
Digitizer Full Scale (V)	0.1
Digitizer Offset (V)	0
Real Time Smooth	OFF
Laser Intensity (%)	35
Laser Frequency (Hz)	250
Laser Shots	13750
Stage (Pa)	3.9E-05
Analyzer (Pa)	2.5E-05
Collision Cell (Pa)	1.2E-05
Mirror (Pa)	2.1E-05
Process Method	
Smoothing Points	-
Subtract Baseline	100
Instrument	
msTornado Control	1.15.6

Figure S78 HRMS spectra of **b7** (as prepared).

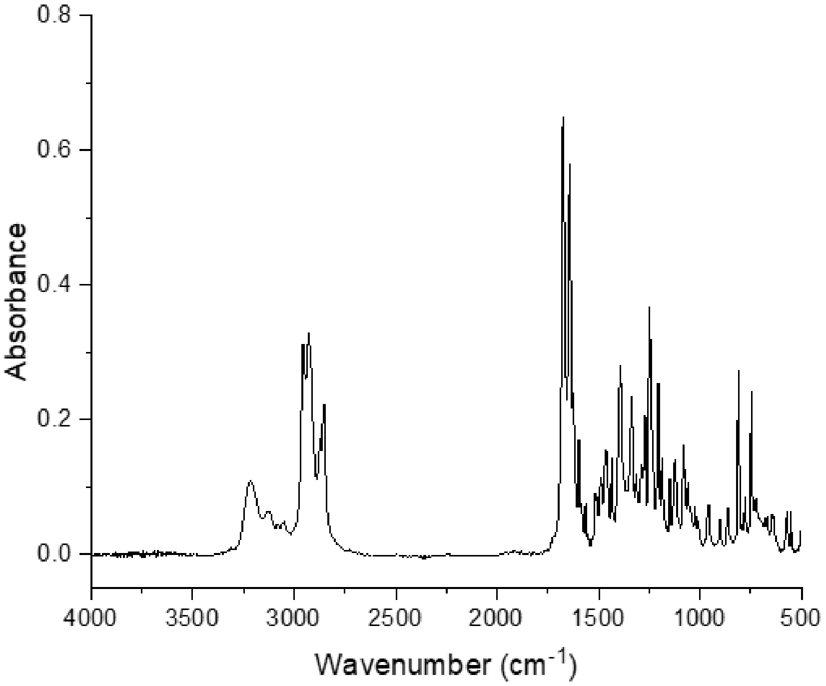

Figure S79 FT-IR spectra of **b7** (as prepared) in KBr.

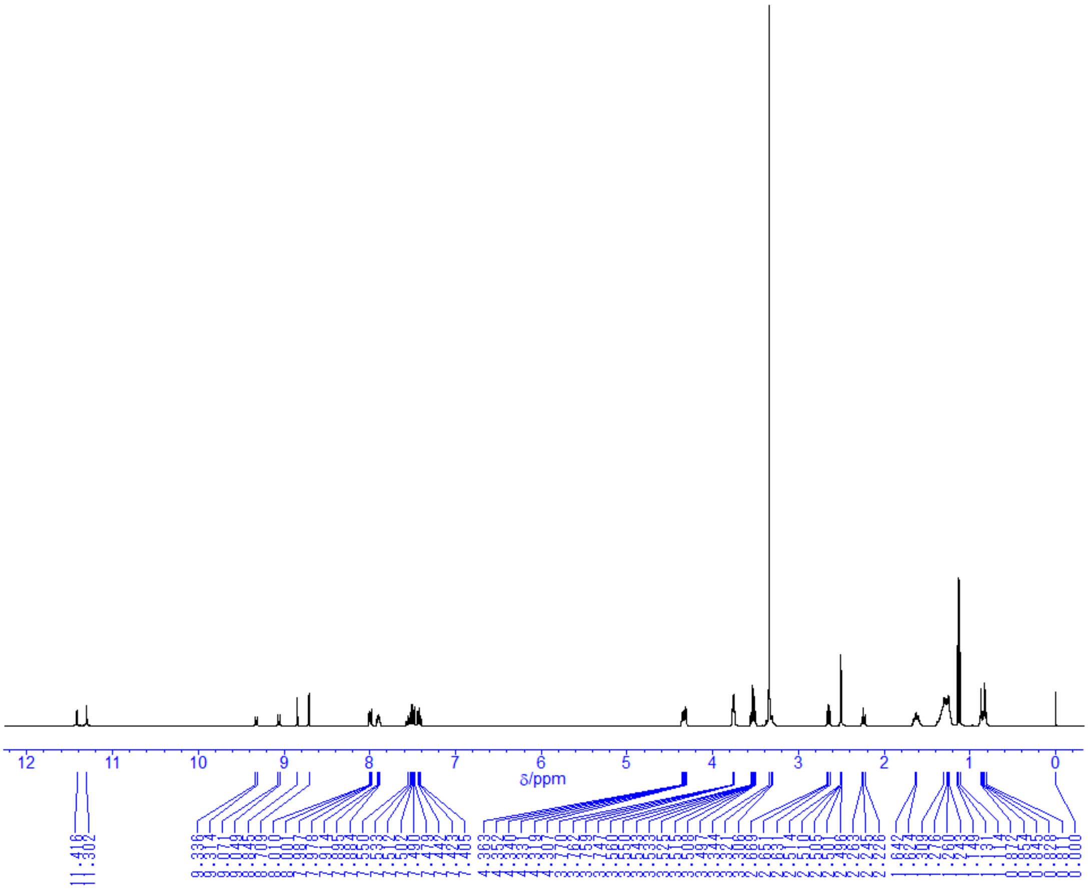

Figure S80 ^{1}H NMR (400 MHz, DMSO-d_6) spectrum of **c7** (as prepared).

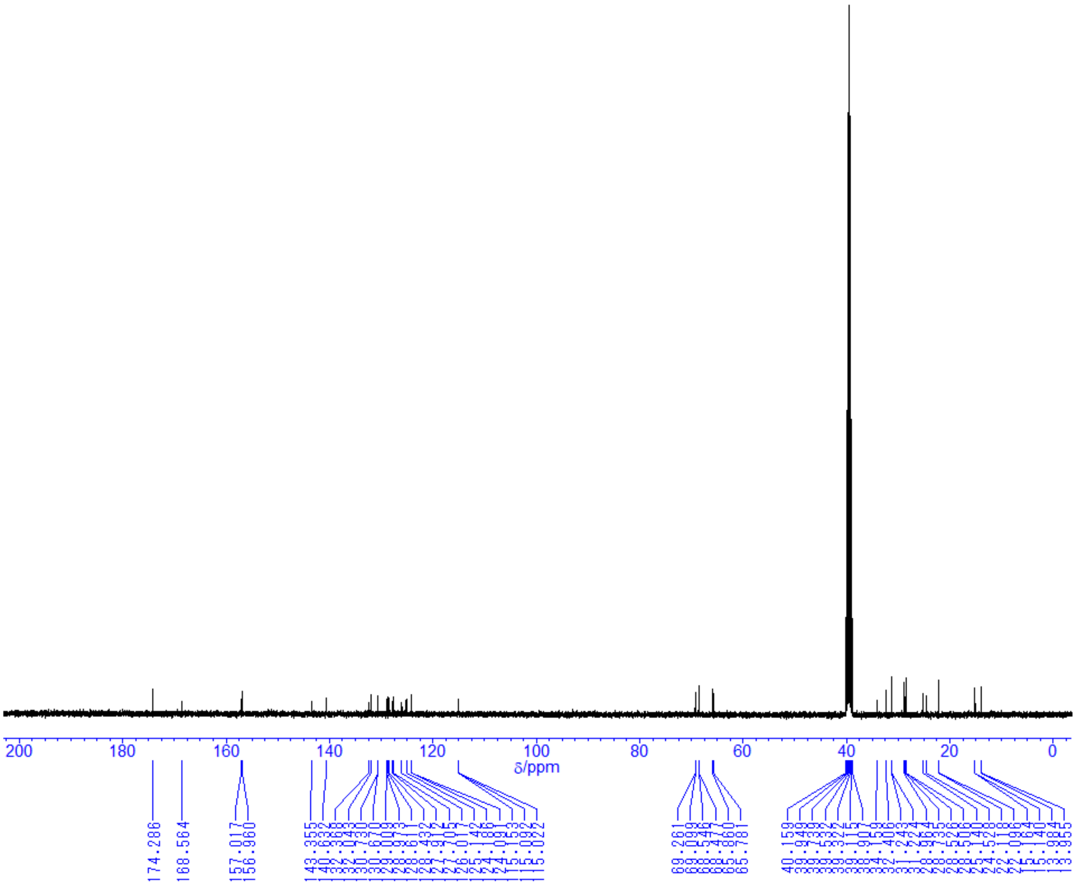

Figure S81 ^{13}C NMR (100 MHz, DMSO-d_6) spectrum of **c7** (as prepared).

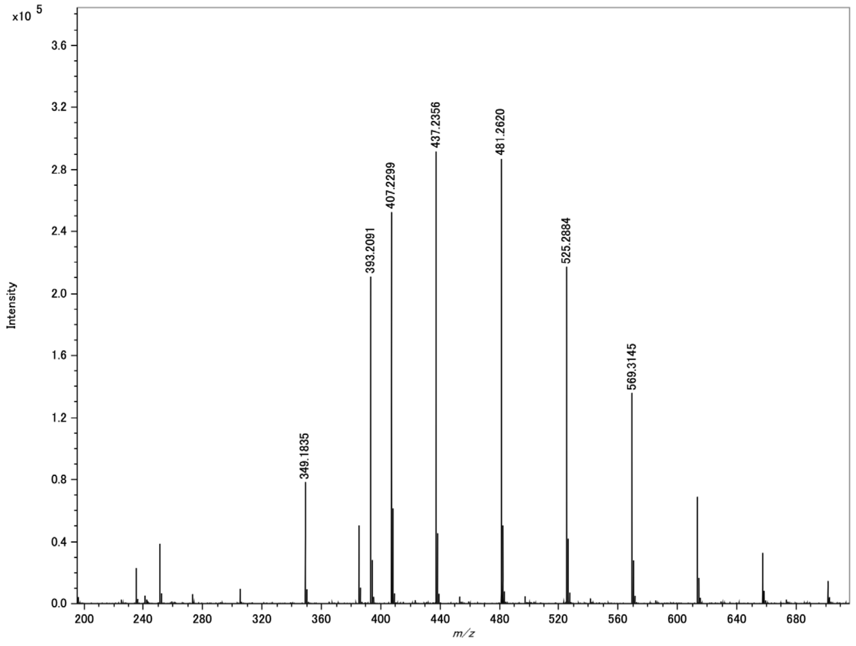

Control Parameters	
Name	SP-2000-df.spcm
Last Saved Date	2022-03-28T14:31:12
Mode	Spiral:POS
Target Plate (V)	20100
Grid (V)	-3000
Inner (V)	-4000
Outer (V)	4000
Matsuda Plate (V)	710
Einzel Lens (V)	2200
Detector (V)	-1550
Delay Time (ns)	160
Mass Range	200-700
Sampling Interval (ns)	0.5
Scan Speed	Normal
Digitizer Full Scale (V)	0.1
Digitizer Offset (V)	0
Real Time Smooth	OFF
Laser Intensity (%)	35
Laser Frequency (Hz)	250
Laser Shots	16250
Stage (Pa)	3.8E-05
Analyzer (Pa)	2.5E-05
Collision Cell (Pa)	1.2E-05
Mirror (Pa)	2.1E-05
Process Method	
Smoothing Points	-
Subtract Baseline	100
Instrument	
msTornado Control	1.15.6

Figure S82 HRMS spectra of **c7** (as prepared).

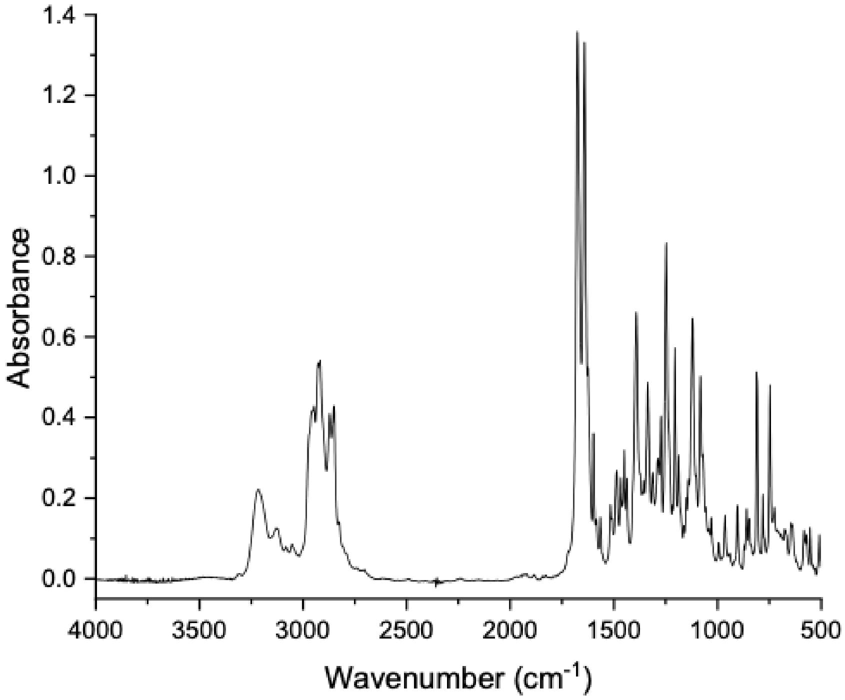

Figure S83 FT-IR spectra of **c7** (as prepared) in KBr.

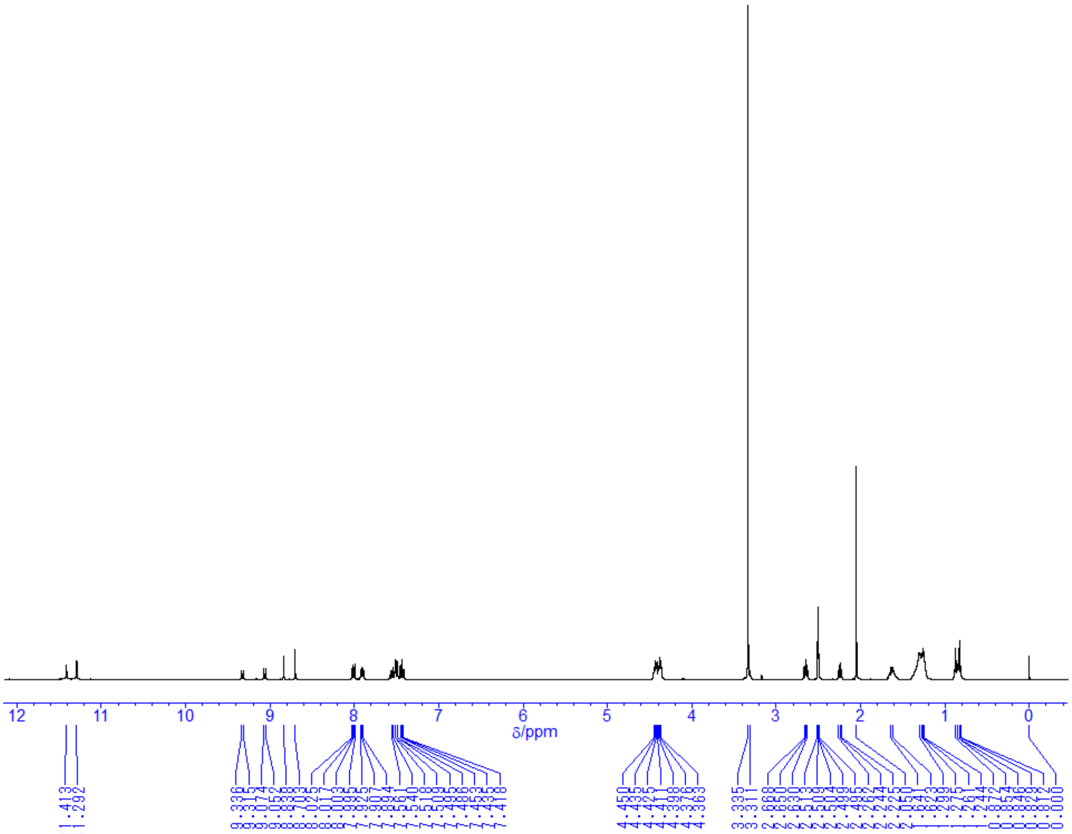

Figure S84 ^{1}H NMR (400 MHz, DMSO-d_6) spectrum of **d7** (as prepared).

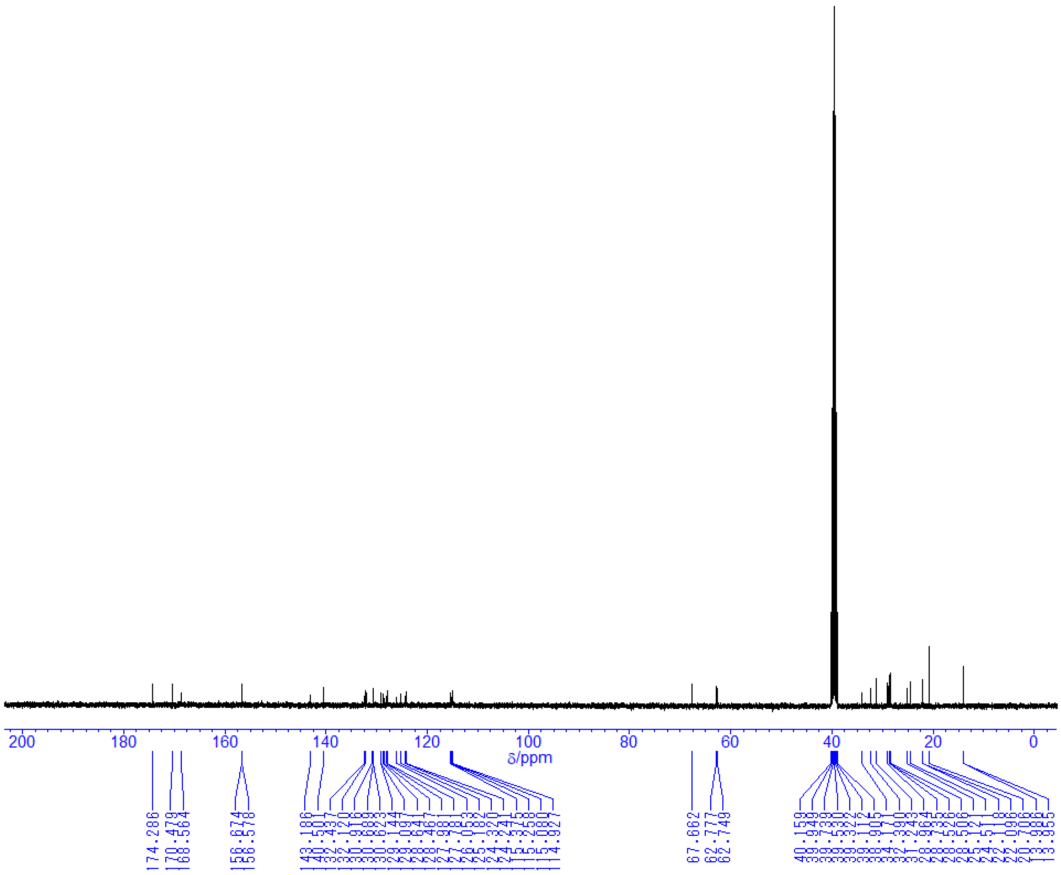

Figure S85 ^{13}C NMR (100 MHz, DMSO-d_6) spectrum of **d7** (as prepared).

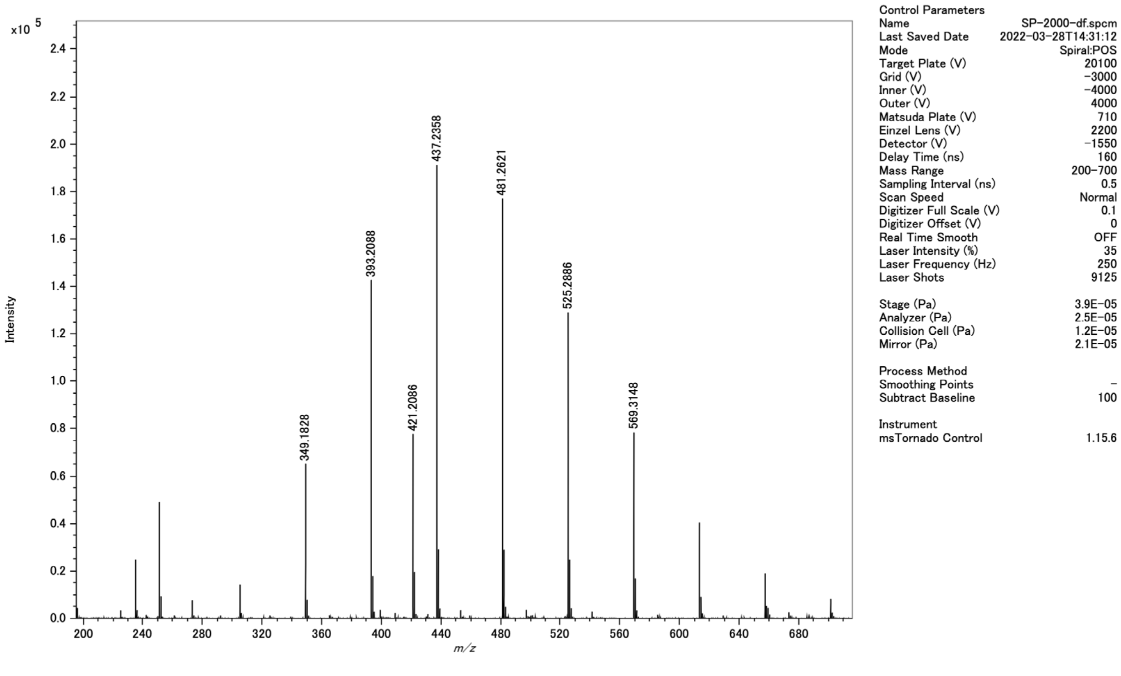

Control Parameters	
Name	SP−2000−df.spcm
Last Saved Date	2022−03−28T14:31:12
Mode	Spiral:POS
Target Plate (V)	20100
Grid (V)	−3000
Inner (V)	−4000
Outer (V)	4000
Matsuda Plate (V)	710
Einzel Lens (V)	2200
Detector (V)	−1550
Delay Time (ns)	160
Mass Range	200−700
Sampling Interval (ns)	0.5
Scan Speed	Normal
Digitizer Full Scale (V)	0.1
Digitizer Offset (V)	0
Real Time Smooth	OFF
Laser Intensity (%)	35
Laser Frequency (Hz)	250
Laser Shots	9125
Stage (Pa)	3.9E−05
Analyzer (Pa)	2.5E−05
Collision Cell (Pa)	1.2E−05
Mirror (Pa)	2.1E−05
Process Method	
Smoothing Points	−
Subtract Baseline	100
Instrument	
msTornado Control	1.15.6

Figure S86 HRMS spectra of **d7** (as prepared).

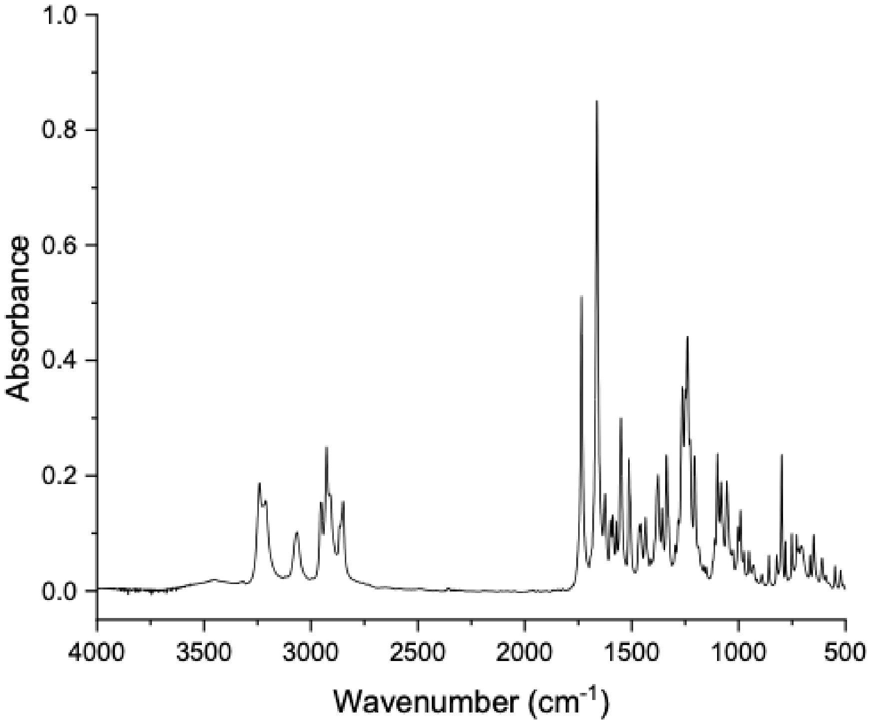

Figure S87 FT-IR spectra of **d7** (as prepared) in KBr.

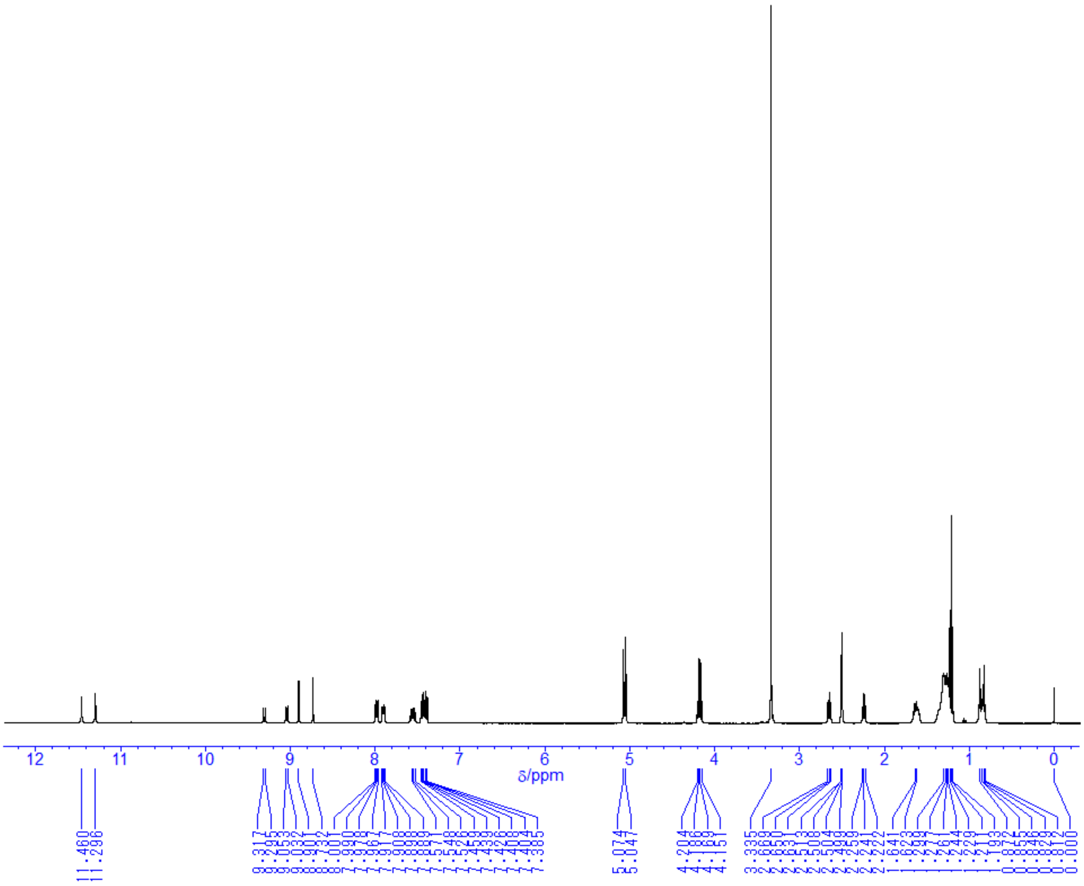

Figure S88 ^{1}H NMR (400 MHz, DMSO-d_6) spectrum of **e7** (as prepared).

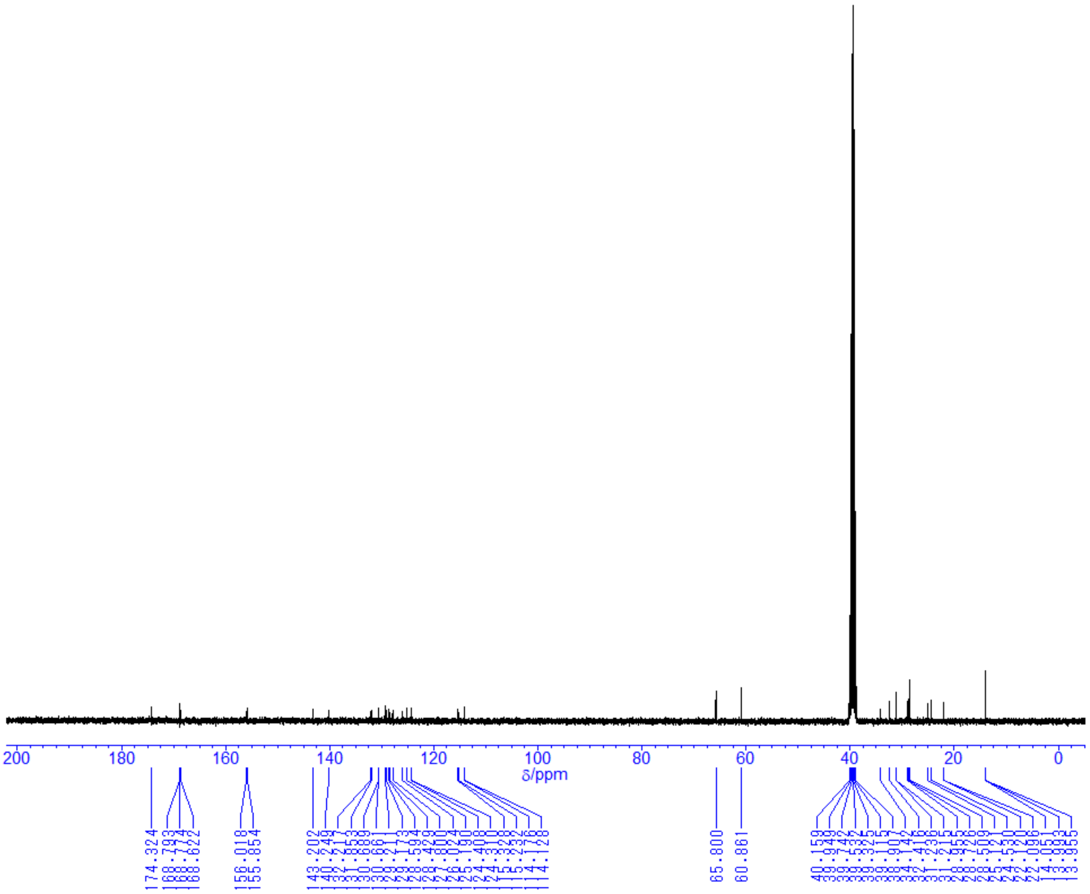

Figure S89 ^{13}C NMR (100 MHz, DMSO-d_6) spectrum of **e7** (as prepared).

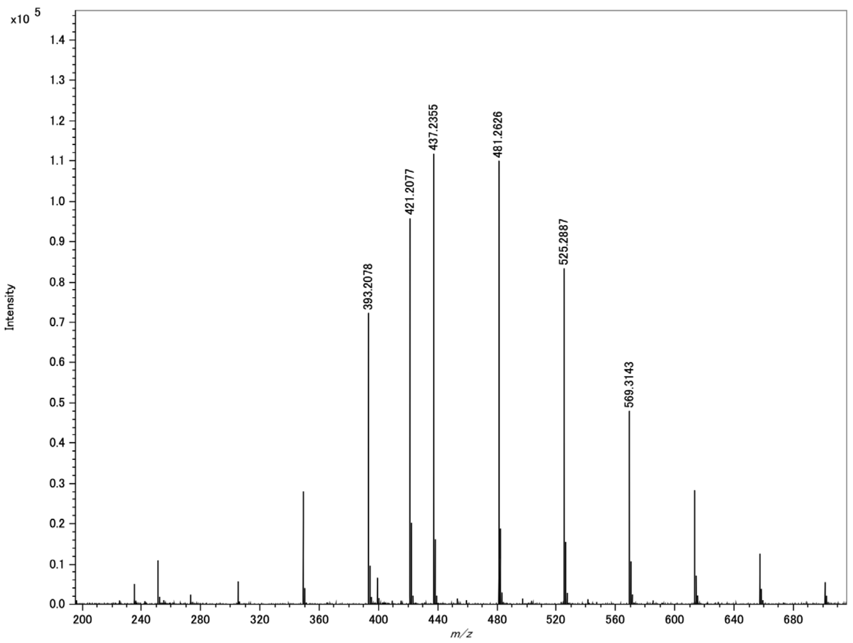

Control Parameters	
Name	SP-2000-df.spcm
Last Saved Date	2022-03-28T14:31:12
Mode	Spiral:POS
Target Plate (V)	20100
Grid (V)	-3000
Inner (V)	-4000
Outer (V)	4000
Matsuda Plate (V)	710
Einzel Lens (V)	2200
Detector (V)	-1550
Delay Time (ns)	160
Mass Range	200-700
Sampling Interval (ns)	0.5
Scan Speed	Normal
Digitizer Full Scale (V)	0.1
Digitizer Offset (V)	0
Real Time Smooth	OFF
Laser Intensity (%)	35
Laser Frequency (Hz)	250
Laser Shots	10375
Stage (Pa)	3.9E-05
Analyzer (Pa)	2.5E-05
Collision Cell (Pa)	1.2E-05
Mirror (Pa)	2.1E-05
Process Method	
Smoothing Points	-
Subtract Baseline	100
Instrument	
msTornado Control	1.15.6

Figure S90 HRMS spectra of **e7** (as prepared).

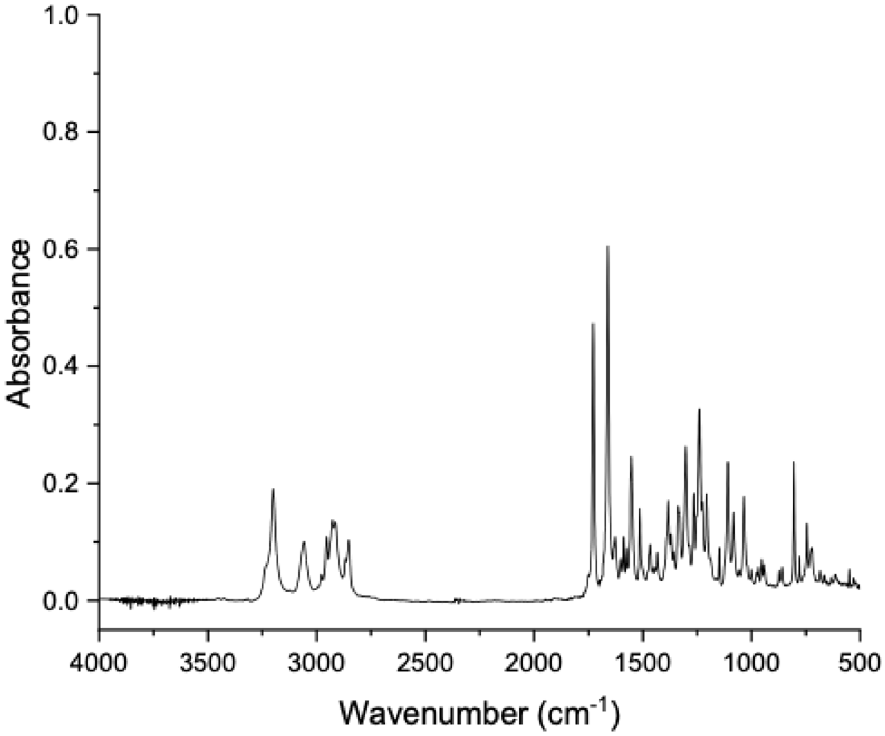

Figure S91 FT-IR spectra of **e7** (as prepared) in KBr.